DISSERTATION

Titel der Dissertation

Molecular insights into the function and regulation of the budding yeast EB1 homolog Bim1p

angestrebter akademischer Grad

Doktor der Naturwissenschaften (Dr. rer.nat.)

Verfasser: Tomasz Zimniak
Matrikel-Nummer: 0748550
Dissertationsgebiet (lt. Studienblatt): Molekulare Biologie
Betreuer: Dr. Stefan Westermann

Wien, am 28. April 2010

Table of content

1. Zusammenfassung

Proteine der EB1 (End Binding 1) - Familie sind konservierte Regulatoren der Mikrotubuli (MT) -Dynamik in allen Eukaryoten. Sie binden spezifisch an die Plus-Enden der Mikrotubuli, transportieren assoziierte Faktoren und regulieren so die Interaktion von Mikrotubuli mit zellulären Strukuren, beispielsweise mit Kinetochoren oder mit dem Zellkortex. Trotz vielfältiger Funktionen in der Zelle sind die molekularen Mechanismen, die der Aktivität dieser Proteine zugrunde liegen, großteils unbekannt.

In dieser Arbeit zeige ich, dass das Hefe EB1 Protein Bim1 von der konservierten Kinase Aurora B/Ipl1 reguliert wird und zwar durch Phosphorylierung an der Linkerdomaene. Detaillierte biochemische Studien haben gezeigt, dass Bim1 physisch mit der Ipl1 Kinase interagiert und dass diese, nach vorangehender Aktivierung durch Sli15, Bim1 an sechs direkt benachbarten Stellen in der flexiblen Linkerdomäne phosphoryliert.

Bim1 wird im Laufe des Zellzyklus in der Anaphase phosphoryliert und kontrolliert so die Kinetik der Spindelelongation und spielt eine wichtige Rolle im effizienten Abbau ausgehend vom Zentrum der Spindel. Rekombinant hergestelltes Bim1 welches vom Ipl1-Sli15 Komplex phosphoryliert wurde oder auch eine Mutante die konstitutive Phosphorylierung imitiert zeigen verminderte Affinität für Taxol- stabilisierte Mikrotubuli.

Meine Experimente demonstrieren, dass für die MT – Bindungsaktivität von Bim1 sowohl die Dimerisierung des Moleküls als auch das Vorhandensein der N-terminalen Calponin Homologie (CH) - Domäne Grundvoraussetzungen sind. Darüber hinaus haben die flexible Linkerregion im Molekül und die CH-Domäne eine synergistische Wirkung auf die MT-Bindungaktivität von Bim1, die durch Phosphorylierung reguliert wird.

Zusätzlich habe ich die Interaktion zwischen Bim1 und dynamischen Mikrotubuli mit *total internal reflection fluorescence* (TIRF) - Mikroskopie *in vitro* rekonstruiert. Bim1-Dimere lokalisieren autonom an das Plus-Ende der Mikrotubuli. Weiters haben die TIRF - Experimente gezeigt, dass die Assoziation von Bim1 mit dynamischen Mikrotubuli von Ipl1 reguliert wird.

Um die Rolle Bim1-abhängiger Rekrutierung von Ipl1 an das Plus-Ende der Mikrotubuli im Detail zu studieren, habe ich Ipl1-Mutanten hergestellt die ihre Fähigkeit an Bim1 zu binden verloren haben. Eine Serie an Experimenten zeigt, dass die physische Interaktion zwischen Ipl1 und Bim1 notwendig ist für die effiziente Lokalisation von Ipl1 an Mikrotubuli in vitro und die

Zusammenfassung

Kinase-Aktivität von Ipl1 in vivo beeinflusst. Zusammenfassend zeigen meine Daten, dass die Linkerdomäne von Bim1 eine wichtige Rolle spielt bezüglich den MT-Bindungseigenschaften des Proteins, und der Fähigkeit das Plus-Ende eines Mikrotubulus zu erkennen. Hieraus ergibt sich ein generelles und ein mögliches Konzept für die Funktion und Regulierung von CH-Domänen in einem EB1-Protein.

2. Abstract

Dynamic instability of microtubules (MTs) is regulated by several MT-associated proteins. A special subgroup of MT-associated factors is constituted by the plus-end tracking proteins (+TIPs), which are characterized by their selective association with the growing ends of tubulin polymers thus linking cellular components to MT plus ends. +TIPs are highly conserved and among them, EB1 (end binding) proteins have emerged as key regulators of microtubules in all eukaryotes. Despite their widespread importance, molecular mechanisms regulating the activity of these proteins still remain unclear.

Here, I performed a comprehensive structure-function analysis of the budding yeast EB1 protein Bim1p. My study shows that Bim1p is regulated by Aurora B/Ipl1 phosphorylation. Bim1p directly associates with the Ipl1p kinase and upon activation by Sli15p, becomes phosphorylated on a cluster of six serine residues in the flexible linker domain. Bim1p phosphorylation occurs during anaphase in vivo, and it is required for normal spindle elongation kinetics and an efficient disassembly of the spindle midzone. Recombinant Bim1p phosphorylated with Ipl1p-Sli15p complex in vitro or a mutant mimicking constitutive phosphorylation display reduced affinity for taxol-stabilized microtubules.

By engineering different Bim1 mutants I could furthermore demonstrate that the MT binding activity of the molecule depends on the dimerization properties of EB1 and that the N-terminal calponin homology (CH) domain of Bim1p is necessary, but not sufficient for stable microtubule association. In contrast, the flexible linker region of the Bim1 molecule synergistically with the CH domain enhances Bim1p MT binding and is critical for the regulation of this EB1 family member.

By using total internal reflection fluorescence microscopy (TIRF) I could visualize dynamic microtubules in vitro and show that Bim1p, like other EB1-proteins, tracks microtubule plus ends autonomously. My data show that the interaction between Bim1p and dynamic microtubules depends on the dimeric form of molecule and that these associations are negatively regulated by Ipl1p phosphorylation of the linker domain.

Finally, I dissected the interaction between the Ipl1 kinase and Bim1p, which is critical for proper kinase function in vivo. I identified two functionally redundant SxIP motifs in the N-terminus of Ipl1p, which mediate the association with the Bim1 EBH domain. The interaction

Abstract

between Bim1p and Ipl1p is negatively regulated by Cdk1 phosphorylation on serine residues immediately adjacent to the SxIP motifs. This suggests a role for Bim1p-mediated translocation of the kinase to the spindle during anaphase.

4

3. Introduction

Proteins are one of the most powerful inventions of nature. They are not only simple building blocks filling the interiors of lipid barriers but because they acquire catalytic activities and can associate with each other, proteins are the main elements to drive cellular functions. The protein-protein interactions are the basis of important biological processes, proteins have co-evolved to fit to each other, working antagonistically or synergistically to regulate the machinery of biological life. One of the remarkable examples of a protein interaction networks are microtubules and the associated proteins which regulate them; this dynamic network of tubular shapes has evolved over several million of years to mechanically support the cell body and maintain crucial intracellular processes.

3.1. Inherent microtubule dynamics

Microtubules (MTs) are an essential element of the cytoskeleton that functions in major cellular activities. These dynamic polymers provide mechanical support for the shape of the cell; they can mediate vesicle or organelle trafficking and during mitosis they are required for chromosome segregation. This diversity of MT function is defined by the extraordinary flexibility of microtubule organization.

Microtubules filaments are composed of globular α- and β-tubulin hetorodimers, which assemble into hollow elongated tubes (Desai and Mitchison, 1997). The αβ-tubulin dimers can self-organize in head-to-tail fashion into polarized protofilaments. In vivo, 13 parallel protofilaments associate laterally to form 25 nm-wide cylindrical structures. Subsequent addition of new heterodimers occurs more quickly at one end (called the plus-end) of the tube. The other, slowly growing end (minus-end) is terminated by an α-tubulin subunit and is usually anchored at centrosomes (spindle pole bodies in budding yeast), specialized microtubule organizing centers (Vinh et al., 2002). Lateral interaction between protofilaments can result in two conformations of microtubule polymers. The so called A-lattice is formed by lateral associations of α-β subunits, conversely a B-lattice is made of α-α or β-β contacts (Amos and Klug, 1974). In animal cells, microtubules are dominated by B-lattice structures, and the A-type can be visualized only at the microtubule seam, a discontinuity of the MT surface required for closing the MT tube (Kikkawa

et al., 1994). The lattice seam has been suggested as an important feature of microtubules, regulating its dynamics and as a structural element recognized by some microtubule associated proteins like the *S. pombe* EB1 homolog Mal3p (Sandblad et al., 2006).

Microtubules are highly dynamic structures and during polymerization, the plus-end switches quickly between phases of relatively slow growth and rapid depolymerization resulting in catastrophes (Mitchison and Kirschner, 1984). This intrinsic feature of tubulin polymers is termed dynamic instability and is a basic property that underlies the re-organization of cellular microtubule networks. The energy that drives switching between catastrophes and rescues of microtubules comes from GTP hydrolysis (Erickson and O'Brien, 1992). The nucleotide hydrolysis and exchange on the β-subunit is not required for polymerization but triggers a conformation change of protofilaments into the more curved GDP-structure, which is more unstable and prone to disassembly (Wang and Nogales, 2005). The catastrophe is initiated by the loss of the so called GTP cap at the microtubule plus-end which then exposes the unstable GDP lattice, leading to rapid depolymerization (Drechsel and Kirschner, 1994). To control microtubule dynamics and function cells regulate the polymerization of microtubules by many microtubule associated proteins.

3.2. Microtubule associated proteins

Under physiological conditions, microtubules interact with an impressive number of proteins that control their role in different biological activities. Microtubule associated proteins (MAPs) initially purified form bovine brain, are the major regulators of microtubule dynamics in cells. They can act as microtubule structural, stabilizing factors or they may be depolymerizers of the tubulin lattice. In addition, some MAPs can generate forces, helping in chromosome or organelles movements or mediating connections of the microtubule ends with many cellular elements.

Examples of the group of structural MAPs are tau or MAP2 which stabilize microtubules by binding all along the microtubule lattice and suppressing catastrophes. They bind to polymeric tubulin via their C-terminal domain while their N-terminus protrudes from the MT surface. During mitosis a number of structural MAPs are phosphorylated which inhibits their MT association (Cassimeris and Spittle, 2001). One special group of microtubule associated proteins that regulate tubulin polymerization is the γ-tubulin ring complex (γ-TuRC). In cells, γ-TuRC helps to over-

come the kinetic barrier of microtubule nucleation by specifically binding to the minus-ends of freshly formed polymers (Moritz et al., 2000).

In contrast to structural and nucleating MAPs, several types of proteins specifically desta-bilize microtubules, most of them are members of kinesin-related families. It was shown that members of the kinesin-13 family such as MCAK can increase the catastrophy frequency of dy-namic MTs up to 10-fold. Instead of moving along MTs like other motor proteins, these proteins use the energy of ATP hydrolysis to catalytically remove tubulin from the ends of microtubules (Newton et al., 2004). Similar effects are observed for Op1/stathmin and in both proteins micro-tubule depolymerizing activities are negatively regulated by the mitotic kinase Aurora B (Gadea and Ruderman, 2006). In budding *S. cerevisae*, a motor from the kinesin-14 family, Kar3p, pre-ferentially destabilizes the minus-ends of microtubules, whereas the kinesin 8-family protein Kip3p specifically affects the plus-ends of microtubules and is required for proper mitotic spindle dynamics (Endow et al., 1994; Gupta et al., 2006). Long after discovery of the first MT-lattice binding MAPs a special subgroup of proteins that modulate microtubule dynamics has been found, factors that can accumulate at the growing plus-ends of microtubules, were termed +TIPs (microtubule plus tip interacting proteins).

3.2.1. +TIPs

CLIP-170 – cytoplasmic linker protein of 170 kDa - was the first protein described that tracks growing microtubule plus ends in vivo (Perez et al., 1999). Since then many of other un-related proteins were described with this peculiar localization to the MT tips in living cells. These proteins show structural diversity, usually with multiple domains and oligomeric properties (Akhmanova and Steinmetz, 2008). Many plus end tracking proteins binds to each other, consti-tuting a dynamic, conserved network of protein interactions at the microtubule ends. Although most of them contain intrinsic microtubule binding activities, they depend on the interactions with EB1 family proteins for their enrichment at MT tips. The main +TIP protein families were assigned according to structural elements underlying their MT tracking properties.

One of the major plus tracking families is constituted by the so-called CAP-Gly proteins (cytoskeleton-associated protein glycine-rich proteins) to which belong mainly CLIPs (CLIP170-like members) and the related p150[glued] subunit of the dynactin complex. They are characterized by the presence of the globular CAP-Gly fold with uniquely conserved GKNDG residues (Weis-brich et al., 2007). Cytoplasmic linker protein CLIP-170 (Bik1p in budding yeast) is a homodi-

meric molecule with two CAP-Gly domains at the N-terminal microtubule binding domain, surrounded with basic serine-rich motifs. In additions it contains a central coiled-coil and a metal binding domain at the C-terminus with a characteristic EE(Y/F) motif. CLIP-170 function was implicated in linking endosomes to microtubules and facilitating kinetochore-microtubule attachments (Pierre et al., 1992; Tanenbaum et al., 2006). Interestingly, CLIP-170 can fold back on itself, as a result of intramolecular interactions. Another microtubule-interacting member of CAP-Gly proteins, the p150^{glued} protein can directly associate with CLIP-170 and release it from its inhibitory conformation by binding to its metal binding "zinc knuckles" and distal EEY motifs (Lansbergen et al., 2004). p150^{glued} contains only one CAP-Gly domain, long coiled-coil regions and, interestingly, it lacks a distal EE(Y/F) motif. Its function was mainly described as important for targeting dynactin to microtubule plus ends and for proper metaphase chromosome alignment (Dujardin et al., 1998; Vaughan and Vallee, 1995). In addition, proteins from the CAP-Gly family associate with other factors called CLASPs (CLIP associated proteins), initially identified as CLASP1 and CLASP2 with microtubule stabilizing activity (Akhmanova et al., 2001). CLASPs associate with growing MT plus ends and contribute to spindle organization and kinetochore alignment (Mimori-Kiyosue et al., 2006).

Another special group of plus tracking proteins are microtubule-based motor proteins that use ATP-driven conformational changes to translocate towards microtubule ends. This includes the plus-directed yeast kinesin Kip2, the *S. pombe* protein Tea2 from the kinesin-7 family, and several plus-end directed kinesins with MT depolymerization activities such as yeast Kip3p or mammalian MCAK.

The last two microtubule +TIP families are characterized by their autonomous tip association properties in vitro. The proteins of the EB1 family and TOG-domain proteins from the family of XMAP215-like proteins. XMAP215 and Stu2p in *S. cerevisae* are elongated molecules containing N-terminal TOG domains. The numbers of TOG domains in these molecules can vary between two to five but each TOG domain is sufficient to bind tubulin dimers (Al-Bassam et al., 2007). The binding to tubulin is mediated within individual TOG domains by six HEAT-repeat elements that fold into paddle-like structures. It was shown that members of this family can stay for extended times at the microtubule plus-ends where they act as a processive polymerases catalyzing repeated rounds of new tubulin subunit addition to existing microtubules (Brouhard et al., 2008). TOG containing proteins increase the rate of tubulin assembly in vivo, a feature that is required for proper mitotic spindle elongation and efficient cortical attachments (Hestermann and Graf, 2004; Severin et al., 2001). The other group of proteins that show primary plus end

tracking activity in vitro are the EB1-like proteins (EBs). In contrast to XMAP215-like proteins, the EBs track growing tips by rapid turn-over rather than a processive polymerization mechanism (Bieling et al., 2007). EB1-like proteins are extremely important in the recruitment of associated factors like other +TIPs to the MT plus end with an intrinsic function to suppress catastrophes and control persistent microtubule growth in mammalian cells (Komarova et al., 2009).

3.3. The family of EB1 - end binding proteins

EB1-like proteins are an evolutionary conserved group of +TIPs that was first visualized for its autonomous MT plus end tracking activity independent of other proteins (Bieling et al., 2007). Human EB1 protein was initially identified as a factor that binds the C-terminus of the adenomatous polyposis coli (APC) protein, a tumor suppressor frequently mutated in colon cancers (Su et al., 1995). EB1 homologues have since been identified in all eukaryotes. Fungal cells contain one copy of the EB1 gene, in *S. cerevisae* called – *BIM1*, and in *S. pombe* called Mal3. There are three genes encoding for human EB1 family proteins: EB1, EB2/RP1 and EB3. In addition, two forms of EB2/RP1 are translated from different initiation codons and also two forms of EB3 are expressed as a result of alternative splicing increasing the complexity of this family of proteins (Su and Qi, 2001).

EB1-like proteins are characterized by the presence of a highly conserved N-terminal microtubule binding domain with a calponin-homology (CH) fold (Hayashi and Ikura, 2003). Although this globular structure is often found in F-actin binding proteins, some other MAPs such as CLAMP or Ndc80/HEC1 contain CH-domains as well, mediating their MT-associations (Dougherty et al., 2005; Wei et al., 2007). A second characteristic feature for EB-like protein structure is their C-terminal homodimerization domain (Fig. 2). This coiled-coil domain is built of four α-helices that form a unique hydrophobic cavity in the end binding homology (EBH) domain (Slep et al., 2005). The two functional regions of EB1-like proteins are connected via a linker sequence, unstructured and flexible and largely lacking conserved determinants. The linker region has been suggested to play an important role in the case of Mal3p-promoted microtubule assembly and in EB3 it is a target region for Aurora kinase phopshorylation (Ban et al., 2009; des Georges et al., 2008). The extreme C-terminus of EB-like proteins form flexible tails, usually marked with the short sequence of EE(Y/F) motifs, similar to that found in α-tubulin and CLIP-170 (Weisbrich et al., 2007).

Despite their sequence similarities individual human EB1-family proteins show various cellular functions, microtubule targeting and they can differentially associate with partner proteins.

Introduction

The growing list of EB-interacting proteins has been focused mainly around APC, p150^{glued}, CLIPs and CLASP1/2 that together with EBs form an interaction network controlling interphase microtubule dynamics and cortex attachments (Bu and Su, 2003; Hayashi et al., 2007; Mimori-Kiyosue et al., 2005). EB1 also has a crucial role in mitosis by promoting growth and association of microtubules within the central spindle and at the cell cortex where it is required for proper spindle orientation and dynamics (Rogers et al., 2002). It was suggested that EB1 can connect kinetochores and centrosomal fibers by binding to the minus-end directed motor Ncd and targeting it to the growing tips of centrosomal microtubules (C-MTs) in *Drosophila* S2 cells. This process is essential in focusing of kinetochore microtubule bundles (K-fiber) and in the formation of a functional bi-polar spindle (Goshima et al., 2005).

Not much is known about the function of other EBs. EB3 as well as EB1 mediate MT plus end tracking of APC, but EB3 can also associate with an F-actin binding protein – debrin, the E3 ubiquitin ligase SIAH-1 and as well with Aurora A and Aurora B kinases (Ban et al., 2009; Geraldo et al., 2008). EB2/RP1 seems to be most divergent compared to the others, as its C-terminus has a lower affinity for MCAK, p150^{glued} and for the best characterized EB1-partner APC (Bu and Su, 2003; Lee et al., 2008). In addition EB2/RP1 is not as effective in suppressing MT catastrophes as other family members which is due to a slightly different sequence composition of its N-terminal CH domain (Komarova et al., 2009). Another interesting feature of mammalian EB1 family proteins is their C-terminal domain-mediated heterodimerization (Komarova et al., 2009). Heterodimerization between different human EB members regulates binding to different partners and affects their microtubule anti-catastrophe activity.

3.3.1. Budding yeast EB1 homolog Bim1p

The *S. cerevisae* genome encodes for only one EB1 homolog which was first found in a two-hybryd screen with the α-tubulin *TUB1* gene (Schwartz et al., 1997). The newly characterized ORF was named Bim1 as it could bind to microtubules. The Bim1 protein is slightly larger than its vertebrate homologs, but shares a high degree of conservation with characteristic EB1 domains.

The deletion of the *BIM1* gene results in severe microtubule-related defects. Yeast cell lacking Bim1p are inviable at extreme temperatures (i.e., ≥ 37°C or ≤ 14°C), display hypersensitivity to microtubule destabilizing drugs such as benomyl, and display aberrant spindle behavior (Schwartz et al., 1997). In addition, deletion of *BIM1* is synthetic lethal with number of other de-

letions such as +TIPs (i.e. *bik1*), kinesins (i.e. *kar3*), check-point proteins (i.e. *bub3)* or conditional alleles of tubulin mutants (Schwartz et al., 1997; Tirnauer et al., 1999). Bim1p associates with every growing plus end of microtubules in budding yeast cells (Fig. 1).
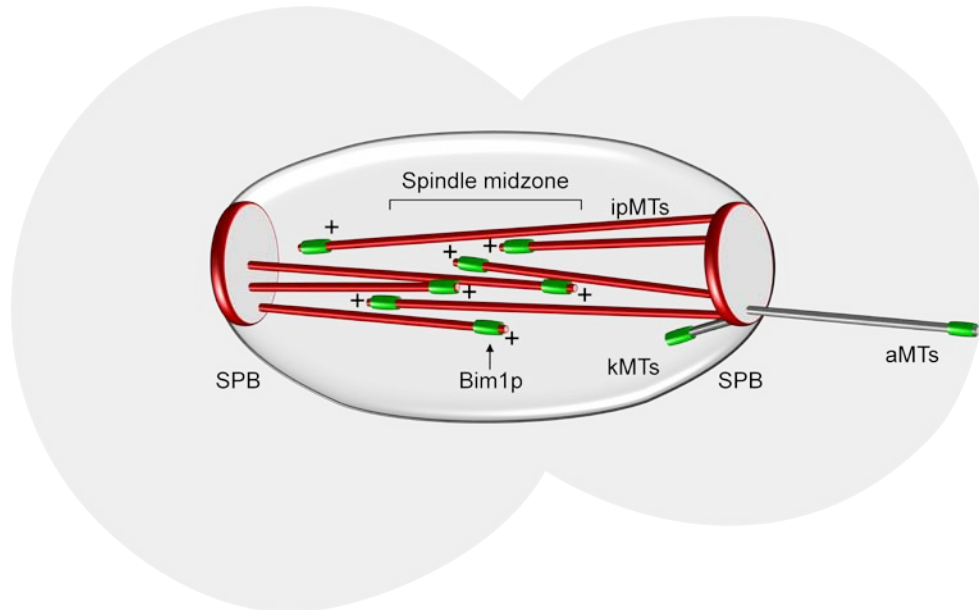
Figure 1. **Multiple localizations of Bim1p in budding yeast cells**
Bim1p associates with MT plus tips emanating for spindle pole bodies (SPB). Bim1p helps anchoring astral microtubules (aMTs) to the cell cortex and modulates the dynamics of nuclear microtubules. It associates with a number of factors at kinetochore mictoubules (kMTs) and supports the anaphase spindle by localizing to overlapping interpolar microtubules (ipMTs). Bim1 is shown in green.

By binding to tubulin polymers Bim1p modulates MT dynamics already in G1 phase (Tirnauer et al., 1999). Microtubules without Bim1p in yeast show impaired dynamics characterized by fewer rescues and catastrophes, and longer pausing times. Bim1p delivers a number of associated factors to the microtubule tip, one of the best characterized examples is its interaction with the Kar9 protein that mediates the cortical attachment of cytoplasmic microtubules and helps to correctly position the mitotic spindle (Lee et al., 2000; Miller et al., 2000). An additional function of Bim1p is present at the anaphase spindle, where it together with the motor Kar3p stabilizes overlapping microtubules and helps maintaining spindle integrity (Gardner et al., 2008).

3.4. The role of EB proteins in mediating plus end binding

Despite the fact that many microtubule +TIPs contain inherent microtubule binding activity, they often depend on EB1-like proteins for the efficient delivery to microtubule plus ends. The recruitment of those factors is done by direct binding to the EBH motif in the dimerization domain or to the distal α-tubulin-like motifs EE(Y/F) of EB-molecules. The interacting factors can be grouped into two classes depending on the domain structure involved in binding to EB1 proteins. The first class is constituted by the CAP-Gly-containing proteins that can symmetrically associate with the hydrophobic cavity of EBH domain or as well with the EE(Y/F) C-terminus of an EB1-like protein (Fig. 2). The latter associations are mediated by a hydrophobic groove of the CAP-Gly domain containing the conserved GKNDG motif (Honnappa et al., 2006).
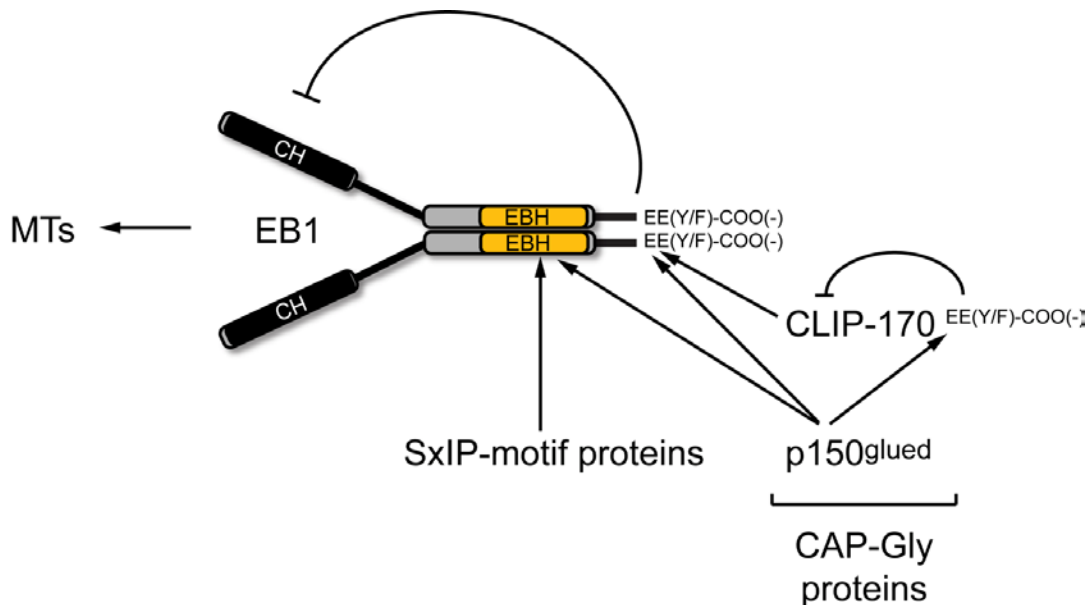
Figure 2. **Hierarchical network of EB-mediated microtubule plus end interactions**
EB1 proteins show autonomous plus tip tracking. By direct association with different +TIPs they can mediate their plus end targeting. The EB1 C-terminal domain offers two binding sites for diverse partners. EB1 EE(Y/F) tail modulates its MTs activity upon binding to CAP-Gly domain-containing proteins. EBH domain serves as a platform for recruiting factors having SxIP motif independently of binding of CAP-Gly proteins (modified from Slep, 2009).

EB1-dependent plus end tracking was described for the CAP-Gly containing CLIP-170 and p150^{glued} (Bieling et al., 2008; Watson and Stephens, 2006). Interestingly, upon binding to CAP-Gly proteins EB1 can be released from an autoinhibitory state mediated by its own EE(Y/F) motif and microtubule binding domain (Manna et al., 2008). The interactions using the EE(Y/F) motif are a very common way of modulating dynamic +TIP networks (Fig. 2). It was recently described that the EE(Y/F) motif mediates associations between EB1-p150^{glued}, p150^{glued} and CLIP-170, as well as between CLIP-170 and α-tubulin tails (Hayashi et al., 2005; Mishima et al., 2007; Weisbrich et al., 2007).

A second group of EB1 interacting factors are the SxIP containing proteins (Honnappa et al., 2009). Members of this class can associate symmetrically via an Ser-x-Ile-Pro (SxIP) motif with the EBH domain of the C-terminal dimeric part of EB-like proteins (Fig. 2). To this group of proteins belong, for example APC (Kar9p in budding yeast), MACF2, MCAK, proteins from the CLASP family and STIM1, displaying structural diversity and no sequence homology. Some of these EB-binding factors can contain multiple SxIP motifs to enhance microtubule tip localization (Honnappa et al., 2009). Sequence analysis of SxIP-proteins suggests that the motif is embedded within basic and proline/serine rich unstructured regions. The interactions with EB-proteins can be additionally regulated by phosphorylation of serines adjacent to the SxIP motif.

3.5. Phosphoregulation of +TIP interactions

Microtubules are negatively charged polymers and many microtubule-associated proteins utilize this property to electrostatically bind tubulin polymers. Phosphorylation is then one possibility to neutralize basic charge and thus regulate MTs-associations. The other way to control targeting to microtubules is phosphorylation-dependent inhibition of the binding to EB1-proteins. It has been suggested that some mitotic kinases could regulate microtubule +TIPs activities in order to control the reorganization of the cytoskeleton during cell division. On example provided a study on the interactions of EB1 and SxIP-containing APC, where CDC2 kinase phosphorylation results in a four-fold reduction of the binding between APC and EB1 (Honnappa et al., 2005). This way of interference was observed also for phosphorylation of MCAK by Aurora B (Lan et al., 2004). MCAK is another SxIP-motif containing protein in which phospho-mimicking mutations of Aurora B sites near this motif decreases its interactions with EB1 and subsequent microtubule plus-end targeting (Honnappa et al., 2009).

3.6. The role of Aurora B/Ipl1 in regulating microtubule ends

One of the major kinases regulating microtubule dynamics by phosphorylation of different MAPs is Aurora B. Aurora B kinase is the catalytic component of the chromosome passenger complex (CPC) which has distinct roles in multiple cellular localizations. The CPC complex consists of the evolutionary conserved proteins Aurora B, INCENP, Survivin and Borealin (Dsra-B), in budding yeast called Ipl1p, Sli15p, Bir1p and Nbl1p, respectively. At metaphase, the CPC is localized to the centromere (Beardmore et al., 2004), but it is effectively translocated to the spindle at anaphase onset (Pereira and Schiebel, 2003). Despite its multiple locations, it is a common theme that Aurora B regulates microtubule tips either in the process of bi-orientation of chromosomes as well during spindle disassembly just before cytokinesis.

3.6.1. Role of Aurora kinase in chromosome bi-orientation

Aurora B kinase controls accurate chromosome segregation, the critical part of cell progression. The process of bi-orientation ensures that sister chromatids are connected to microtubules emanating from opposites cell poles and are subsequently segregated to two daughter cells. Multiple lines of evidence suggest that the mechanism governing chromosome bi-orientation critically depends on the evolutionary conserved mitotic kinase Aurora B (Lampson et al., 2004; Tanaka et al., 2002).

The role of Aurora kinase in bi-orientation has been studied extensively in budding yeast where each sister kinetochore is connected to only one microtubule (Winey et al., 1995). In yeast, after chromosome replication, both sister chromatids are occasionally captured by MTs form the same pole, an aberrant geometrical configuration known as syntelic attachment. This situation brings both kinetochores close together and affects tension forces produced by the mitotic spindle (Dewar et al., 2004). This lack of tension between sister kinetochores triggers the activity of Aurora kinase Ipl1p that then helps to correct improper kinetochore-MT attachments (Fig. 3) (Tanaka et al., 2002).

In yeast, Ipl1p targets a number of kinetochore and microtubule binding proteins, lowering their kinetochore or MT associations (Cheeseman et al., 2002; Shang et al., 2003). Among them, the Dam1 protein is a particularly important target of Ipl1p as its allele mimicking constitutive phosphorylation can suppress the kinase compromised *ipl1-2* mutant (Cheeseman et al., 2002). The Dam1 protein is a subunit of a heterodecameric complex, which is essential in bridg-

ing the plus ends of microtubules and the centromeres in *S. cerevisae* (Kiermaier et al., 2009). Ipl1p phosphorylation affects Dam1 complex function at the microtubules and prevents its interaction with the Ndc80 complex allowing the correction of maloriented chromosomes (Lampert et al., 2010; Shang et al., 2003).
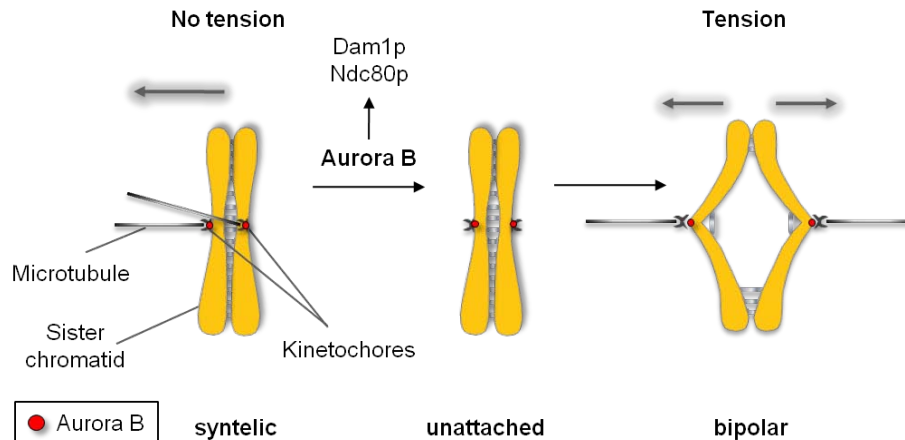
Figure 3.   The role of Aurora B kinase in bi-orientation process
Lack of tension across sister kinetochores activates the kinase Aurora B/Ipl1 that by phosphorylation of microtubule binding kinetochore components allows correcting improper attachments of chromosomes to the mitotic spindle.

In human cells, Aurora B regulates Ndc80/HEC1, which is the main microtubule attachment module at the outer kinetochore. In the absence of tension Aurora B phosphorylates the N-terminal tail of Ndc80, thereby reducing its affinity for microtubules (Cheeseman et al., 2006). In addition, Aurora B can control microtubule disassembly by regulating the activity of a mitotic centromere-associated kinesin MCAK/Kif2C (Andrews et al., 2004). Aurora phosphorylation of MCAK inhibits its microtubule depolymerase activity but also targets it to the centromere where it is believed to regulate aberrant merotelic attachments (Lan et al., 2004). Aurora B also phosphorylates Op18 (oncoprotein)/Stathmin, another microtubule destabilizing protein whose localized inhibition is important during spindle assembly (Gadea and Ruderman, 2006). Recent findings also suggest that Aurora A and B activity regulates microtubule dynamics by controlling the stability of EB2 and EB3 proteins (Ban et al., 2009).

3.6.2. Regulation of anaphase spindle disassembly and mitotic exit

Aurora B has a second role in regulating microtubules at the time when sister chromatids are separated and cell progresses into anaphase. At the beginning of this process the CPC and Aurora B are translocated from centromeres to the spindle midzone. In budding yeast, the trigger for this transfer is separase activated Cdc14p dephosphorylation of Sli15p (Pereira and Schiebel, 2003). Dephosphorylated Sli15p targets other components of the passenger complex to the anaphase microtubules, where the activity of Aurora/Ipl1p first helps to organize the spindle via phosphorylation of microtubule bundling proteins such as Ase1p and later the kinase activity helps in the timely dissasembly of the spindle before cytokinesis (Buvelot et al., 2003; Kotwaliwale et al., 2007).

In vertebrate cells, the transfer of CPC is dependent on a kinesin superfamily member MKLp2 (mitotic kinesin-like protein-2), which can recruit the CPC to the central spindle in anaphase (Gruneberg et al., 2004). MKLp2 directly binds Aurora B and also interacts with Cdc14A which in addition regulates spindle localization of INCENP/Sli15p. Cdc14A dephosphorylates INCENP and this contributes as well to the relocation of Aurora B to the central spindle in anaphase. At telophase and cytokinesis Aurora B concentrates to the midbody and helps in the formation of the cleavage furrow (Eckley et al., 1997). In budding yeast the Ipl1p-dependent NoCut pathway timely regulates cytokinesis and prevents chromosome breakage by regulating aniline-like proteins (Norden et al., 2006). A similar role of Aurora B is observed in human cells, where the kinase is a part of a mechanism that in response to unsegregated chromatin controls cytokinesis and prevents tetraploidization (Steigemann et al., 2009).

4. Aim of the work

Proteins from the EB1-family are conserved regulators of microtubule dynamics. They can primarily associate with growing microtubule plus ends in vivo and recruit associated factors in order to regulate the interactions of microtubules with cellular structures such as kinetochores or cortical attachment sites. Despite their widespread importance, some important questions concerning EB1 related proteins have still remained unanswered.

Not much is known how these proteins bind microtubules and how this activity is regulated in different cellular processes. Moreover, it is also not clear how the mitotic kinase Aurora B regulates microtubule ends in the process of resolving improper microtubule-kinetochore attachments or during anaphase spindle disassembly.

The primary aim of this work was to identify novel Ipl1p/Aurora B targets in *S. cerevisae* that contribute to kinase function at the microtubule plus ends. The yeast EB1 homolog was initially identified as an Ipl1p phosphorylation target, opening the question for the importance of this phenomenon in vivo. First I tried to understand how the phosphorylation affects Bim1p function on dynamic or static microtubules, to define the molecular mechanism regulating microtubule binding activity of EB1-like proteins. This study helped me also to address the structural requirements of Bim1p for its plus end association and the role of Bim1p during disassembly of the anaphase spindle.

In addition, I characterized functional interactions between Ipl1 kinase and Bim1p to understand how they modulate kinase function in living cells. My study provides insight into regulation and functions of microtubule end binding proteins and helps to reveal the role of functional interactions between EB1-Aurora B at microtubule plus ends.

5. Results

5.1. Regulation of the EB1 homolog Bim1p

5.1.1. Bim1p is phosphorylated by the Ipl1p-Sli15p complex in vitro and in vivo

In the initial experiment I purified the budding yeast EB1 homolog Bim1p to determine its potential posttranslational modifications in vivo. For this purpose, Bim1p was tagged at the C-terminus with a tandem affinity tag (TAP-tag) and the protein was purified from yeast extracts of logarithmically growing cells. Purification was performed under stringent conditions with 300 mM KCl and the resulting peptides were analyzed after tryptic digestion by mass spectroscopy. Under these conditions only Kar9p was co-purified with Bim1p (Fig. 4A).
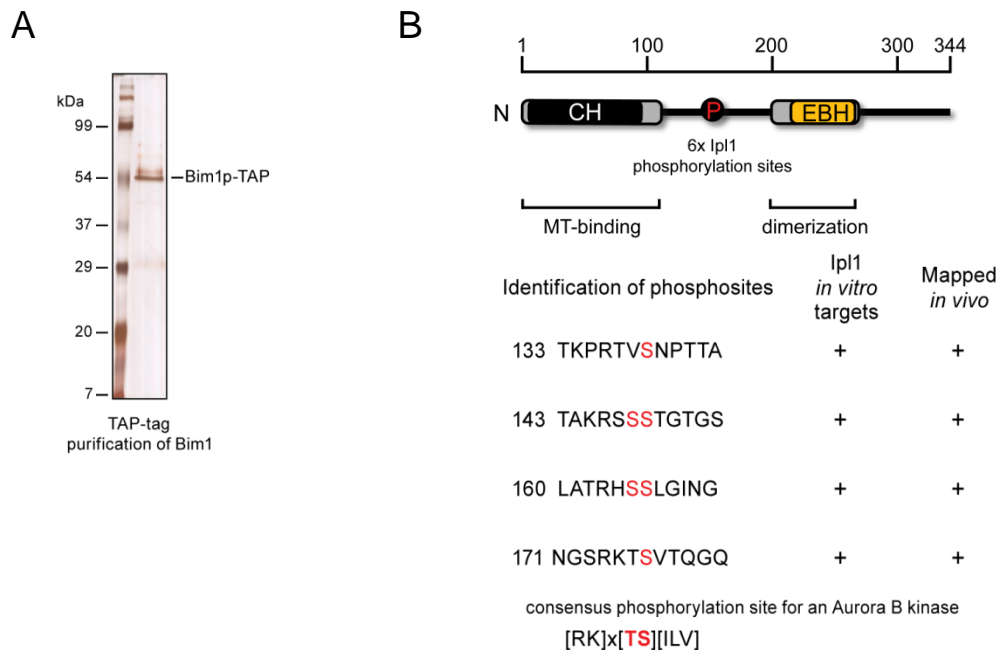
Figure 4.   Bim1p is a target of Ipl1/Aurora B phosphorylation

(A) Silver stained gel of purified Bim1p-S Tag-TEV-ZZ from yeast extracts made from logarithmically growing cells.

(B) Schematic representation of phosphorylation sites found by mass spectroscopy of Bim1p purified from yeast extracts or phosphorylated by recombinant Ipl1p-Sli15p complex in vitro.

Kar9p is the adenomatus polyposis coli (APC) homolog and a known interaction partner of Bim1p. While no additional co-purified proteins were detected, further phospho-peptide analysis determined six phosphorylation sites (Ser-139, -148, -149, -165, -166, and -176) in the central, 40 aa long, unstructured region of Bim1p that connects the conserved calponin homology CH- and the EB1- like domain (Fig. 4B). A functional role for this region of the Bim1p molecule has not been described so far. Most of the phosphorylation sites matched the consensus sequence targeted by the Ipl1p/ Aurora B kinase (Cheeseman et al., 2002). This suggested that Bim1p may be a target for Ipl1p. To confirm that, recombinant Bim1p was phosphorylated in vitro with purified Ipl1p in complex with its activator Sli15p. The phosphorylation state of Bim1p was then analyzed by mass spectroscopy and interestingly the same six serine residues in the linker domain of Bim1p were found to be phosphorylated. To further validate the specificity of the kinase for the mapped sites, Bim1p variants were expressed with mutations of the six serines into alanines (Bim1^{6A}) to prevent phosphorylation or into aspartic acids (Bim1^{6D}) to mimic constitutive phosphorylation (Fig. 5A).

Figure 5.   Analysis of Ipl1 kinase specificity for Bim1p.

(A) Recombinant Bim1^{WT} and mutants preventing (6A) or mimicking (6D) phosphorylation were assayed with Ipl1p-Sli15p complex and [P^{32}] γATP. Mutation of the mapped sites results in elimination of phosphorylation.

(B) Bim1p is not able to activate Ipl1p alone and its phosphorylation by the kinase depends on the presence of Sli15p.

Results

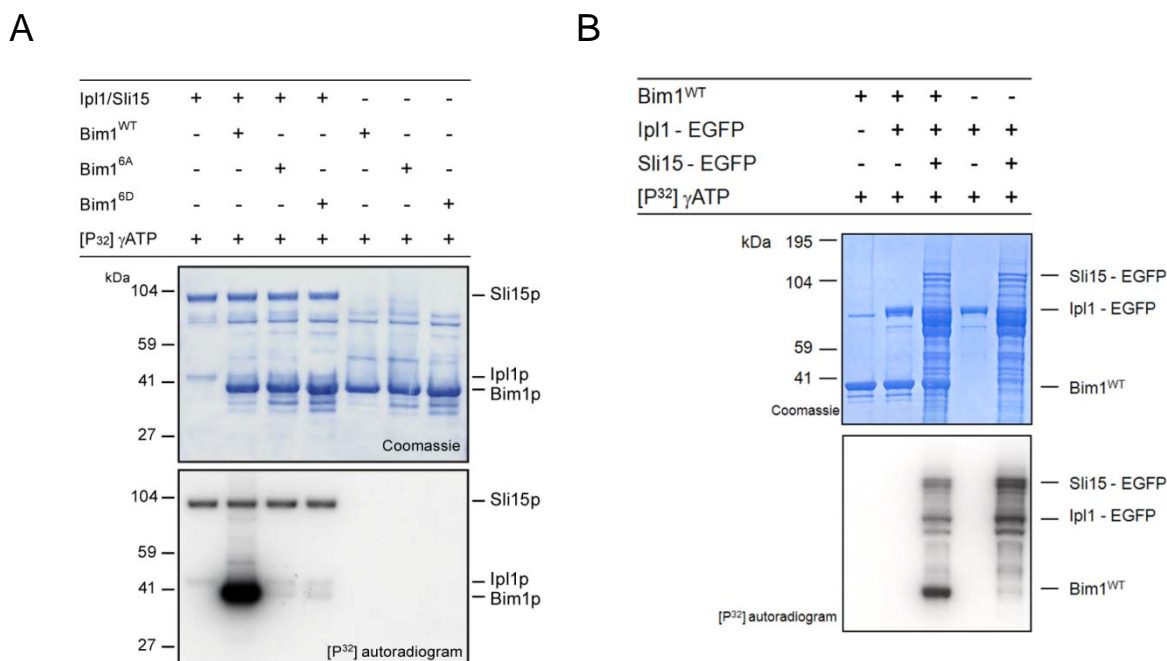The mutated recombinant proteins were then subjected to Ipl1p-Sli15p phosphorylation in vitro, which resulted in abolishment of phosphorylation by Aurora kinase and confirms the high specificity of the kinase for mapped sites (Fig. 5A). To further examine the functional requirements for Bim1p phosphorylation, the kinase assay was performed in the absence of the known activator Sli15p. Under these conditions Bim1p phosphorylation was not detectable but could only be seen after addition of Sli15p, suggesting that phosphorylation of Bim1p depends strictly on the presence of Sli15p (Fig. 5B).

5.1.2. Bim1p phosphorylation depends on Ipl1p and occurs during anaphase in vivo

In the next set of experiments I tried to analyze the phosphorylation status of Bim1p in vivo by studying the migration pattern of myc-tagged Bim1p using WB. A potential phospho-shift was enhanced by addition of 30 µM Mn^{2+} Phos-tag reagent to the SDS-PAGE (Kinoshita et al., 2006). Under these conditions slower migrating forms of phosphorylated Bim1p were detected in the yeast extracts expressing the wild-type allele of *IPL1*. These forms were eliminated after shifting the cells to the restrictive temperature in an *ipl1-2* mutant, further confirming that Bim1p phosphorylation is Ipl1p-dependent in vivo (Fig. 6A).
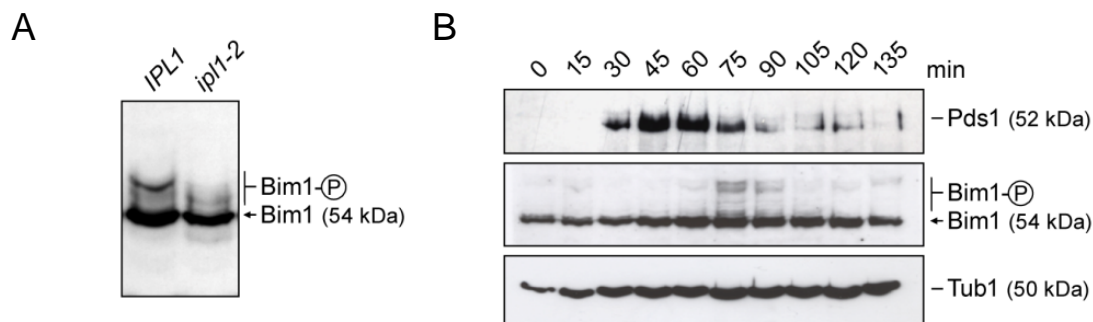
Figure 6.   Bim1p phosphorylation occurs during anaphase in vivo

(A) Western-blotting analysis of myc-tagged Bim1p in *WT* cells or with *ipl1-2* temperature sensitive allele. Shifting to restrictive temperature eliminates slower migrating phosphorylated forms of Bim1p confirming that the phosphorylation is Ipl1p-dependent.

(B) WB analysis of Bim1p's phosphorylation status during the cell cycle. Phosphorylated forms of Bim1p are detectable after degradation of yeast securing Pds1p that marks anaphase onset.

To determine the timing of Bim1p phosphorylation in vivo, cell were arrested in G1 phase using α-factor, and samples taken every 15 min after release were analyzed by Phos-tag WB. This time course analysis detects phosphorylated forms of Bim1p in a short 15-30 min time window following degradation of the yeast securin Pds1 (Fig. 6B). This demonstrates that Bim1p phosphorylation occurs mainly in anaphase during the yeast cell cycle and is caused by Ipl1p kinase activity.

5.1.3. Phosphorylation affects Bim1p binding to microtubules

The major function of Bim1p in living cells is determined by its microtubule binding properties. To study the effects of phosphorylation on Bim1p function, I therefore first looked at consequences on Bim1p microtubule-binding. Although on dynamic microtubules Bim1p specifically recognizes growing MT plus-ends, in vitro it also can bind to static microtubules. This feature was used first to determine the apparent dissociation constant (K_d) for MTs in a co-sedimentation assay (Fig. 7).
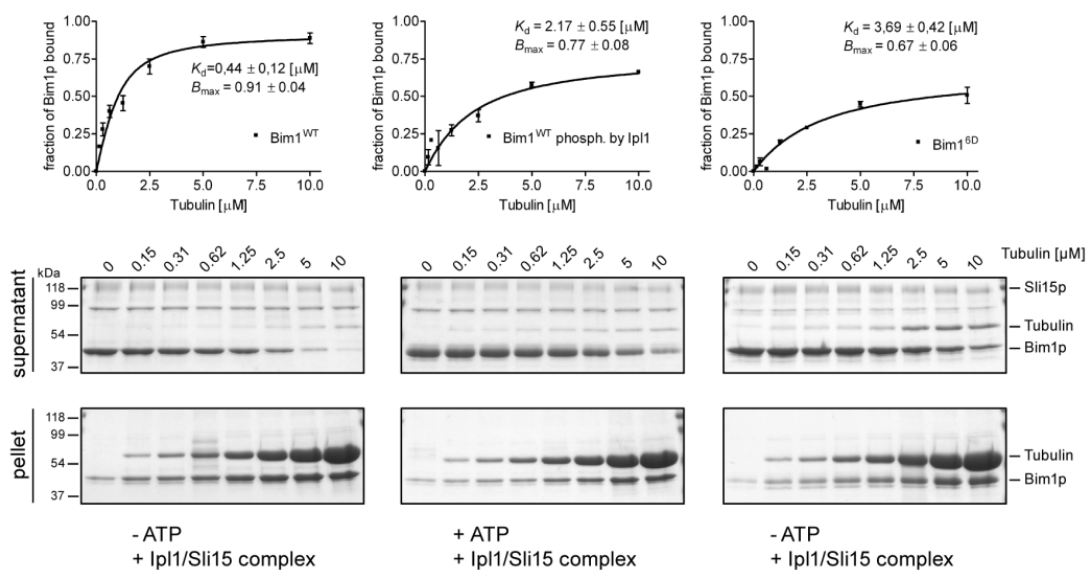
Figure 7.   **Multisite phosphorylation of Bim1p regulates its MT binding**

Equal amounts (1 μM) of Bim1^{WT}, Bim1p phosphorylated by Ipl1p-Sli15p and phospho-mimicking Bim1^{6D} were incubated with increased concentrations of taxol-stabilized microtubules (0-10 μM). Bim1p bound to MTs was separated from the unbound fraction by ultracentrifugation and the amounts of protein in supernatant and pellet were quantified from Coom-

masie stained gels. The binding affinity curves represent averaged data from three indepen-
dent experiments. Error bars represent SEM.

Wild type Bim1p binds microtubules with a relatively high affinity of 0.44 µM. In contrast, the multisite phosphorylation on the linker region decreases its affinity for taxol-stabilized MTs and the apparent K_d is raised about fivefold. The Bim1p variant that mimics constitutive Ipl1p phosphorylation (Bim1^{6D}) shows an even lower affinity for stabilized microtubules (Fig. 7).

To test whether phosphorylation of Bim1p is sufficient to remove it from stable microtu-bules, Bim1p was pre-bound to taxol-stabilized MTs and then incubated with increasing amounts of kinase complex in the presence or absence of ATP. The fraction bound to MTs was separated after centrifugation. Only in the presence of ATP Bim1p was significantly released from MTs showing that phosphorylation by Ipl1 is sufficient to remove Bim1p from stable micro-tubules (Fig. 8).
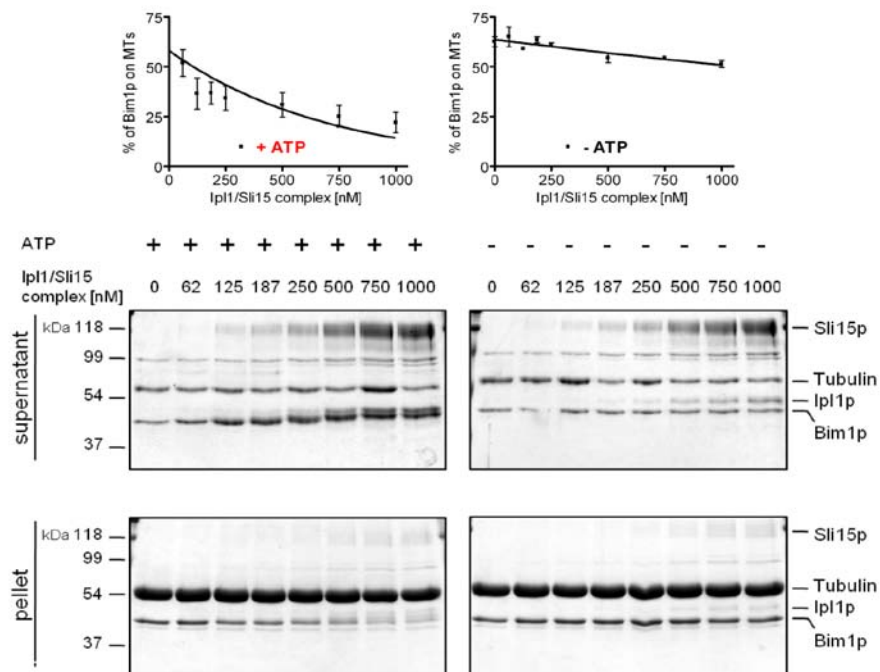
Figure 8.   Phosphorylation of Bim1p removes it from stable MTs

MTs (2.5 µM) were loaded with Bim1^{WT} and then incubated with increasing amounts of Ipl1p-Sli15p complex (0-1 µM) in the presence or absence of ATP. The fraction of Bim1p bound was analyzed by SDS-PAGE upon centrifugation and quantified. Release curves display the quantifications from two independent experiments. Error bars denote SEM.

5.1.4. Dissecting Bim1p microtubule binding activity

Previous studies have demonstrated that EB1-like proteins form dimers and the dimerization properties are required for efficient microtubule plus-end tracking in vivo (Slep and Vale, 2007). In order to determine the interface of Bim1p's microtubule binding activity, I first analyzed its hydrodynamic features to elicit its molecular organization. Bim1p indeed forms homodimers like other EB1 proteins as judged from its glycerol gradient sedimentation profile (Fig. 9).
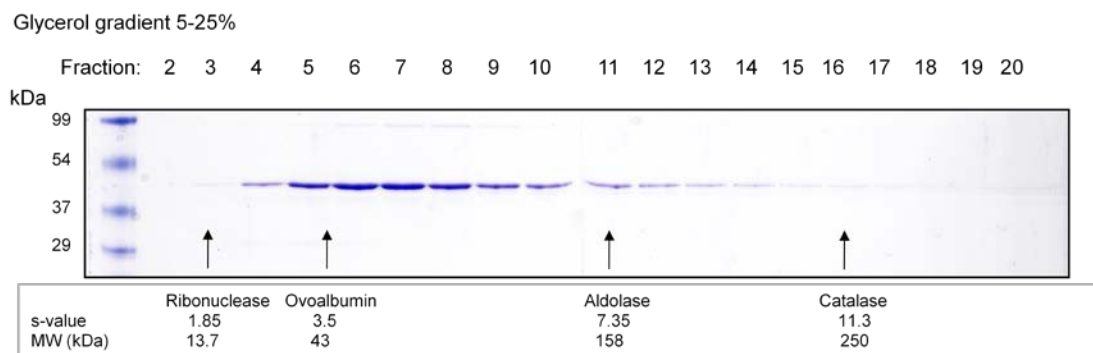
Figure 9. **Glycerol gradient sedimentation of Bim1p**

Bim1p was loaded on a 5-25% glycerol gradient and ultracentrifuged. Samples were collected from the top of the gradient and analyzed by SDS-PAGE. The position of the protein standards from a parallel experiment is marked. Bim1p sediments with an s-value of 4.12 and MW= 98 kDa.

The calculated molecular weight of Bim1p is 98 kDa, which is more than twice its theoretical MW (38 kDa). Despite its small size Bim1p elutes as a highly elongated molecule on analytical size exclusion chromatography with a Stokes radius of about 57 Å (Fig. 10).
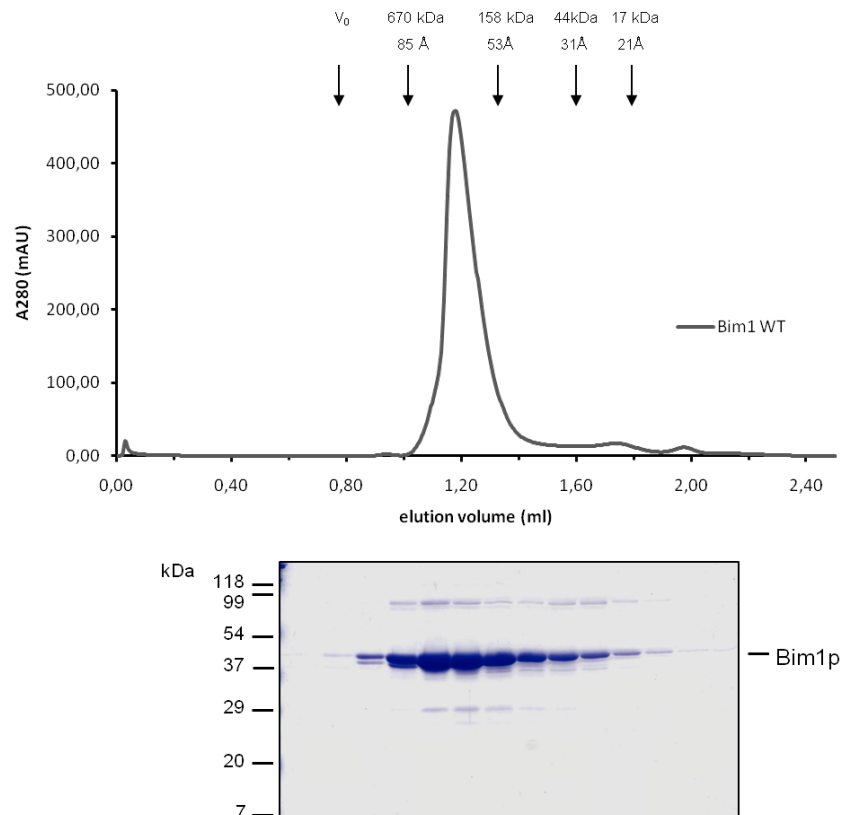
Figure 10. Size exclusion chromatography analysis of Bim1p

Bimp1 elutes from a Superdex 200 column as a highly elongated dimeric molecule with a Stokes radius of 57.4 Å

The molecular interface that underlies the MT binding activity of an EB1-like protein was previously assigned to its N-terminal calponin-homology (CH) domain (Hayashi and Ikura, 2003). However, the phosphorylation sites on Bim1p were found in the unstructured region, which is not part of the conserved CH domain at the N-terminus of the protein, yet they show the ability to decrease the affinity of Bim1p for MTs. To understand this intriguing finding I next studied the molecular requirements for Bim1p's microtubule association. To dissect the binding interface various C-terminally EGFP-tagged Bim1p truncations (variants lacking either calponin homology domain, linker region or dimerization region at the C-terminus as well their phospho-mutant derivatives) were expressed as recombinant proteins in *E. coli* (Fig. 11) and subjected to co-sedimentation assay with taxol-stabilized MTs.
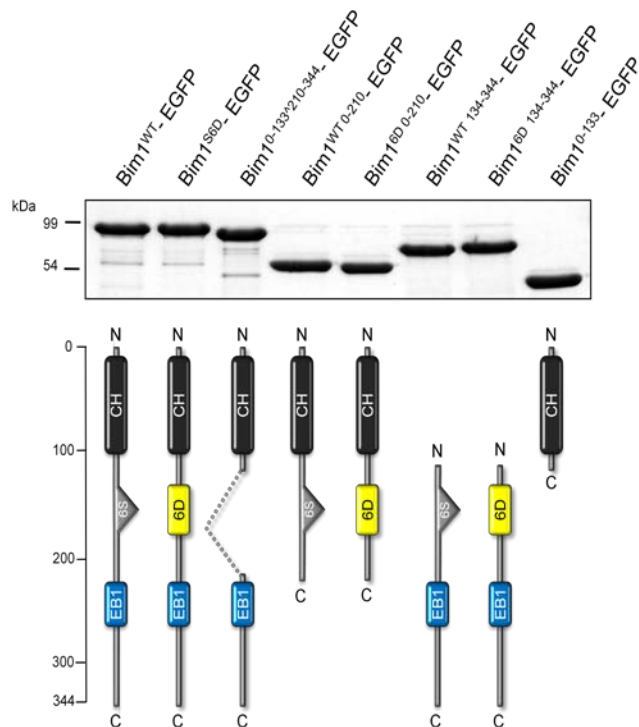
Figure 11. Bim1p variants used in MT-binding activity assay

Bim1p[WT], mutants lacking -CH, unstructured middle region, or C-terminal dimerization domain were expressed as EGFP fusion proteins in *E. coli*. Upper Coomassie-stained gel represents respective Bim1p variants.

As Bim1p forms homodimers I first investigated the microtubule binding properties of monomeric (lacking C-terminal domain) versus dimeric molecules (Fig. 12). Full-length dimeric Bim1p-EGFP (residues 1-344) binds to MTs with an apparent K_d of 0.2 µM. In contrast the monomeric CH domain alone (Bim1[1-133]) displayed a very low affinity for MTs (K_d= 8.9 µM), which was surprisingly raised upon addition of residues from the adjacent unstructured linker region to the molecule (Bim1[1-210]). The binding of the monomeric molecule (Bim1[1-210]) to MTs was significantly reduced compared to full-length Bim1p and the apparent dissociation constant of the monomeric form of Bim1p that mimics the Ipl1p phosphorylation raised the K_d even more from 3.5 to 4.8 µM.

Results

Figure with y-axis "fraction of Bim1 bound" (0.00 to 1.00) and x-axis "Tubulin [μM]" (0.0 to 10.0). Curves labeled:
- Bim1^{WT}- EGFP
- Bim1$^{WT\ 1-210}$- EGFP
- Bim1$^{6D\ 1-210}$- EGFP
- Bim1$^{1-133}$- EGFP

	Bim1^{WT}- EGFP	Bim1$^{WT\ 1-210}$- EGFP	Bim1$^{6D\ 1-210}$- EGFP	Bim1$^{1-133}$- EGFP
K_d	0.2 ± 0.02 μM	3.52 ± 1.48 μM	4.81 ± 2.4 μM	8.98 ± 4.19 μM
B_{max}	0.98 ± 0.01	0.59 ± 0.11	0.27 ± 0.06	0.24 ± 0.06
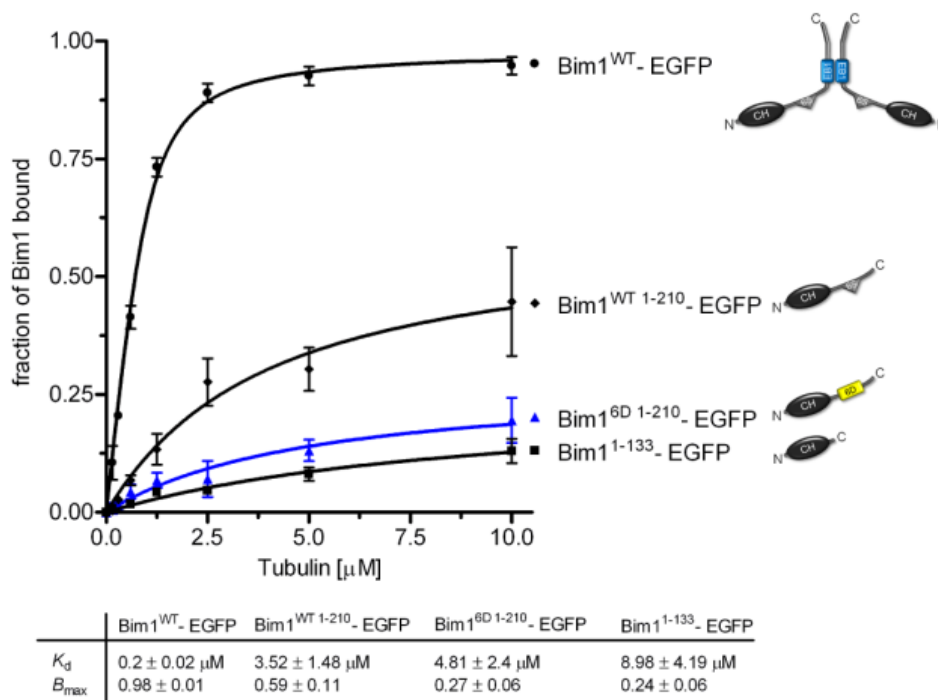
Figure 12.   Comparison of MT-binding activities of dimeric vs. monomeric Bim1p variants

Constant amount of the respective Bim1p construct (1 μM) was subjected to MT binding.
The fraction bound to MTs was separated by centrifugation and quantified fluorometrically.
The affinity binding curves represent averaged data from three independent experiments.

In order to determine the role of the linker region in MT-binding of Bim1p and in phospho-regulation of the molecule, the dimeric forms of Bim1p lacking the CH domain or the unstructured middle part were subjected to MT binding in the context of mutations mimicking Ipl1p-phosphorylation (Fig. 13).
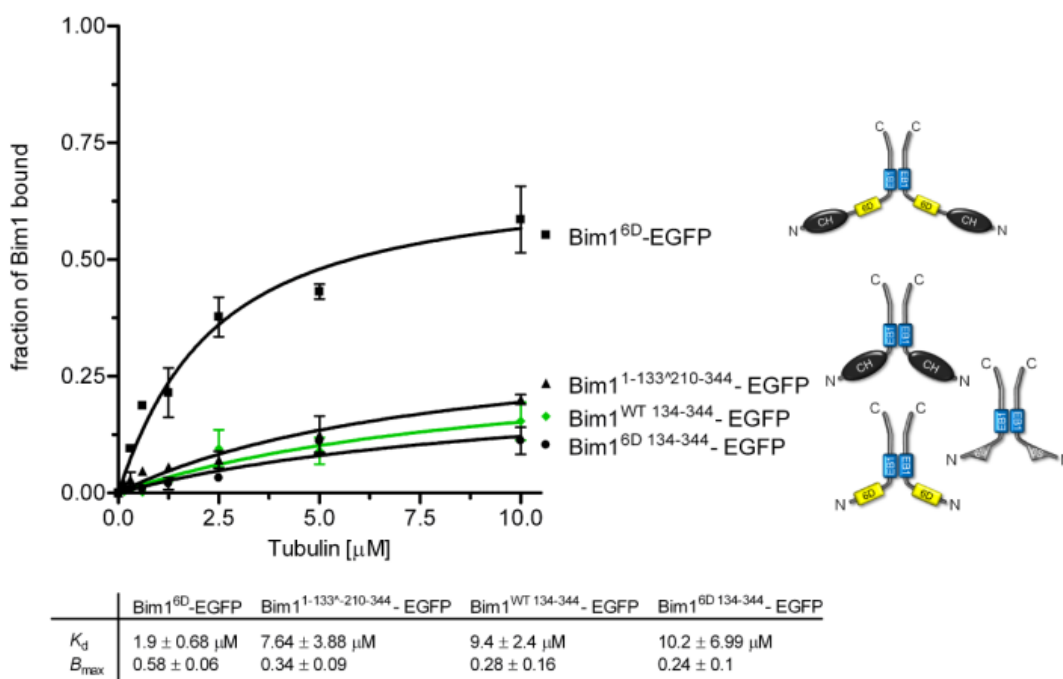
Figure 13.   Comparison of MT-binding activities of different dimeric Bim1 constructs

Constant amount of Bim1p construct (1 µM) was subjected to MTs binding. The fraction bound to MTs was separated by centrifugation and fluorometrically quantified. The affinity binding curves represent averaged data from three independent experiments.

K_d and B_{max} values of different variants are summarized in the table.

Surprisingly the weak association of a single N-terminal calponin homology domain to MTs was not enhanced upon direct fusion with the C-terminal coiled-coil dimerization domain (Bim1$^{1-133^210-344}$). Interestingly, the construct lacking both CH domains displayed an affinity for MTs that was as low as the variant missing the central linker region. The binding activity of the latter was even more reduced upon multisite phosphorylation by Ipl1p.

To further determine the role of dimerization and the function of the unstructured central part of Bim1p, different truncated Bim1p forms were tested for their effects on microtubule po-lymerization in a light-scattering assay (Fig. 14). The full-length Bim1p enhances tubulin self-assembly as previously reported for the EB1 protein (Vitre et al., 2008). Under the same experimental conditions, the Bim1 construct encompassing the CH domain alone was completely ineffective in promoting microtubule polymerization.

Results
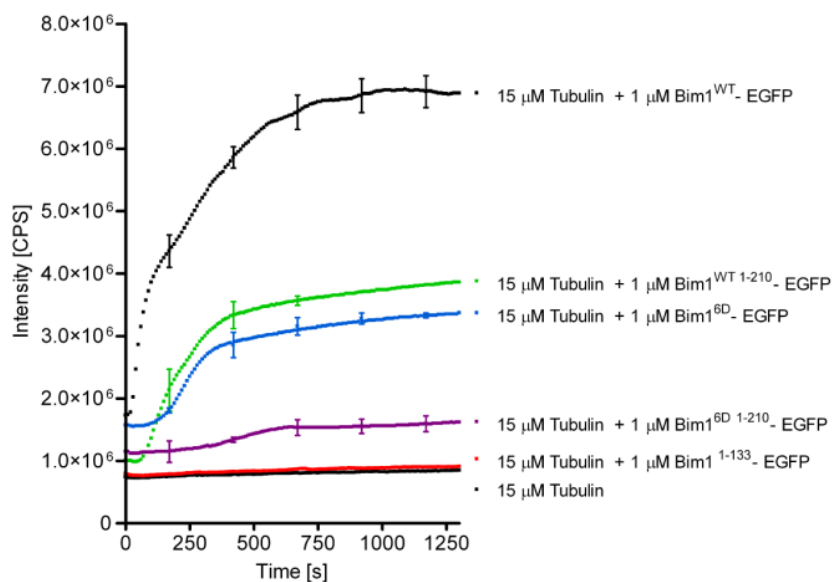
Figure 14. Light-scattering analysis of Bim1 promoted microtubule assembly
Constant amounts of different Bim1p variants were added to tubulin solution at 30°C and tubulin self-assembly was monitored spectrometrically at 350 nm.

The longer monomeric form showed improved but still significantly lower ability to stimulate MT assembly compared to the most effective dimeric full-length molecule. The Ipl1p phosphorylation reduced Bim1p stimulated polymerization in both the dimeric or monomeric form.

Taken together this demonstrates that the MT-binding activity of Bim1p depends on the dimerization properties of the EB1-like molecule and that the CH domains of Bim1p dimers are necessary but not sufficient for stable microtubule association. In contrast, the flexible linker region of Bim1p, acting synergistically with the CH domain is of critical importance for MT binding.

5.1.5. Reconstitution of Bim1p microtubule plus-end tracking in vitro

As mentioned previously in the paragraph 3.3.1, Bim1p like other members of the EB1-family exhibits a peculiar microtubule association in living cells. It specifically recognizes the dynamically growing plus-end of a MT. To study the function of Bim1p on dynamic microtubules and ask if this behavior requires any other molecules, I aimed to reconstitute Bim1p plus-end tracking in vitro. First, in microscopy flow cells, short, rodamine-labeled, biotinylated GMPCPP-MT seeds were adhered to the cover slip surface using biotin-avidin interactions (Fig. 15)
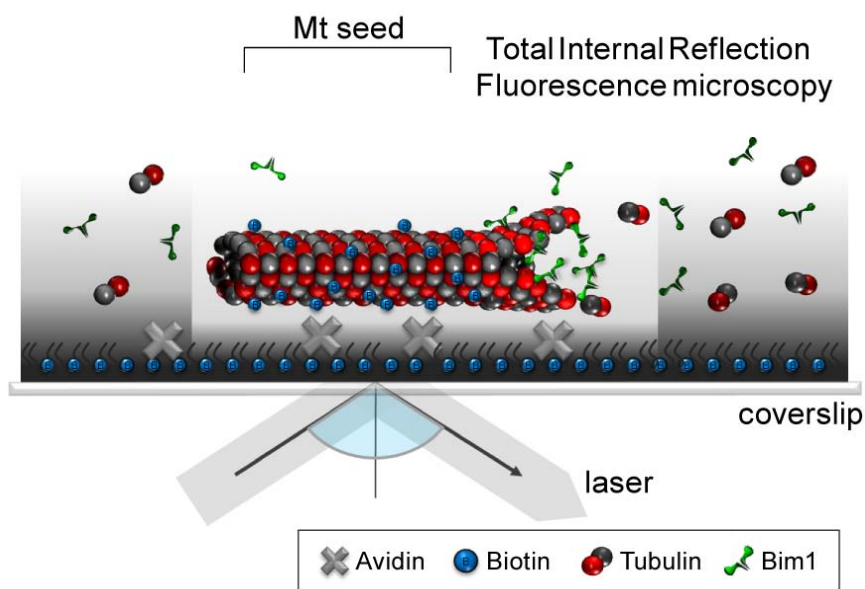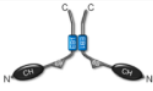
Figure 15.   Experimental setup for TIRF microscopy

Cells pre-equalibrated with assay buffer were next filled with free, dimly labeled rhodamine-tubulin (15 µM) to promote microtubule growth in the presence of fluorescent Bim1p-EGFP variants. Microtubule dynamic instability was visualized at 30°C using total internal reflection microscopy in order to eliminate background fluorescence. The plus-end tracking assay was then used to analyze the molecular requirements for autonomous plus-end association (Tab. 1). First, the full-length protein (70 nM) was tested and two-color time lapse imaging revealed preferential accumulation at MT ends during phases of growth but the protein was rapidly lost during MT disassembly. Despite prominent plus-end binding the full-length protein demonstrated also weak lattice association that was ionic-strength and protein concentration dependent (Fig. 16A)

Results

Table 1. Summary of the abilities for plus-end tracking or lattice association of different Bim1p constructs

Bim1p construct [aa]	MT plus-end tracking	Lattice association
1-344 WT	+	+
1-210	−	+
1-133	−	−
1-133^210-344	−	−

Next the monomeric construct lacking the C-terminal EB1-like domain (Bim1$^{1-210}$) was tested for its microtubule association. The plus-end association of this variant was not detectable under conditions in which full-length Bim1p showed prominent tracking, and did not change upon raising the concentration of the protein in assay to 1 µM. Only weak lattice association was still detectable (Fig. 16). The construct encompassing the CH domain alone or the CH domain directly fused to the dimerization domain did not display tip-tracking activity or lattice association (Tab. 1).

A

Microtubule growth   Bim1 plus-end tracking

⊖ seed ⟶ ⊕

Time

120 s
4 µm

■ microtubule   ■ Bim1^{EGFP} Merge

B

Microtubule growth

⊖ seed ⟶ ⊕

Time

120 s

4 μm

■ microtubule   ■ Bim1 1-210 EGFP   Merge
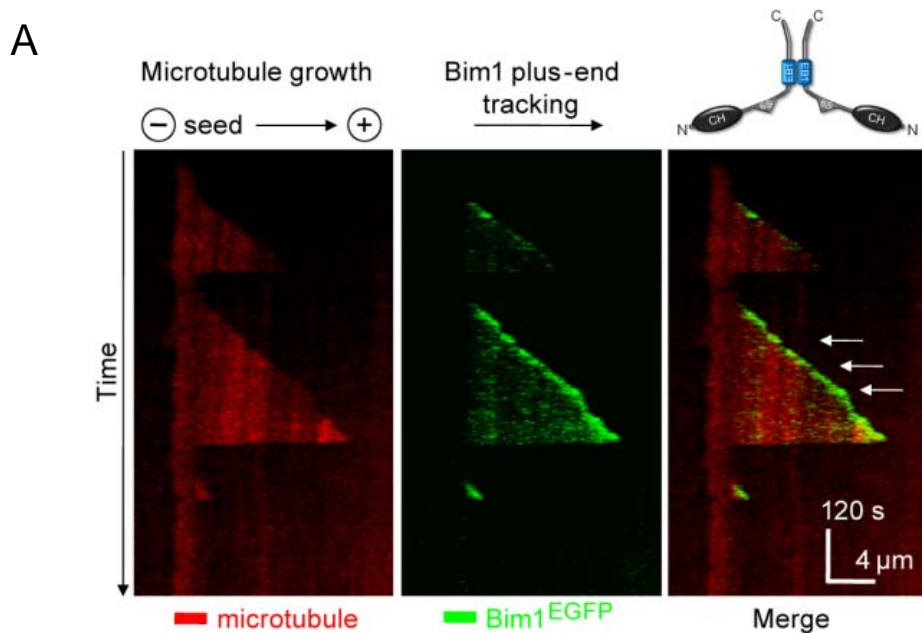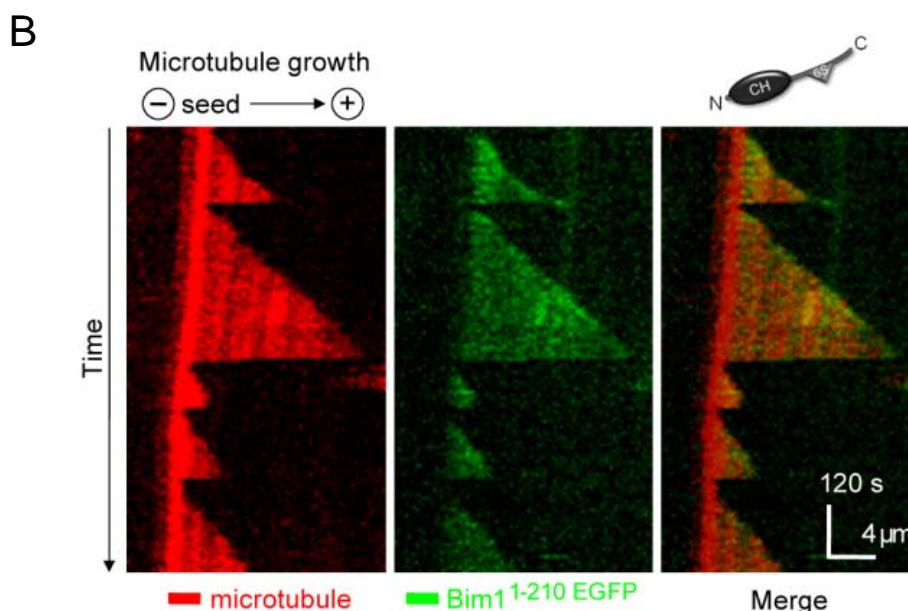
Figure 16. **Reconstitution of Bim1p microtubule plus-end tracking**

(A) Full-length Bim1p-EGFP autonomously tracks growing microtubules in vitro. TIRF micro-
scopy demonstrates tip-tracking activity of Bim1p (70 nM).

(B) A monomeric variant of Bim1$^{1-210}$ (1 μM) fails to accumulate at growing ends and weakly
associates with the lattice of dynamic microtubules. Bar, 5 μm,

Collectively, the tip-tracking abilities of Bim1p depend on a proper spatial orientation of
two CH domains in one dimeric molecule. Furthermore, it seemed that the presence of the un-
structured linker region modulates the general microtubule binding activity of Bim1p and as well
affects its tip tracking. To study the effects of the Ipl1p phosphorylation on that region in regula-
tion of Bim1p binding to dynamic microtubules, the tip-tracking assay was used as described
above. In the flow chamber, in addition to Bim1p and rhodamine-tubuline, the Ipl1p kinase com-
plex was supplemented together with ATP. Upon initial tip tracking behavior, in the experiments
in the presence of ATP and Ip1p-Sli15p, the signal of Bim1p on MT plus-ends quickly disap-
peared. This was not the case in control assays lacking either ATP or kinase complex in the
reaction. This demonstrates that linker phosphorylation is sufficient to remove Bim1p from dy-
namic microtubules (Fig. 17).
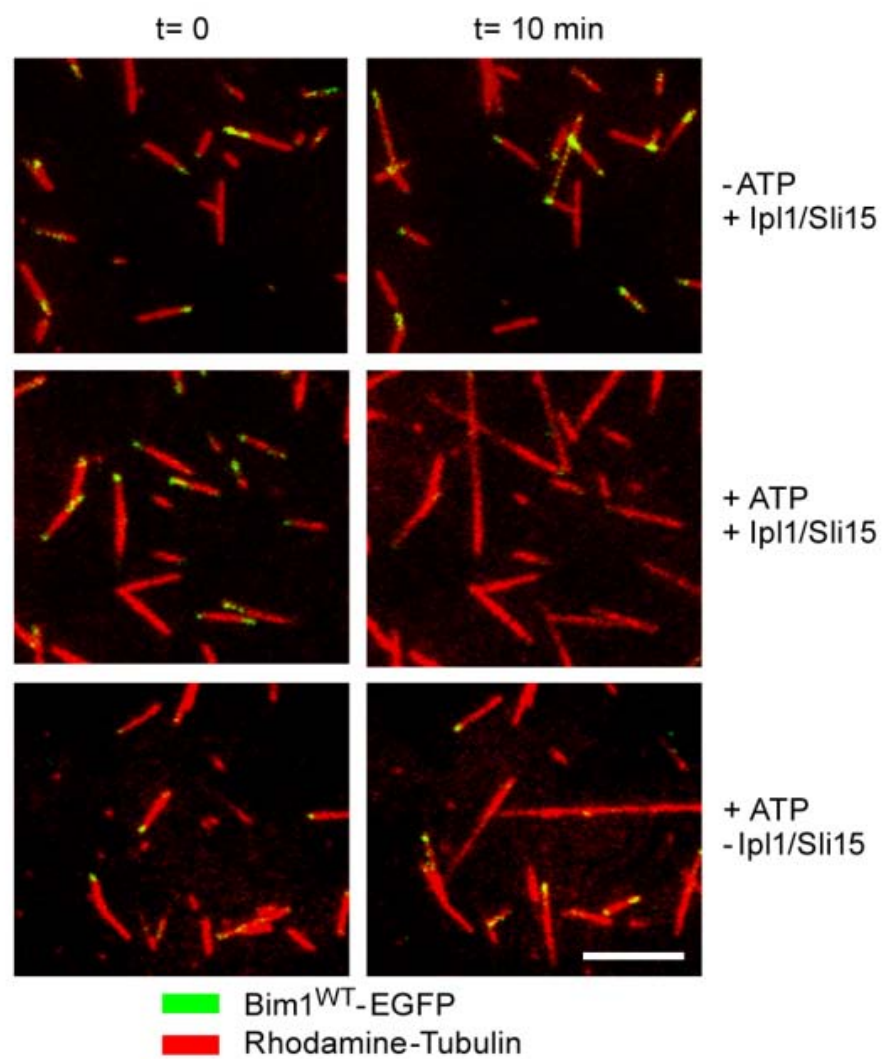
Figure 17. Bim1p phosphorylation removes it from dynamic microtubules in vitro

In the presence of the Ipl1p-Sli15p complex and ATP the signal of Bim1p on growing microtubules decreases, suggesting that phosphorylation inhibits binding of Bim1p to the dynamically growing MT tips. Bar, 5 µM.

5.1.6. Effects of phosphorylation on Bim1p function in vivo

In budding yeast cells, Bim1p preferentially accumulates at tips of astral and kinetochore microtubules and additionally it associates with the interpolar MTs of the anaphase spindle. The phosphorylation of the protein as described above occurs prominently in anaphase (Fig. 6); therefore to reveal its function, I first studied the effects of Bim1p phosphorylation on spindle elongation kinetics. Using time-lapse live cell microscopy, microtubules were visualized by expressing GFP-tubulin in a strain with either Bim1p wild-type, the 6A mutant to prevent phosphorylation (Bim1^{6A}) or the phospho-mimicking form- Bim1^{6D}. Spindle dynamics was compared to a strain with a deletion of *BIM1* that, as previously described, shows impaired microtubule dynamics in cells (Tirnauer et al., 1999). The elongation of the spindle in wild-type cells occurs with typical biphasic kinetics consisting of a fast initial phase and subsequent slower phase of final growth (Fig. 18)
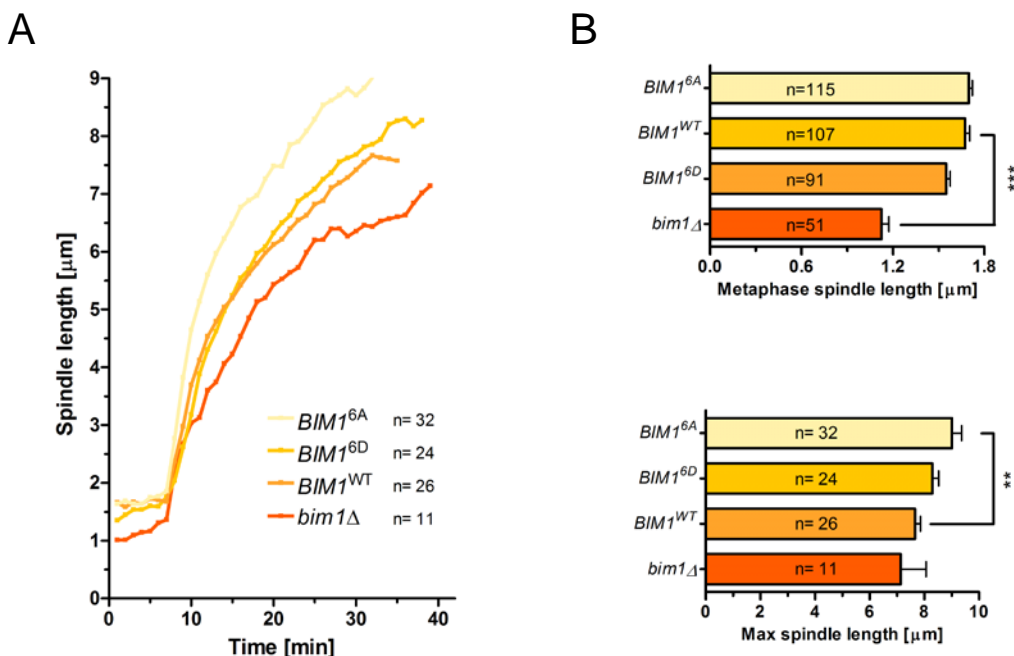
Figure 18. Anaphase spindle elongation kinetics in different *bim1* mutant backgrounds

Cells were arrested at G1 stage with α-factor, released and visualized every minute by time-lapse microscopy.

(A) Averaged kinetics of anaphase spindle growth quantified from GFP-tubulin live cell imaging recorded in *BIM1*^{WT}, *bim1*^{6A}, *bim1*^{6D}, and Δ*bim1* cells.

(B) Maximal metaphase and anaphase B spindle length quantified from cells expressing different Bim1p variants

Results

In contrast, the elongation rate of the spindle in Δ*bim1* cells was reduced and the spindle length in metaphase was decreased by 50%. The elongation speed of the spindle in the Bim1^{6A} mutant, which fails to be phosphorylated by Ipl1p, was significantly enhanced and the spindle reached an increased final length compared to wild-type cells. The behavior of the phospho-mimicking mutant resembled the kinetics of the Bim1^{WT} cells. This suggests that Bim1p phosphorylation is necessary for the normal kinetics of anaphase spindle elongation. Interestingly, even though the spindle overextended, the averaged duration of anaphase B was shorter when Bim1p was compromised in the Ipl1p phosphorylation and significantly longer in case of *bim1* deletion or phospho-mimicking mutant (Fig. 19).
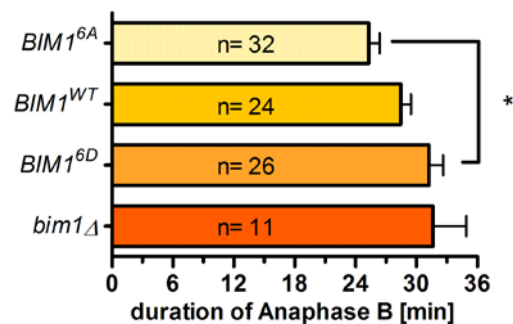
Figure 19. **Averaged duration of anaphase B in different *bim1* backgrounds**
Measurements of anaphase B duration from the beginning of spindle elongation to spindle break down in cells expressing GFP-*TUB1*, in α-factor arrest/release experiment.

To test if the observed effects on spindle dynamics were due to altered Bim1p localization on microtubules, cells expressing a sole copy of GFP-tagged *bim1* phosphomutants were fixed and visualized using fluorescent microscopy (Fig. 20). Despite similar expression levels, as judged from WB α-GFP analysis, Bim1^{6D} showed a significant reduction of the signal on the spindle compared to Bim1^{WT} or Bim1^{6A} mutant. Interestingly, the signal of GFP-tagged Ipl1p was very similar to that observed for Bim1^{WT} suggesting that the co-localization might be due to direct Ipl1p-Bim1p interaction (Fig. 20).

A

Bim1^{WT}-3xGFP   Bim1^{6A}-3xGFP   Bim1^{6D}-3xGFP   Ipl1-3xGFP
DNA
Cell outline
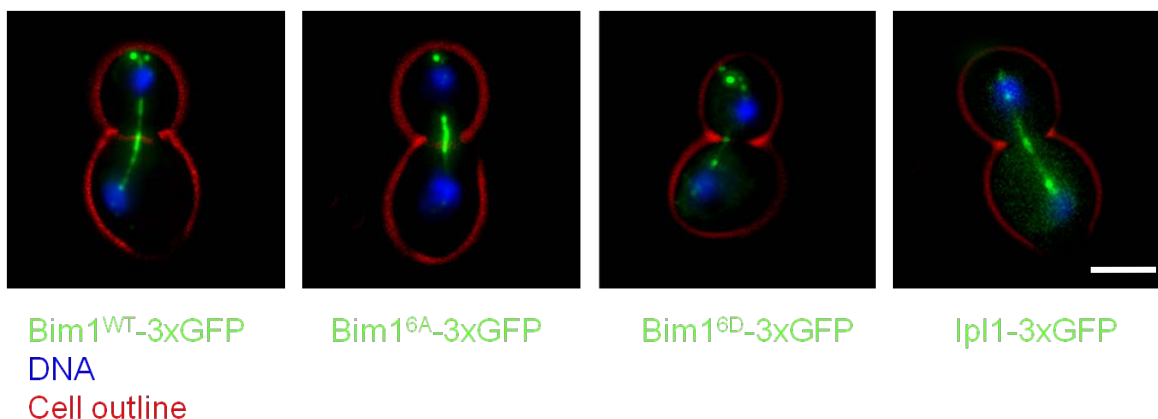
B
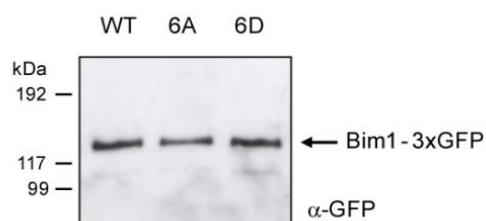
Figure 20. Comparison of Bim1p-3xGFP phospho-mutants and Ipl1p on anaphase spindle

       (A) Triple GFP tagged Bim1p variants integrated into strain with Δ*bim1* or Ipl1p-3xGFP in *BIM1*^{WT} cells were fixed with p-formaldehyde and visualized together with DAPI stain. Fluorescence images were merged with bright field pictures to indicate the outline of the cell. Bar, 3 μm.

       (B) Western-blot analysis of Bim1p expression levels of the indicated mutants.

In order to directly visualize the effects of Ipl1p phosphorylation on Bim1p interaction with the anaphase spindle, triple GFP-tagged Bim1p was visualized by live cell microscopy together with microtubules labeled by expression of mCherry-tubulin. Time lapse imaging of anaphase spindles showed that after an initial prominent localization to the spindle midzone, the length of the Bim1^{WT} signal gradually decreased as the cells progressed towards the end of anaphase. In contrast, the Bim1p phospho-deficient mutant Bim1^{6A} stayed much longer on the spindle without significant unloading and remained on the disassembling half-spindles (Fig. 21)

Results
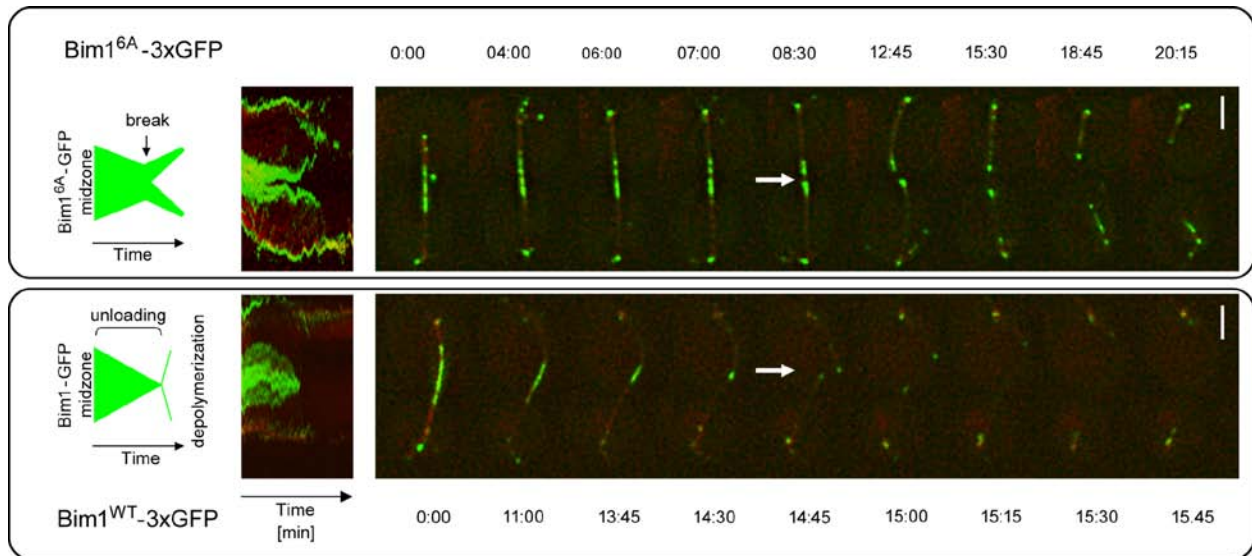
Figure 21. Different localization behavior of Bim1p during anaphase progression

Bim1[6A]-3xGFP and Bim1[WT]-3xGFP were visualized by live cell microscopy in strains expressing mCherry-*TUB1*. The individual frames form the movies are plotted as kymographs. Arrows show moment of the spindle separation. Bars, 3 µm.

Time lapse microscopy of the Bim1[6A] mutant, has shown that in some extreme cases the spindle had even more severe problems in proper disassembly, as instead of depolymerizing the spindle started to grow again (Fig. 22).
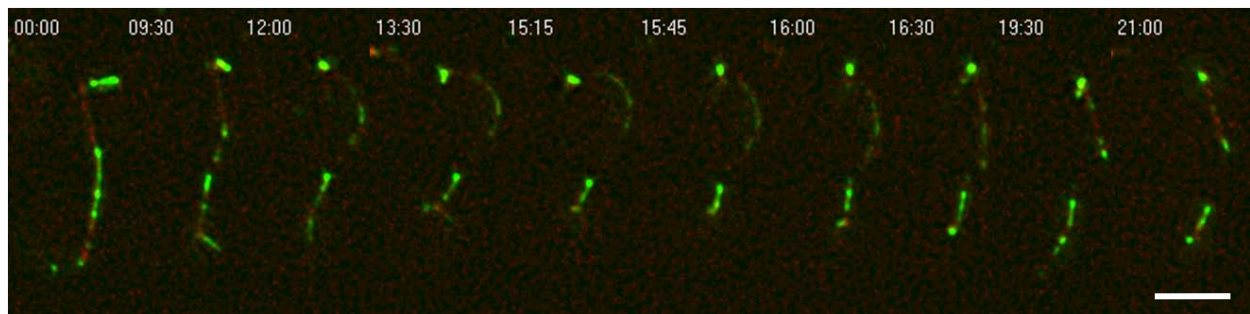
Figure 22. Bim1[6A] mutant shows aberrant spindle behavior

Bim1[6A]-3xGFP on anaphase spindle was visualized by live cell microscopy in strains expressing mCherry-tubulin. Bar, 3 µm

In spite of this abnormal spindle disassembly, all Bim1[6A] cells are able to progress into telophase, and do so with even faster kinetics than wild-type. These results suggest that phosphorylation of Bim1p plays an important role in proper spindle disassembly but there are additional Ipl1p-dependent mechanisms involved (e.g. by controlling the microtubule plus-end specific depolymerase Kip3p) as well as Ipl1p-independent mechanisms such as the degradation of spindle stabilizers like Ase1p prior telophase (Juang et al., 1997).

5.2. Functional analysis of the Bim1p-Ipl1p interaction

The results in previous paragraphs have demonstrated that Bim1p is phospho-regulated by the Aurora/Ipl1p kinase. Fluorescence microscopy has shown that both proteins co-localize at the anaphase spindle and likely interact with each other. To ask whether apart from a kinase-substrate relationship, the interaction between the plus-end tracker Bim1p and the kinase Ipl1p is also important in another context, I performed detailed functional analyses of the binding interface between these two proteins.

5.2.1. Size exclusion chromatography analysis of Bim1p-Ipl1p complex

The initial experiments have shown that binding of the kinase Ipl1p to Bim1p was stronger than a typical kinase-substrate interaction. Bim1p and Ipl1p form a stable complex which is strong enough to be detected by gel filtration in buffers with ionic strength of 100-150 mM KCl (Fig. 23).
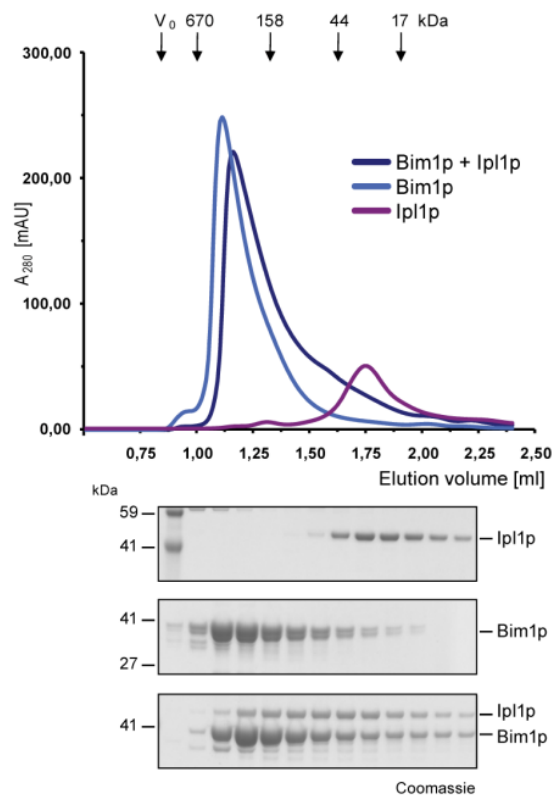
Figure 23. Bim1p forms a complex with Ipl1p

Analytical size exclusion chromatography of the Bim1p-Ipl1p complex. Proteins were diluted into the same buffer and loaded on a Superdex 200 column. Samples were analyzed by SDS-PAGE and Coomassie staining.

Interestingly, upon binding to the kinase the elution profile of Bim1p shifts towards a smaller stokes radius suggesting that interaction with Ipl1p stabilized a more compact conformational state of the Bim1p molecule. The phosphorylation state of Bim1p did not have an influence on the binding of the Ipl1p kinase as analyzed by a GST-pull down assay (Fig. 24). The phospho-mimicking Bim1[6D] mutant could bind as efficiently to the kinase as the wild-type form.
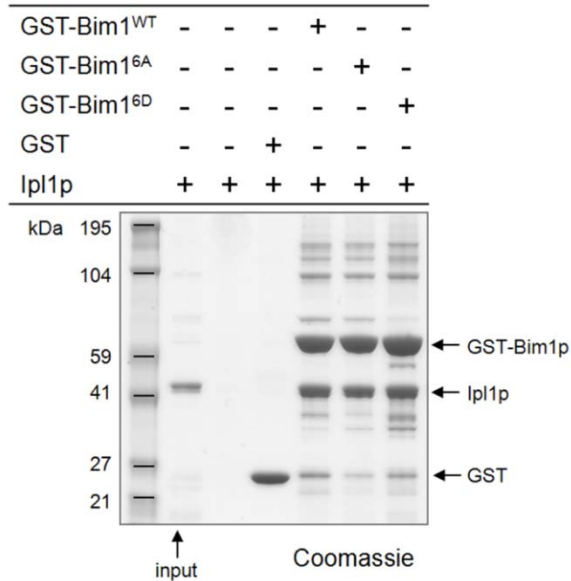
Figure 24. Effects of Bim1p phosphorylation state on binding to the Ipl1p kinase
Recombinant Bim1p, N-terminally fused to GST can efficiently pull-down 6xHis-tagged Ipl1p kinase independently of its phosphorylation state.

Results

5.2.2. The C-terminal region of Bim1p mediates its binding to Aurora kinase

Because of the direct interaction between Ipl1p kinase and Bim1p, I next tried to determine the molecular interface that mediates this interaction. Truncated versions of Bim1p were expressed recombinantly as N-terminal fusions with GST. The Bim1p variants were next used in GST-pull down assays with full-length 6xHis-tagged Ipl1p. The minimal construct that could bind the kinase was the C-terminal coiled-coil domain encompassing residues 185-344, lacking the region of Ipl1p phosphorylation. Interestingly the same fragment of Bim1p mediates interactions between Bim1p and Ipl1p in complex with its activator Sli15p (Fig 25). The residues mediating Bim1p-kinase interactions were further narrowed to the region 197-283 aa of Bim1p (Section 5.2.5.)
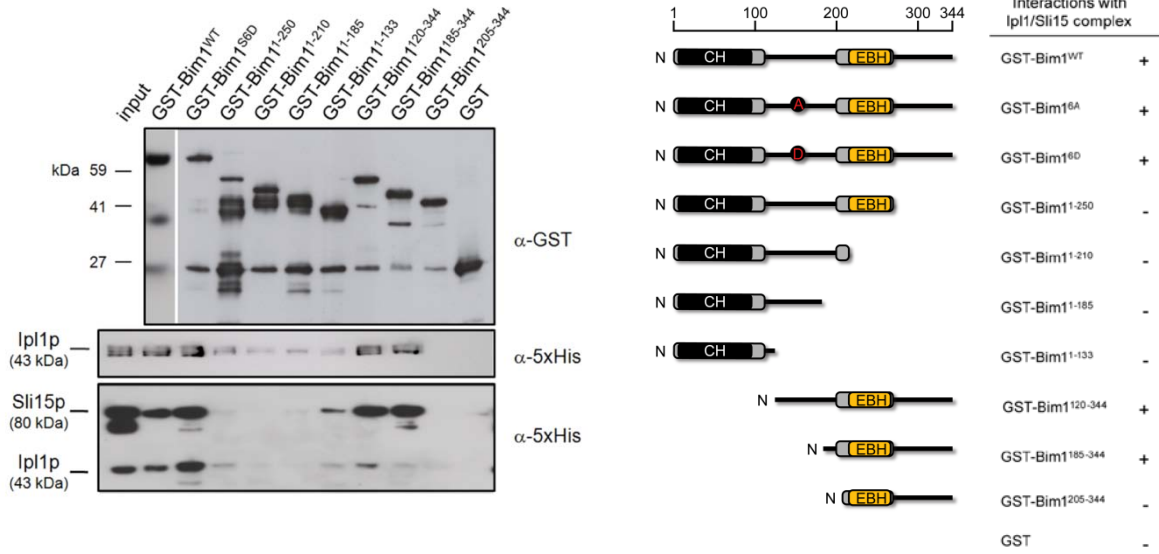
Figure 25.   Mapping the region of Bim1p mediating interaction with the Ipl1 kinase

Series of GST-truncations of Bim1 were expressed in *E.coli* and subjected for Ipl1p binding. The minimal interacting region encompasses residues 185-344 of Bim1p.

5.2.3. Bim1p can be phosphorylated without strongly binding Ipl1p kinase

To test if the mapped C-terminal domain, which is responsible for the interaction with Ipl1p, contributes also to the efficiency of Bim1p phosphorylation, Bim1p truncations missing the C-terminus or N-terminal CH-domain were in vitro phosphorylated by Ipl1p/Sli15p complex and the reaction analyzed by autoradiography. Interestingly, Bim1p lacking the Ipl1p-binding domain (Bim1p$^{1-210}$), could still be efficiently phosphorylated by the kinase. The amount of incorporated [P^{32}] phosphate was slightly lower compared to the construct lacking only the N-terminal CH-domains (Bim1p$^{134-344}$) indicating that this part enhances phosphorylation but is not necessary (Fig. 26). The specificity of reaction was confirmed by using Bim1p variants in which the Ipl1p sites were mutated (Bim1p $^{6D\ 134-344}$). Taken together this suggests that the kinase-substrate relationship does not require strong interaction of Ipl1p with the cargo-binding domain of Bim1p.
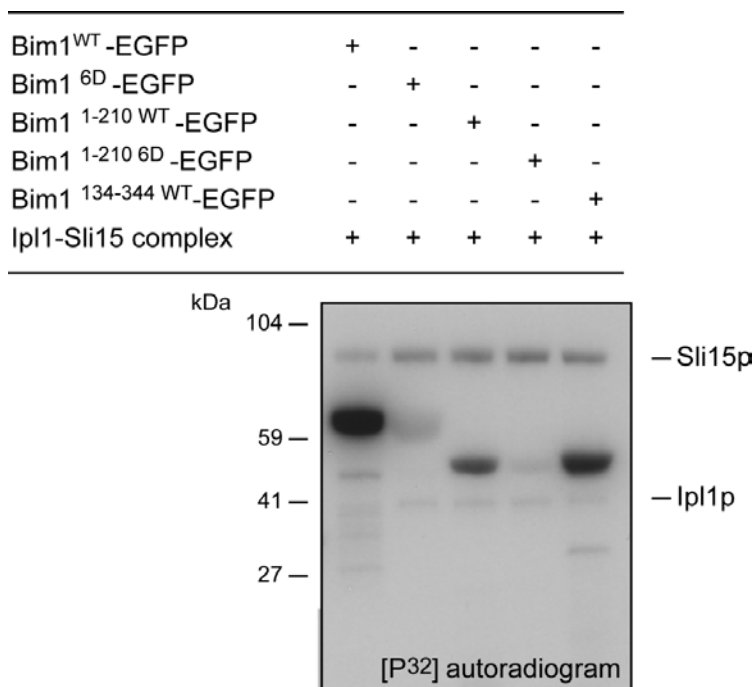
Figure 26. Ipl1p can phosphorylate Bim1p even in the absence of its cargo-binding domain
Indicated Bim1p-EGFP variants were phosphorylated in vitro with purified recombinant Ipl1p-Sli15p complex. Samples were next separated by SDS-PAGE and analyzed by autoradiography.

Results

5.2.4. Ipl1p kinase interacts with Bim1p via its N-terminal region

To study structural requirements for Ipl1p binding to Bim1p, several truncations of 6xHis-tagged Ipl1p were purified as recombinant proteins and used in pull-down assays with full-length GST-Bim1p. Sequence analysis of Ipl1p showed in addition to the conserved Serine/Threonine protein kinase catalytic domain, the presence of an N-terminal region of predicted unstructured nature. Elimination of this region in pull-down assay resulted in impaired binding of remaining kinase domain to the yeast EB1 homolog (Fig. 27).
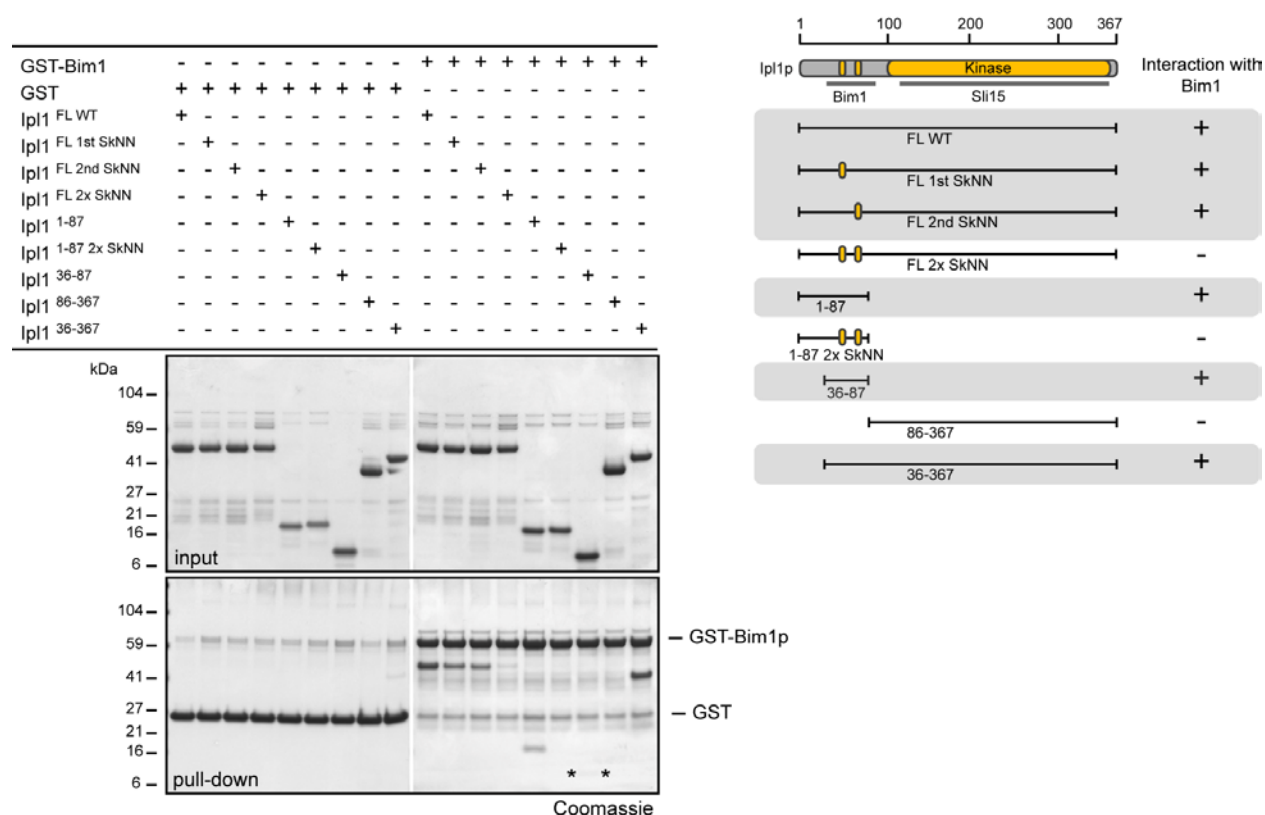
Figure 27. Mapping the region of Ipl1 mediating its interactions with Bim1p

Various 6xHis-tagged Ipl1 mutants lacking N-terminal residues, the kinase domain or with SkIP motif mutations were expressed as a recombinant proteins in *E. coli* and subjected for binding with the full-length GST-Bim1p. Asterisks indicate the minimal Ipl1 fragment (residues 36-87) that bind Bim1p.

In contrast the N-terminal region alone was sufficient to bind to Bim1p. Interestingly, the region contains two short SxIP sequences (residues 46-49 and 72-75) which were recently proposed to act as plus-tip localization signals by providing a minimal binding motif of many EB1

interacting proteins. (Honnappa et al., 2009). Elimination of either of the two SkIP motifs individually by mutating the residues to alanines or to asparagines (1x SkAA or 1x SkNN) did not inhibit binding of Ipl1p to Bim1p. Interestingly, however, upon alteration of both SkIP motifs (2x SkNN) Ipl1p could not bind to Bim1p in the pull-down assay. The minimal fragment of the kinase that exhibited Bim1p-binding activity encompassed two SkIP motifs on the Ipl1p N-terminus between residues 36-87. Taken together this demonstrates that Ipl1p kinase associates with Bim1p via two redundant SkIP motifs in its N-terminal domain.

5.2.5. Analysis of Bim1p-Ipl1p interaction by isothermal titration calorimetry

In order to determine the molar stoichiometry as well as the dissociation constant of the Bim1p-Ipl1p complex, the cargo-binding domain of Bim1p (residues 197-283) was titrated calorimetrically with the Ipl1p minimal interacting domain (residues 36-87). This analysis demonstrated that one dimer of Bim1p binds 2 molecules of the Ipl1p kinase with a dissociation constant of 2.5 µM, thus forming a ternary complex (Fig. 28). As expected, an Ipl1p construct with mutations in both SkIP EB1-interaction motifs, showed a significant decrease in binding to a Bim1p dimer.
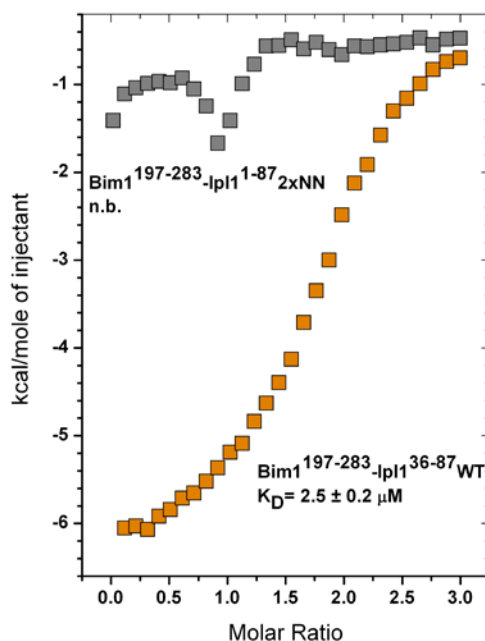
Figure 28.   Isothermal titration calorimetry analysis of Bim1-Ipl1 complex

10 µM of Bim1p (residues 197-283) was titrated with 0.1 mM Ipl1p variant and dissociation constant from was estimated from non-linear curve fitting.

Results

5.3. The role of Bim1p-mediated regulation on Ipl1p function

5.3.1. Genetic evidence for a role of Bim1p in Ipl1 kinase function

In order to study the role of Bim1p in Ipl1p kinase function in vivo, temperature sensitive alleles of *IPL1* and its activator *SLI15* were crossed to a conditional allele of *BIM1* created by placing the *BIM1* gene under the control of the *GAL1* promoter. This allows regulation of its expression depending on the carbon source in the medium. The *ipl1-2* or *sli15-3* alleles display reduced kinase activity even at the permissive temperature (Kim et al., 1999) and I found that both of these mutants depend on *BIM1* expression for viability at 25°C, suggesting an important role of Bim1p in the Ipl1 kinase function in vivo (Fig. 29).

Figure 29. *ipl1-2* and *sli15-3* mutants depend on *BIM1* for viability

Serial dilutions of indicated strains were spotted on plates containing raffinose/galactose in order to switch on expression of Bim1p, or on glucose containing medium to repress its expression at 25°C.

5.3.2. *bim1*[6A] overexperssion partially suppresses *ipl1-2* temperature sensitivity

Because deletion of *BIM1* gene causes lethality in strains compromised for Ipl1p kinase function in vivo, I next tested the effect of *BIM1* overexpression in the kinase mutant background. Yeast cells containing *IPL1*[WT] or the *ipl1-2* allele in the background of *BIM1*[WT] were transformed with 2µ ARS plasmids for *GAL1*-driven overexpression of Bim1 phospho-mutants. In the strains containing the wild-type copy of the *IPL1* gene, overexpression of *BIM1*[WT] did not affect growth at any temperature from the range 25-37°C tested, in contrast to growth defects shown in a previous study (Schwartz et al., 1997). However, overexpression of the phospho-deficient *bim1*[6A] mutant compromised strain growth at all temperatures tested. Interestingly, overexpression of *bim1*[6A] in the *ipl1-2* background partially suppresses the temperature sensitivity at 34°C (Fig. 30).
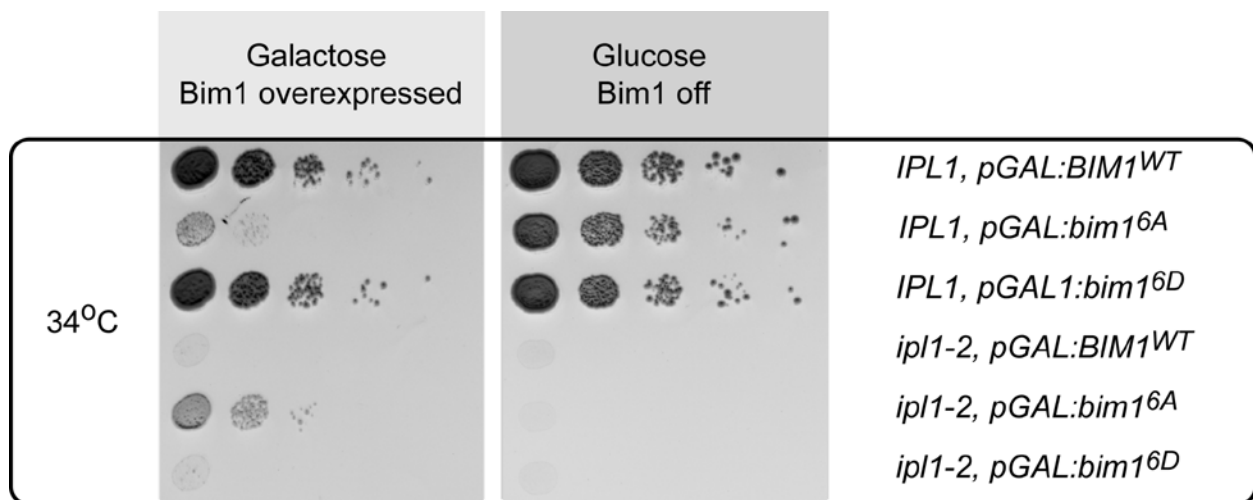
Figure 30.   The effect of Bim1 overexpression on the Ipl1 kinase function in vivo
Serial dilutions of indicated strains were spotted on galactose medium to overexpess or glucose medium to repress expression of Bim1 variants. Overexpression of Bim1[6A] is lethal in a wild-type background but can suppress *ipl1-2* temperature sensitivity at 34°C.

Results

To further investigate the role of Bim1p phosphorylation on Ipl1p kinase function in vivo, the *ipl1-2* allele was crossed to strains containing *bim1* phospho-mutants, expressed from the native promoter of the *BIM1* gene. Under these conditions expression of *bim1*[6A] did not affect cell viability at any tested temperature (25-37°C), but interestingly the combination of a kinase compromised allele with the phospho-mimicking *bim1*[6D] mutant increased its temperature sensitivity from 34 to 30°C (Fig. 31). This together indicates that Bim1p alone and its phosphorylation status are important for the Ipl1p kinase function in vivo.
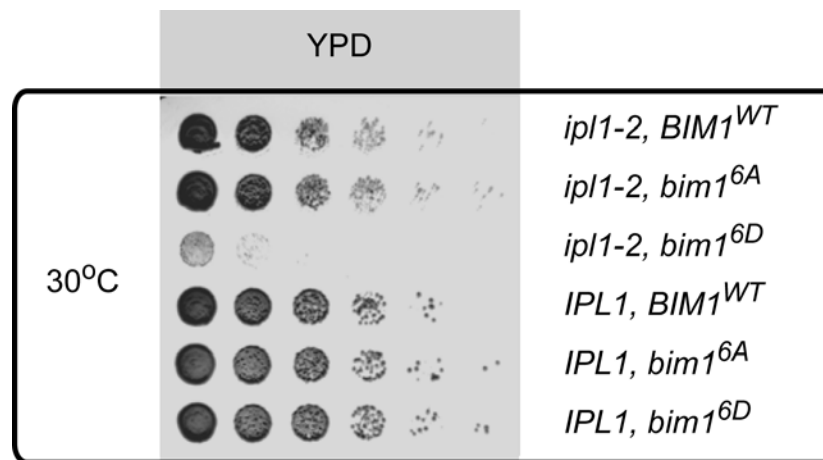
Figure 31.   A phospho-mimicking *bim1*[6D] mutant decreases *ipl1-2* restrictive temperature

Serial dilutions of indicated strains were spotted on rich glucose-containing medium at 30°C.

5.3.3. Bim1p targets Ipl1p to microtubules in vitro

While Ipl1p has been found to bind to microtubules in vitro (Kang et al., 2001), one possible role of a Bim1p-Ipl1p interaction could be to enhance the association of the kinase with microtubules. To test this, the microtubule binding properties of the kinase alone were studied first. Ipl1p co-sediments weakly with taxol-stabilizied MTs (Fig. 32), with an apparent dissociation constant of K_d=2.2 µM. Interestingly, when it was pre-incubated with Bim1p the affinity of Ipl1p raised 14-fold to an apparent dissociation constant similar to that of Bim1p alone (see paragraph 5.1.3.). This suggests a possible role for Bim1p in regulating Ipl1p localization on microtubules.

	Ipl1-EGFP	Ipl1- EGFP + Bim1[WT]
K_d	2.28 ± 0.63 µM	0.16 ± 0.07 µM
B_{max}	0.63 ± 0.06	0.78 ± 0.04
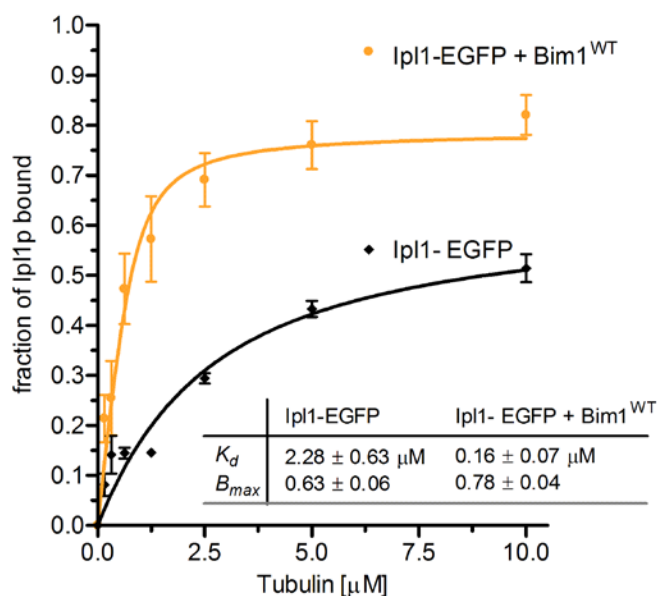
Figure 32. **Bim1p mediates Ipl1p association with stable microtubules**

Equal amounts of Ipl1-EGFP (1 µM) were incubated with increasing amounts of taxol-stabilized microtubules (1-10 µM) and the fraction bound to MTs after centrifugation was quantified fluorometrically. Affinity binding curves represent averaged data from three independent experiments. Error bars represent SEM.

Results

5.4. Probing Bim1p-Sli15p interactions

5.4.1. Mapping the domain mediating binding of Sli15p to Bim1p

Initial experiments have shown that Bim1p can associate not only with the kinase alone but also with its activator Sli15p separately or together with the Ipl1p-Sli15p complex. In addition two-hybrid interactions have been reported not only between Bim1p and Ipl1p, but also between Bim1p and Sli15p (Wong et al., 2007). To define the molecular interface of these activities, I first decided to perform a sequence survey to search for EB-targeting motifs in Sli15p that could be responsible in mediating the Bim1p interaction. I found that Sli15p contains two SxIP-like motifs (residues 305-306 and 382-385) without any other known EB-interacting interfaces such as CAP-Gly domains. Due to the larger size and lack of defined protein domains of Sli15p, three similarly sized truncations were expressed in *E. coli* as 6xHis-tagged proteins and first subjected to binding with full-length GST-Bim1p (Fig. 33). Only the central part of the Sli15 molecule showed significant binding activity. It contains two putative EB1 targeting motifs (SSIP). I decided to test whether these motifs play a role in mediating Bim1p-Sli15p associations. Elimination of these motifs however, only weakly affected binding to Bim1p, suggesting the presence of other targeting elements or a more complicated binding interface in the fully folded molecule (Fig. 33).
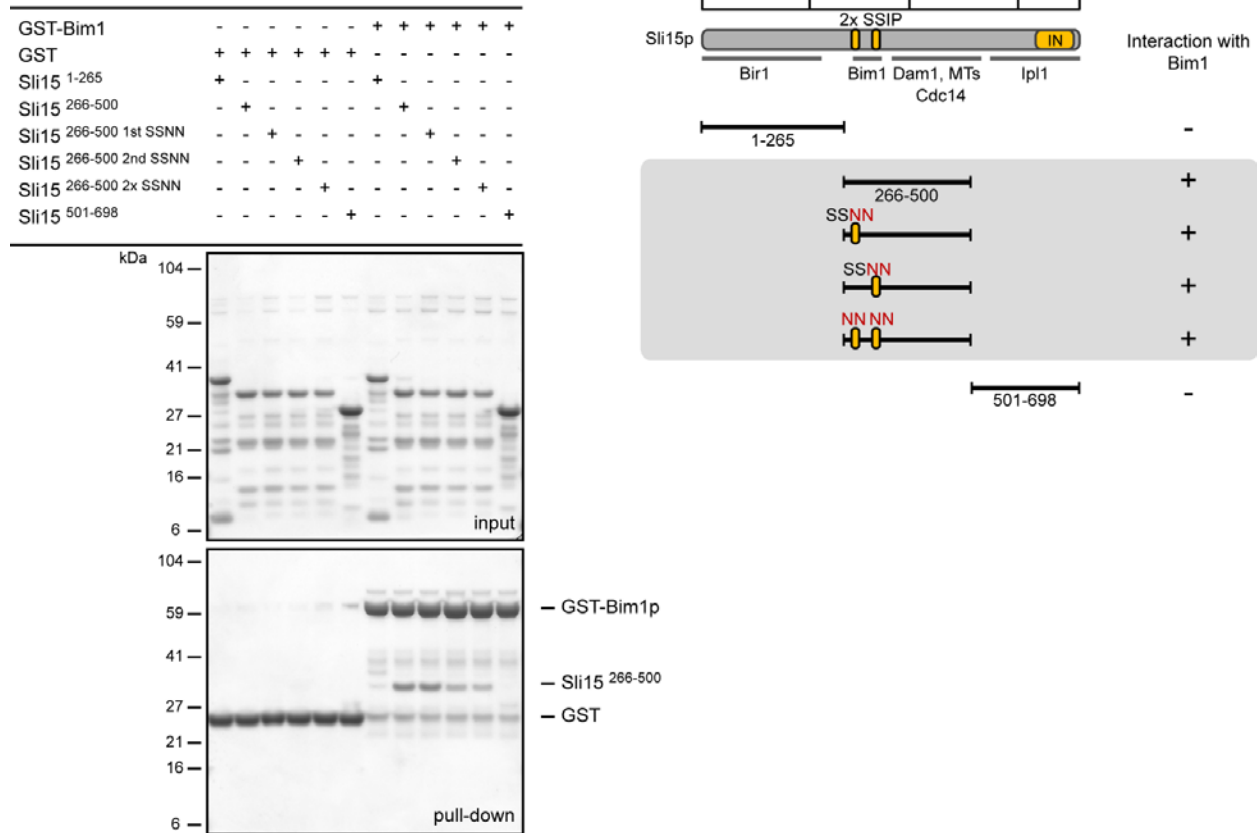
Figure 33. Bim1p binds to the central part of Sli15p

Indicated Sli15p- constructs were expressed in *E. coli* as 6xHis-tagged proteins and sub-jected to Bim1p binding in vitro. The central part of Sli15p mediates its interactions with Bim1p but it does not depend strongly of the presence of SxIP-like motifs.

5.4.2. Bim1p interacts with the Ipl1p-Sli15p complex via the N-terminus of the ki-nase

Next I tested the requirements for Bim1p binding in the context of the full Ipl1p-Sli15p complex. The recombinant kinase complex was purified from *E. coli* and consisted of Sli15p and Ipl1p with either separate or combined mutations of the SxIP-motifs. Any variant of the complex carrying 2x SkNN mutations on Ipl1p exhibited reduced binding to Bim1p (Fig. 34). This suggests that in the context of the kinase-Sli15p complex, Bim1p binding depends only on the unstructured N-terminus of Ipl1p. The complex with only Sli15p mutations showed unaf-

fected binding to Bim1p which indicates that the two SSIP motifs in Sli15p are not critical for the binding activity. In addition, my analysis indicated that overall the Ipl1p-Sli15p complex binds more weakly to Bim1p compared to its components separately; suggesting that Bim1p-mediated microtubule delivery may not be affected by Sli15p activation.
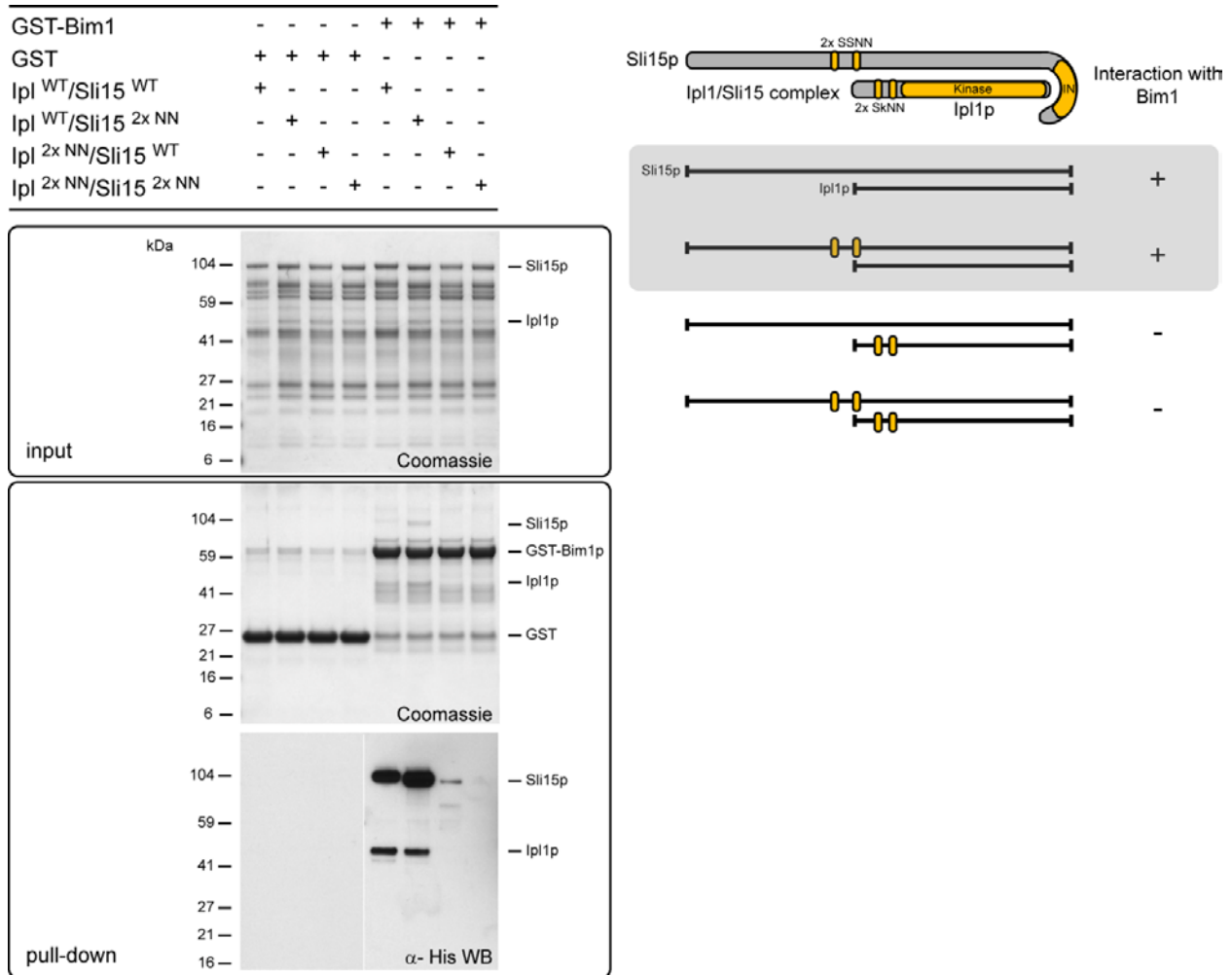
Figure 34. **The Ipl1p-Sli15p complex associates with Bim1p via the N-terminus of Ipl1p**

Recombinant Ipl1p-Sli15p complex with either of the components mutated in their potential Bim1p-binding motifs were pulled-down with GST-Bim1p.

5.5. Regulation of the interaction between Ipl1p and Bim1p

5.5.1. Elimination of Bim1p-binding motifs does not affect kinase activity in vitro

My previous data indicated that the ability of the kinase to phosphorylate Bim1p does not depend of the direct binding to the Bim1p C-terminal domain. In addition I performed an in vitro kinase assay to test if the Ipl1p kinase activity is compromised in the mutant specifically affected in Ipl1p-Bim1p interactions. I found that mutation of the SkIP motifs in Ipl1p did not affect kinase activity, supporting the distinction of the phospho-regulation domain from the Bim1p-Ipl1p binding function on the Bim1p molecule (Fig. 35).
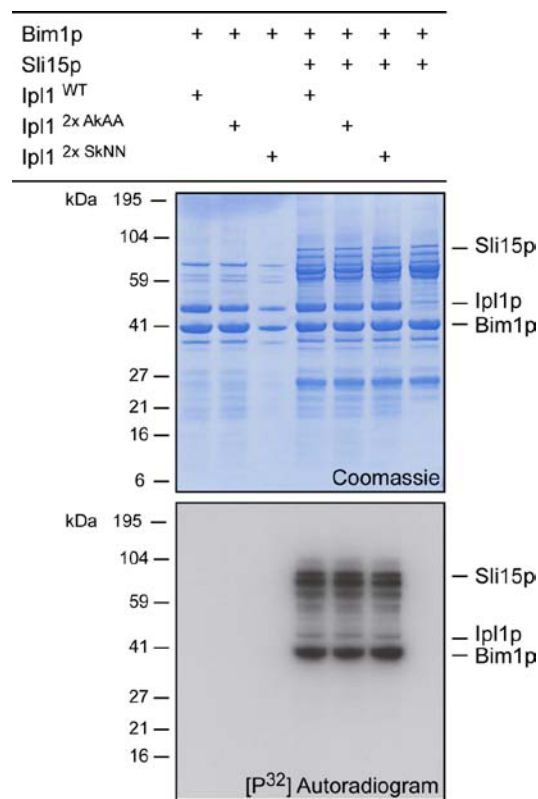
Figure 35.   Ipl1p mutants affected in Bim1p binding display normal kinase activity in vitro

Ipl1^{WT} or mutants in Bim1p-binding motifs (2x AkAA or 2x NN) were incubated with the activator protein Sli15p and Bim1p as a substrate in the presence of P^{32} γATP. Kinase activity was then analyzed by autoradiography.

Results

5.5.2. Ipl1p is phosphorylated by Cdc28/Cdk1

A recent study showed that Ipl1p might be a target for Cdk1/Cdc28 phosphorylation during mitosis (Holt et al., 2009). To test this possibility, an in vitro Cdk1 kinase reaction was performed with recombinant, purified Ipl1p or Ipl1p-EGFP (Fig. 36A). Indeed, under my assay conditions, Ipl1p was effectively phosphorylated by cyclin dependent kinase Cdc28/Cdk1 without obvious Ipl1p auto-phosphorylation in the absence of Cdk1.
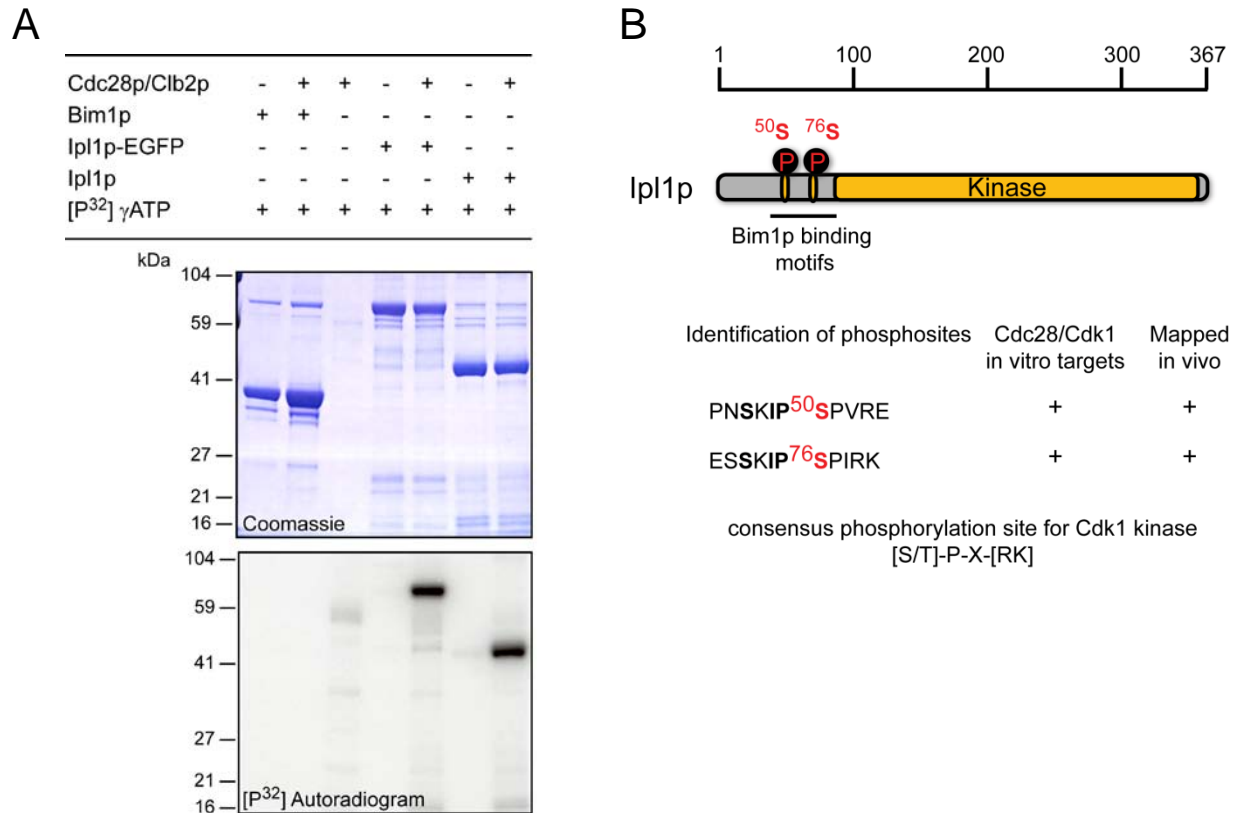
Figure 36.   Ipl1p is a target for Cdc28/Cdk1 phosphorylation

(A) In vitro kinase assay showed that Ipl1p but not Bim1p is phosphorylated by the major cell-cycle progression kinase Cdc28

(B) Identification of phosphosites by mass spectrometry from in vitro kinase reaction revealed the same two serines at the N-terminus of Ipl1p as mapped from a Sli15p-TAP tag purification (personal communications, Fabienne Lampert)

The phosphorylation reaction was also performed with Bim1p to validate Cdk1 kinase specificity. As expected, in contrast to Ipl1p, Cdk1/Cdc28 did not target Bim1p. In order to map phosphorylation sites, mass spectroscopy analysis was performed on in vitro phosphorylated Ipl1p and as well on Sli15p-TAP tag purified Ipl1p. Interestingly, the same two serine residues

(Ser-50 and Ser-76) were found in both samples, strongly suggesting that Ipl1p is a physiological target for Cdk1/Cdc28 phosphorylation (Fig. 36B). These two sites are directly adjacent to motifs that my previous analysis described to mediate interactions with Bim1p, indicating that Cdk1 phosphorylation may regulate the association of Ipl1p to Bim1p.

5.5.3. Cdk1 phosphorylation regulates Ipl1p-Bim1p binding

To test how the Cdk1 phosphorylation on the two serines adjacent to SkIP motifs would affect the association of Ipl1p with Bim1p, the binding properties of the Ipl1p kinase were tested using GST-Bim1p is a pull-down assay (Fig. 37).
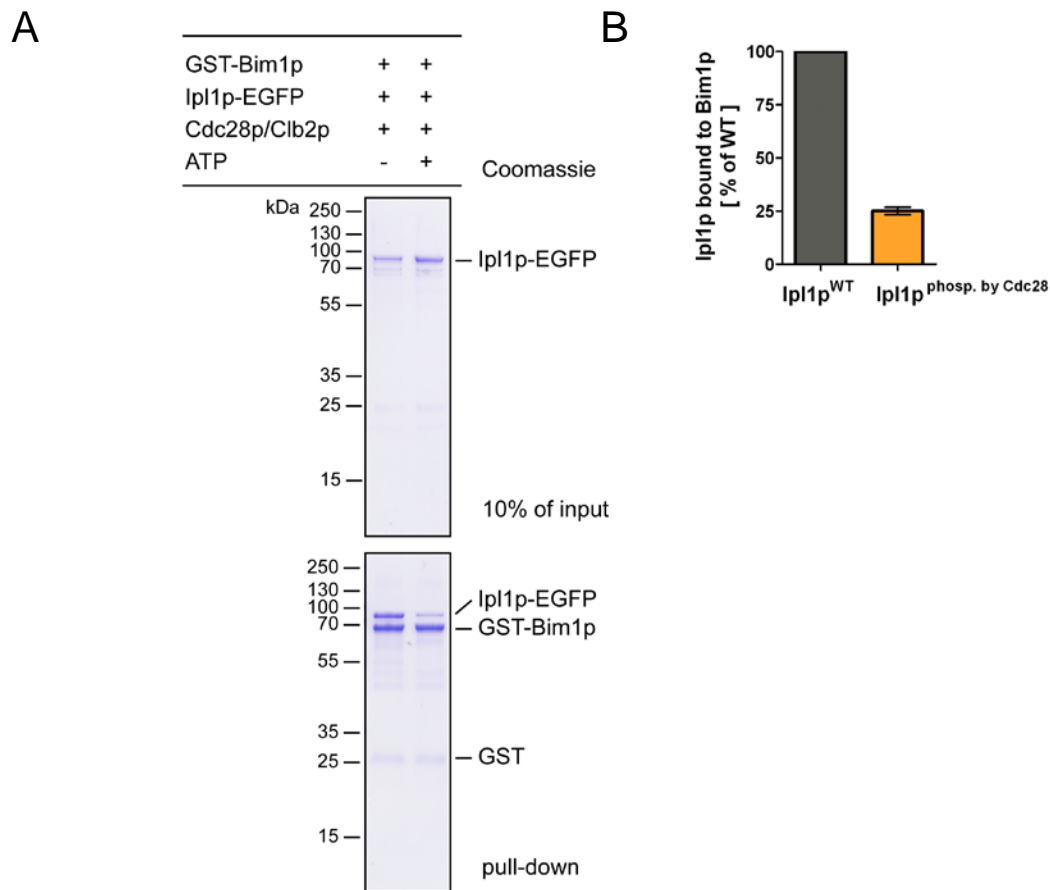
Figure 37. Ipl1p phosphorylated by Cdk1/Cdc28 displays reduced binding to Bim1p

      (A) GST-Bim1p pull-down of Ipl1p-EGFP. Cdk1/Cdc28 phosphorylation on Ser-50 and Ser-76 of Ipl1p affects its binding to Bim1p.

      (B) Quantification of Ipl1p binding from Coomassie-stained gels in three independent experiments

Results

As predicted, Cdk1 phosphorylation compromises Ipl1p binding to yeast EB1, suggesting a mode of regulating Ipl1p function by inhibiting its binding to Bim1p in living cells.

6. Discussion

To understand the molecular mechanisms underlying Ipl1p function at the kinetrochore or at the spindle midzone, it is necessary to identify all physiological kinase substrates. In this study, I present that budding yeast Bim1p, a member of the highly conserved EB1 family of proteins, is a crucial target for Aurora/Ipl1p kinase phosphorylation. EB1 proteins have widespread importance in modulating microtubule dynamics but so far the molecular mechanisms regulating their activities at MT plus ends have largely remained elusive. My analysis has shown that the phosphorylation of Bim1p is a way to regulate its microtubule-binding activity. The Bim1p phosphoregulation is not only important for proper spindle dynamics but in addition the direct Bim1p-Ipl1p interaction modulates the mitotic kinase function in vivo.

6.1. Insights into the functional organization of EB1-proteins

Previous studies have characterized EB1 proteins extensively. They showed that the EB1-protein dimers are built from two globular calponin homology domains (CH) connected via a short linker region to the coiled-coil dimerization region at the C-terminus (Hayashi and Ikura, 2003; Honnappa et al., 2005). However, a crystal structure of the linker region was not determined during any of the EB1-crystalization attempts and because it is primarily cleaved after limited proteolysis, this EB1 part is widely regarded to be flexible and unstructured (Slep, 2009). My study has shown that this domain is critical for regulating the microtubule binding activity of yeast Bim1p in vitro and in vivo. So far, the molecular activity of microtubule end binding proteins was assigned to the N-terminal CH domains of the EB1-molecule (Hayashi and Ikura, 2003). Interestingly, Bim1p phosphorylation by Ipl1p on the linker region reduces its MT binding activity. In addition, molecules lacking this region showed decreased MT-binding properties (Fig. 38).

Discussion
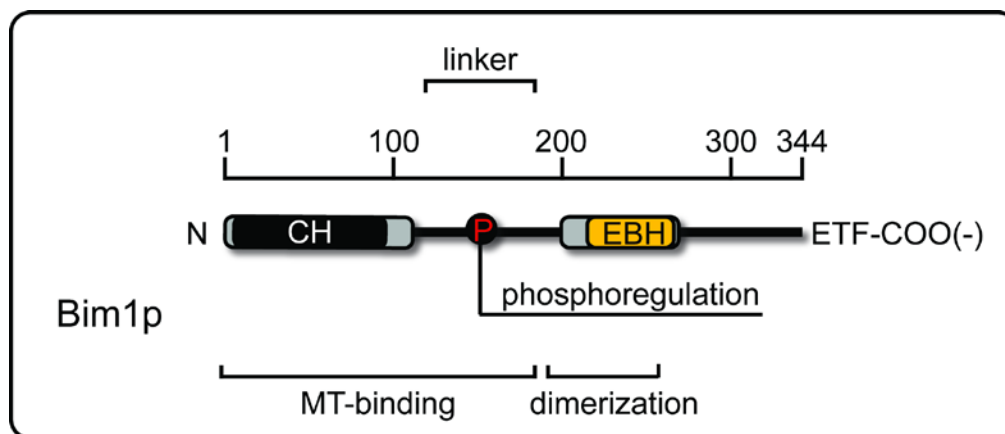
Figure 38. The functional organization of the Bim1p molecule

The N-terminal calponin-homology domain (CH) is connected to the coiled-coil four helix-bundle (EBH) via an unstructured, flexible linker. The linker region of Bim1p is the target of multisite phosphorylation by Aurora B/Ipl1p kinase. The C-terminal residues show similarities to the consensus EE(Y/F) signature motif for EB1 proteins or to α-tubulin tails.

In the EB- family of proteins, the linker region is more evolutionary diverse than other functional regions. Nevertheless, its presence, predicted unstructured nature, approximate length and basic electrostatic character are common features in all end-binding homologues. The molecular importance of the linker region was also suggested in studies on the *S. pombe* EB1 homolog –Mal3 (des Georges et al., 2008). The authors demonstrate that a C-terminal truncation of a monomeric construct (lacking the short polyarginine sequence located in a flexible linker) affects its ability to stimulate tubulin self-assembly in vitro. Moreover, the linker regions are suggested to play regulatory roles in other EB-like proteins. Human EB2 and EB3 are phosphorylated by Aurora A and Aurora B kinases, respectively, on Ser-176 located as well in the unstructured linker region of the molecule (Ban et al., 2009). In contrast to multisite phosphorylation of Bim1p, the phosphorylation of EB3 does not seem to affect its microtubule binding but regulates its stability during mitosis and contributes to mitotic progression. Phosphorylation by an Aurora kinase disrupts a complex between EB3 and SIAH-1 (E3 ubiquitin ligase) increasing the levels of EB3 (Ban et al., 2009). The flexible linker may also allow intramolecular folding of the EB-molecules. It has been suggested that the activity of MT-catastrophe suppression of the EB1 proteins can be auto-inhibited by folding of the CH-domains onto the C-terminal tails (Hayashi et al., 2005; Manna et al., 2008). The C-termini of many EB1 proteins contain the EE(Y/F) se-

quence that resembles the distal part of the tyrosinated EE(Y/F)-COO(-) tails of α-tubulin. Upon binding to interacting CAP-Gly proteins, the auto-inhibition is released and the EB1 protein can bind more effectively to microtubules. It is believed that these interactions are enhanced by the presence of tyrosinated α-tubulin tails. Interestingly, this type of regulation of the MT-activity was never clearly observed for Bim1p during my studies. Bim1p can efficiently stimulate tubulin polymerization or track growing plus ends. The amino acid composition of the Bim1p C-terminus ETF-COO(-) is slightly different from the consensus motif EE(Y/F) and it has been suggested that Bim1p tip-tracking does not significantly depend on the distal amino acid of tubulin tails. In a study where the yeast α-tubulin (*TUB1*) tail was modified from EEF to EEE the localization of Bik1p (CLIP-170 homolog) on MTs was affected but not Bim1p (Badin-Larcon et al., 2004). In addition, my analysis suggests that Bim1p is not in any intramolecular fold as it elutes on size exclusion chromatography as a highly elongated protein and its activity state is rather regulated by creating a negatively charged patch of phosphorylated serines in the linker domain than by autoinhibition.

6.2. Regulation of the CH domains in MT binding proteins

Calponin homology (CH) domains are present in many actin cross-linking and signal-transducing proteins and have been proposed to function either as an autonomous actin binding motif or serve a regulatory function (Djinovic Carugo et al., 1997). The architecture of the CH domain is composed of four α-helices connected by long loops and despite the overall structural conservation of the unique CH domain fold, the use of this module displays functional variability (Gimona et al., 2002). Surprisingly, the CH fold was also found in microtubule binding proteins like Bim1p or Ndc80/HEC1 and is used as a part of their MT binding interfaces (Wei et al., 2007). Interestingly, phosphoregulation of Bim1p as presented in this study and the regulation mode proposed for Ndc80 share striking similarities. In both proteins an unstructured protein region is present adjacent to the globular CH domain and both are targets for Aurora B phosphorylation (Ciferri et al., 2008; Guimaraes et al., 2008; Miller et al., 2008). Aurora B phosphorylation of Ndc80 weakens its interaction with microtubules and helps to release improper microtubule-kinetochore attachments. In addition, phosphorylation by Ipl1p kinase of purified Ndc80 complex decreases its affinity for the microtubules up to three-fold (Cheeseman et al., 2006). This is similar to the reduction of MT-affinity of Bim1p, which I can observe upon Ipl1p phospho-

Discussion

rylation of its linker, suggesting a common way of regulating the activity of the CH domains in microtubule binding proteins.

6.3. Contribution of the linker region in the regulation of Bim1p MT-binding

How can the phosphorylation of the linker region affect the microtubule binding activity of Bim1p? The end binding proteins show a characteristic way of interacting with microtubules, specifically recognizing the growing, dynamic plus ends (Bieling et al., 2007). The molecular requirement for this specific binding is not clear. It was proposed that EB1 can recognize the GTP state of the tubulin cap at the growing end (Zanic et al., 2009). Alternatively, from studies on the *S. pombe* homolog Mal3 it has been proposed that EB1-like proteins can act as molecular zippers for tubulin polymers by aligning and stabilizing the microtubule lattice seam (Sandblad et al., 2006). Moreover, a three-dimensional cryo-EM reconstruction of this EB1 homolog suggested, that the CH domains can mediate binding of the molecule to freshly formed microtubules by occupying the groove between protofilaments (des Georges et al., 2008). In this context, the basic linker region of Bim1p would contribute to these associations by mediating binding to the negatively charged E-hooks of αβ-tubulin. In support of that idea is a recent report showing that EB1 lattice-binding depends on the unstructured peptide located on the outer surface of the microtubule (E-hooks of tubulin), as EB1 fails to localize to subtilisin treated microtubules (Zanic et al., 2009). In a similar way, the flexible basic N-terminal tail of Ndc80 contributes to the binding of the adjacent globular CH domain at the interface between tubulin dimers (Wilson-Kubalek et al., 2008). This region is, as in a Bim1p, the key regulatory element controlling microtubule binding of Ndc80 and it is as well a target for Aurora B phosphorylation. The multisite phosphorylation can efficiently regulate the binding properties of CH domains by creating an additional negatively charged domain in the flexible regions directly connected to the calponin-homology folds. This interferes with electrostatic interactions between unstructured fragments of either Bim1p or Ndc80 and tubulin C-terminal tails regulating their MT-binding.

6.4. Molecular requirements for microtubule plus-end tracking

The characteristic MT plus-end association of Bim1p is negatively regulated by Ipl1p phosphorylation. But what are the molecular properties defining tip tracking itself? To address this question I reconstituted Bim1p MT plus-end tracking in vitro. Using TIRF microscopy recombinant Bim1p autonomously tracks growing tubulin polymers. Tip tracking seems to be a general, characteristic feature of end binding proteins as it can be demonstrated for *S. pombe* homolog Mal3 or *Xenopus leavis* or human EB1 (Bieling et al., 2008; Bieling et al., 2007; Komarova et al., 2009). The tip-tracking activity of Bim1p was dissected using fluorescently labeled constructs and showed, consistent with microtubule co-sedimentation experiments, dependency on the flexible linker region in the Bim1p molecule. The Bim1p variant lacking this domain failed to show both MT tip associations and MT lattice binding. In addition, also the monomeric calponin homology CH domain alone could not reconstitute plus-end tracking. Summarizing, the activity of MT plus-tip tracking of Bim1p depends on proper orientation of the dimeric CH domains and enhancing effects of the unstructured adjacent linker region. The dimeric requirements for tip associations were shown for EB1 proteins as well as for many +TIPs (Slep and Vale, 2007). Interestingly, the functional plasticity of the CH domain in end-binding homologues allows the plus-end tracking activity of even a monomeric version of human EB3 (Komarova et al., 2009). However, the MT tip tracking properties are not common for all CH domain-containing proteins as yeast Ndc80 complex does not track growing MTs (Lampert et al., 2010)

6.5. The physiological function of Bim1p phoshorylation in vivo

Why does Bim1p become phosphorylated by Ipl1p? The Ipl1p kinase is a part of the conserved chromosome passenger complex whose diverse roles in coordinating chromosome segregation and cytokinesis were extensively described over the past years. Interestingly, in anaphase Ipl1p localizes to the spindle midzone, where it regulates the disassembly of the spindle (Buvelot et al., 2003). Fluorescently labeled Bim1p follows the tips of the elongated microtubules during this process and it finally also localizes to the spindle midzone to stabilize its integrity. It was reported that Bim1p together with Kar3p and Ase1p plays a key role in maintaining the stable zone of overlapping inter-polar microtubules by promoting its assembly (Gardner et al., 2008). But for proper spindle disassembly prior to telophase, these microtubule bundles must be destabilized. A role for Ipl1p in this process was already suggested as the *ipl1* temperature sensitive mutants show a delay in spindle disassembly (Buvelot et al., 2003). In addition,

Discussion

the activity of Ipl1p increases before spindle break down which can be correlated with the detection of a phosphorylated fraction of Bim1p from mobility shifts on SDS-PAGE, in a narrow time window after the beginning of securin degradation. Moreover, I found that the signal of the wild-type form of Bim1p gradually decreases just before spindle disassembly suggesting an unloading mechanism and the reduction of its microtubule binding activity. Analysis of a mutant Bim1[6A] that cannot be phosphorylated by Ipl1p showed its prolonged association with the spindle midzone and an inefficient unloading before spindle disassembly. Strikingly, in the Bim1[6A] background the spindle polymerizes to a longer extent compared to WT and it disassembles earlier by breakage rather than plus-end depolymerization (Fig. 39).
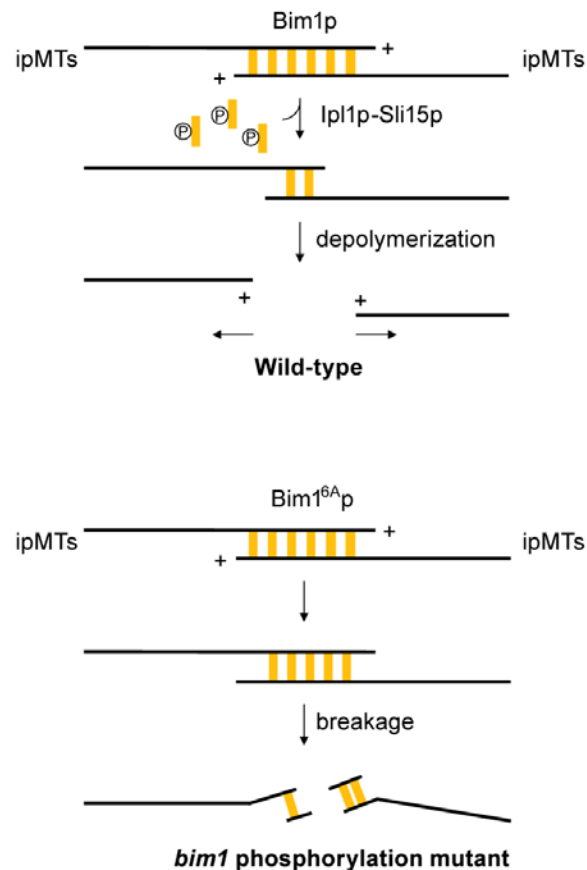
Figure 39. The role of Bim1 phosphorylation in the process of spindle disassembly.
In a wild-type Bim1 cell, Ipl1p-Sli15p phosphorylation facilitates the removal of Bim1p from the midzone and allows proper spindle disassembly. In contrast, the phospho-deficient mutant Bim1[6A] persists longer at the midzone, which leads to defects in disassembly and spindle breakage.

60

The Bim1[6A] mutant may on the one hand by direct binding increase Ipl1p kinase localization at the spindle midzone where it could phosphorylate other midzone factors (e.g. Kip3p) to decrease the time of disassembly but on the other hand Bim1p would not be properly unloaded from microtubules in this scenario, which would affect microtubule dynamics and explain the extended spindle growth.

The measurements of spindle kinetics showed also that the phosphorylation-deficient Bim1[6A] mutant has an impact on the initial, kinesin-dependent fast phase of elongation of the anaphase spindle. This suggests that even in that case, a higher amount of Bim1p on the MTs promoted growth of the microtubules and organized the spindle for a better activity of motor proteins or for Ipl1p function. However, it has been reported that the *ipl1-321* temperature sensitive allele does not have a significant effect on anaphase kinetics (Buvelot et al., 2003). In contrast, Bim1p with eliminated Ipl1p phosphorylation sites as mentioned above showed enhanced kinetics of spindle elongation which does not exactly phenocopy the *ipl1* mutant. This can be explained by the presence of additional Ipl1p phosphorylation targets important for spindle elongation and microtubule bundling factors such as Ase1p (Kotwaliwale et al., 2007). Bim1p is probably not the only key Ipl1p substrate in the spindle disassembly process as the deletion of Bim1p does not arrest cells in anaphase. Nevertheless, the Bim1p deletion affects spindle length already in metaphase, and without Bim1p the anaphase spindle shows impaired growth, microtubule density and cells need more time to properly disassemble the spindle.

6.6. Bim1p-mediated regulation of Aurora function in vivo

The interface of interaction between the Ipl1p kinase and Bim1p is separated on the molecule from the module regulating Bim1's microtubule binding activity (Fig. 40). In addition, the phosphorylation occurs independently of the cargo-binding domain at the C-terminus of Bim1p, which is on the other hand necessary for the direct kinase-Bim1p binding. This implies that this EB1 homologue is not just a typical Aurora substrate but probably acts as another important factor that modulates kinase function in vivo.

What would be the biological role of Aurora-EB1 associations in budding yeast? The genetic analysis revealed that proper Ipl1p kinase function depends on the presence of Bim1p. Interestingly, only overexpression of the Bim1 variant deficient in Aurora phosphorylation can partially suppress the *ipl1-2* allele. This suggests that Bim1p mediated targeting of Ipl1p to the

Discussion

MT tips modulates Ipl1p function in vivo. Indeed, I have identified the functional binding interface between the kinase and Bim1p and I showed that the Bim1p-Ipl1p interaction can target the kinase to microtubules in vitro. The two proteins bind to each other via two redundant SxIP motifs in the N-terminus of Ipl1p and the four helix-bundle domain of Bim1p (Fig. 40).
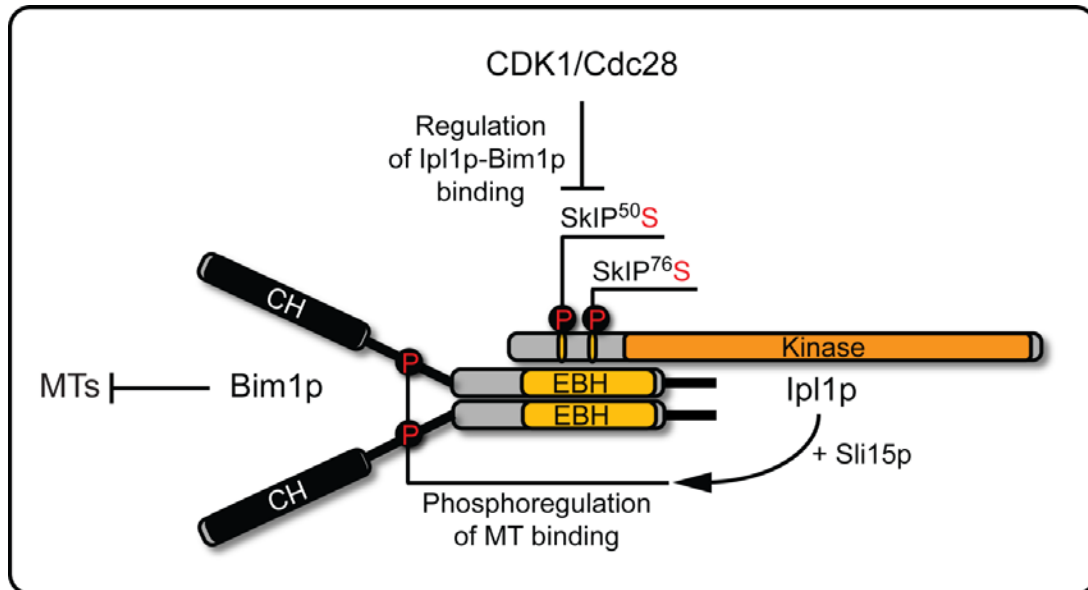
Figure 40. The binding interface between the Aurora/Ipl1p kinase and Bim1p mediates the Ipl1p MT-targeting and phospho-regulation of Bim1p MT-activity

Two SkIP motifs on the N-terminus of Ipl1p target the kinase to the cargo-binding domain of Bim1p. Upon activation by Sli15p, the kinase can phosphorylate Bim1p and release it from microtubules. Ipl1p is phosphorylated by Cdc28 at two serines next to the SkIP motifs which negatively controls its Bim1p-mediated microtubule targeting.

Interestingly, Ipl1p like other EB1 interacting proteins, contains two short SkIP motifs at the N-terminus. These motifs have been characterized as minimal EB1 binding sequences that could target interacting proteins to microtubule plus-ends (Honnappa et al., 2009). Mutation of the isoleucine and proline residues of the motifs in Ipl1p specifically affects its docking to Bim1p. Direct interactions were as well reported for human Aurora B and EB1 suggesting that the interaction between EB1 and Aurora kinase might to be evolutionary conserved (Ban et al., 2009; Sun et al., 2008). Using co-immunoprecipitation and two-hybrid analysis it was found that human the EB1 binds to the mitotic kinase Aurora B and that these two proteins co-localize on the

central spindle in anaphase and in the midbody during cytokinesis. In case of EB1 and Aurora B, the direct interactions antagonize effects of dephosphorylation by phosphatase PP2A on Aurora B activity.

The yeast Ipl1p as a part of the chromosome passenger complex (CPC) is also translocated from the centromere to the midzone of the anaphase spindle (Pereira and Schiebel, 2003). Its localization pattern on the anaphase spindle is strikingly similar to that observed for Bim1p. This suggests that not only the Ipl1p-Bim1p interactions help in proper disassembly of the spindle but also that Bim1p could play a role in transferring CPC components to the midzone of the early anaphase spindle. The major role in this characteristic transfer was however suggested for the Sli15p protein and its dephosphorylation by Cdc14p (Pereira and Schiebel, 2003). The Bim1-dependent targeting could contribute to this process by bringing Ipl1p to microtubules, as it does in the in vitro co-sedimentation assay. Ipl1p itself demonstrates microtubule-binding activity but relies on Sli15p for efficient microtubule association in vivo (Kang et al., 2001). Bim1p can be another important element for targeting Ipl1p to microtubules. This hypothesis is especially attractive, since Bim1p can differentiate between various microtubule populations within the spindle. At the onset of anaphase, kinetochore microtubules shorten (Anaphase A), while interpolar microtubules polymerize to form the spindle midzone (Anaphase B). Bim1's ability to specifically target growing microtubule plus-ends would therefore naturally transfer cargoes to the spindle midzone. In support of this idea is the finding that Ipl1p is phosphorylated by the cyclin dependent kinase Cdk1/Cdc28 at two serines adjacent to the SkIP-motifs. The phosphorylation weakens the interaction between the kinase and Bim1p during onset of mitosis where high Cdk1/Cdc28 activity is observed. At the beginning of anaphase degradation of mitotic cyclins lowers Cdk1 activity and release of the Cdk1-opposing phosphatase Cdc14 helps to dephosphorylate Cdk1 targets such as Sli15p or Ipl1p. This would allow direct Bim1p-Ipl1p interactions and a transfer of the kinase from kinetochores to the anaphase spindle. It has been shown that different subcomplexes of CPC elements might exist in the cell, suggesting that Ipl1p could exist in transient complex with Bim1p (Thomas and Kaplan, 2007). The study of the Ipl1p mutants, identified in this study, which are either specifically defective in the interaction with Bim1p (SxIP motif mutants) or constitutively interacting with Bim1p (Ipl1 S50A, S76A) will help in the future to understand the mechanism of Ipl1p regulation in more detail. Ultimately, this will allow novel insights into how the chromosome passenger complex travels within the cell.

7. Material and methods

7.1. Material

7.1.1. DNA constructs

Plasmid number	Description
TZP12	pGEX-TEV-*BIM1*^{WT}
TZP33	pGEX-TEV-*bim1*^{6A}
TZP34	pGEX-TEV-*bim1*^{6D}
TZP15	pGEX-TEV-*BIM1*$^{1-133}$
TZP38	pEGEX-TEV-*BlIM1*$^{1-185}$
TZP14	pGEX-TEV-*BIM1*$^{1-210}$
TZP18	pGEX-TEV-*BIM1*$^{1-250}$
TZP13	pGEX-TEV-*BIM1*$^{120-344}$
TZP39	pGEX-TEV-*BIM1*$^{185-344}$
TZP40	pGEX-TEV-*BIM1*$^{205-344}$
TZP187	pGEX-TEV-*BIM1*$^{197-283}$
TZP169	pET-28a-*IPL1*
TZP110	pET-28a-*IPL1*-EGFP
TZP108	pET-28a-*SLI15*
TZP19	pET-28a-*SLI15*-rbs-*IPL1*
TZP86	pET-28a-*BIM1*^{WT}-EGFP
TZP87	pET-28a-*bim1*^{6A}-EGFP
TZP102	pET-28a-*bim1*^{6D}-EGFP
TZP105	pET-28a-*BIM1*$^{1-133}$-EGFP
TZP89	pET-28a-*BIM1*$^{1-210}$-EGFP
TZP90	pET-28a-*BIM1*$^{1-210\ 6D}$-EGFP
TZP114	pET-28a-*BIM1*$^{1-133^210-344}$-EGFP
TZP116	PET-28a-*BIM1*$^{134-344}$-EGFP
TZP118	pET-28a-*BIM1*$^{134-344\ 6D}$-EGFP
TZP217	pET-28a-*IPL1*$^{1-87}$
TZP220	pET-28a-*IPL1*$^{1-87\ NN}$

TZP218	pET-28a-*IPL1*$^{36\text{-}87}$
TZP168	pET-28a-*IPL1*$^{86\text{-}367}$
TZP219	pET-28a-*IPL1*$^{36\text{-}367}$
TZP170	pET-28a-*ipl1 1*$^{st\ SkNN}$
TZP180	pET-28a-*ipl1 2*$^{nd\ SkNN}$
TZP179	pET-28a-*ipl1 2x*^{SkNN}
TZP209	pET-28a-*SLI15-ipl1*^{2xNN}
TZP210	pET-28a-*sli15*^{2xNN}*-IPL1*
TZP208	pET-28a-*sli15*^{2xNN}*-ipl1*^{2xNN}
TZP192	pET-28a-*sli15*$^{1\text{-}265}$
TZP193	pET-28a-*sli15*$^{266\text{-}500}$
TZP205	pET-28a-*sli15*$^{266\text{-}500 1st\ SSNN}$
TZP206	pET-28a-*sli15*$^{266\text{-}500\ 2ndSSNN}$
TZP207	pET-28a-*sli15*$^{266\text{-}500\ 2x\ SSNN}$
TZP199	pET-28a-*sli15*$^{500\text{-}698}$

7.1.2. Yeast strains used in this study

Strain number	Genotype
SWY167	*Mat a, leu2, ura3-52, trp1, prb1-1122, pep4-3, pre1-451, BIM1–S-Tag-TEV-ZZ::KanMX*
TZY39	*Mat α, his3Δ200, leu2-Δ1, ura3-52, ade2-101, lys2-801, TUB1-LYS2, bim1Δ::URA3, BIM1*^{WT}*– 3x GFP::HISMX5*
TZY40	*Mat α, his3Δ200, leu2-Δ1, ura3-52, ade2-101, lys2-801, TUB1-LYS2, bim1Δ::URA3, bim1*^{6A}*–3x GFP::HISMX5*
TZY41	*Mat α, his3Δ200, leu2-Δ1, ura3-52, ade2-101, lys2-801, TUB1-LYS2, bim1Δ::URA3, bim1*^{6D}*–3x GFP::HISMX5*
TZY114	*Mat a, his3Δ200, leu2-3,112, lys2-801, trp1-1, BIM1*^{WT}*::KanMX, GFP-Tub1::URA*
TZY115	*Mat a, his3Δ200, leu2-3,112, lys2-801, trp1-1, bim1*^{6A}*::KanMX, GFP-Tub1::URA*
TZY116	*Mat a, his3Δ200, leu2-3,112, lys2-801, trp1-1, bim1*^{6D}*::KanMX, GFP-Tub1::URA*
TZY143	*Mat α, his3Δ200, leu2-3,112, lys2-801, trp1-1, bim1Δ::KanMX, mCherry-Tub1::URA, BIM1*^{WT}*– 3x GFP::HISMX5*

TZY144	*Mat α, his3Δ200, leu2-3,112, lys2-801, trp1-1, bim1Δ::KanMX, mCherry-Tub1::URA, bim1^{6A}–3× GFP::HISMX5*
TZY145	*Mat α, his3Δ200, leu2-3,112, lys2-801, trp1-1, bim1Δ::KanMX, mCherry-Tub1::URA, bim1^{6D}–3× GFP::HISMX5*
TZY146	*Mat a, his3Δ200, leu2-3,112, lys2-801, trp1-1, bim1Δ::KanMX, GFP-Tub1::URA*
TZY147	*Mat α, lys2-801am, leu2-3,112, his3Δ200, ura3-52, 2μ ARS Bim1^{WT}-13myc::URA*
TZY148	*Mat α, lys2-801am, leu2-3,112, his3Δ200, ura3-52, 2μ ARS Bim1^{6A}-13myc::URA*
TZY149	*Mat α, lys2-801am, leu2-3,112, his3Δ200, ura3-52, 2μ ARS Bim1^{6D}-13myc::URA*
TZY150	*Mat a, his3Δ200, leu2-3,112, ura3-52, lys2-801, trp1-1, ipl1-2, 2μ ARS Bim1^{WT}-13myc::URA*
TZY151	*Mat a, his3Δ200, leu2-3,112, ura3-52, lys2-801, trp1-1, ipl1-2, 2μ ARS Bim1^{6A}-13myc::URA*
TZY152	*Mat a, his3Δ200, leu2-3,112, ura3-52, lys2-801, trp1-1, ipl1-2, 2μ ARS Bim1^{6D}-13myc::URA*
TZY153	*Mat a, his3Δ200, leu2-3,112, ura3-52, lys2-801, trp1-1, ipl1-2, pGAL1-HA-BIM1::HIS*
TZY154	*Mat a, his3Δ200, leu2-3,112, ura3-52, lys2-801, sli15-3, pGAL1-HA-BIM1::HIS*
TZY155	*Mat a, his3Δ200, leu2-3,112, ura3-52, lys2-801, trp1-1, ipl1-2, BIM1^{WT}::KanMX*
TZY156	*Mat a, his3Δ200, leu2-3,112, ura3-52, lys2-801, trp1-1, ipl1-2, bim1^{6A}::KanMX*
TZY157	*Mat a, his3Δ200, leu2-3,112, ura3-52, lys2-801, trp1-1, ipl1-2, bim1^{6D}::KanMX*

7.2. Methods

7.2.1. Yeast strain construction

Yeast strains were constructed using standard procedures. C-terminal S-Tag-TEV-ZZ (tandem affinity purification) tags, deletions, and conditional alleles of *BIM1* were constructed by PCR as described previously (Longtine et al., 1998). Phosphorylation site mutants were generated using QuikChange Multi Site-Directed Mutagenesis (Agilent Technologies) on *BIM1* ORF together with both 200 bp UTRs cloned into *XhoI* and *EcoRI* sites of pBS II KS plasmid with additional *KanMX* resistance insertion at *BamHI* site in the 3'UTR of *BIM1* gene, or *BIM1* gene with single 200 bp 5' UTR cloned into *BamHI* site of modified pRS303–3x GFP. Constructs were integrated into a *bim1Δ* strain by cutting *XhoI* and *EcoRI* or *NheI,* respectively. Growth experiments were conducted as indicted typically in YPD (YP + 2% dextrose) YP Raf/Gal (YP + 2% galactose and raffinose) or in minimal medium supplemented with dropout TRP and 2% dextrose.

7.2.2. Tandem affinity purification of Bim1p–S- (TEV)–ZZ from yeast extracts and mass spectrometry analysis

The C-terminally tagged Bim1p-S-TEV-ZZ strain was grown to OD_{600} = 1.2, washed with water, resuspended in small amount of water, and drop frozen in liquid N_2. Cells were lysed four times in a Waring blender with liquid N_2. An equal volume of 2x lysis buffer (1x lysis buffer: 50 mM bis-Tris propane, pH 7.0, 100 mM KCl, 5 mM EDTA, 5 mM EGTA, 10% glycerol) plus protease inhibitors as well phosphatase inhibitor cocktail (containing 20 mM Sodium pyrophosphate, 10 mM NaN_3, 20 mM NaF, 0.8 mM Sodium orthovanadate, and 0.1 M ß-glycerophosphate) was added to the cell powder. Triton X-100 was next added to the thawed extract to a final concentration of 1%. The extract was centrifuged at 10 k rpm in a SS-34 rotor for 20 min and at 45 k rpm in a Ti70 rotor for 30 min at 4°C. The supernatant was passed over Q sepharose resin (Amersham Pharmacia Biotech), and the salt concentration of the flow through was adjusted to 300 mM KCl. The flow through was then added to IgG sepharose and washed with lysis buffer containing 300 mM KCl, 1 mM DTT and 0.1% Tween-20. The IgG sepharose was incubated overnight with TEV protease 0.1 mg/ml in final wash buffer. The supernatant was then removed from the IgG sepharose and added to S protein agarose (Novagen) for 3 h. Next the 20 mM Glycine pH=2 buffer was added to elute the protein from beads. The purified proteins

were next analyzed by mass spectrometry after in solution digest. Phopsho-mapping was conducted on purified Bim1p from two independent preparations.

7.2.3. Cloning, expression, and purification of proteins

PCR amplified *Saccharomyces cerevisiae BIM1* ORF was ligated into modified pGEX-4T-TEV, or modified pET28a(+)-EGFP plasmids. QuikChange Multi Site-Directed Mutagenesis was used to selectively mutate serines on pBSII KS-Bim1^{WT} full length (Ser139, -148, -149, -165, -166, and -176) into alanines or aspartic acids, and mutations were verified by sequencing. *IPL1* ORF was ligated to pET28a vector and residues I^{48}, P^{49}, I^{74}, and P^{75} of two SkIP motifs were mutated into Asn (N) or Ala (A). Similarly, residues of two SSIP motifs on *SLI15* ORF (I^{307}, P^{308}, I^{384} and P^{385}) were mutated to asparagines (Asn).

7.2.3.1. Purification of GST-tagged Bim1 form *E. coli*

GST-TEV-Bim1^{WT}, -Bim1^{6A}, and -Bim1^{6D} variants were expressed overnight at 18°C after induction with 0.1 mM IPTG. Bacteria were disrupted by sonication in the presence of protease inhibitors (Roche), and fusion proteins were purified from cell lysates using glutathione-Sepharose (GE Healthcare). Phosphate buffer A (25 mM NaH$_2$PO$_4$/Na$_2$HPO$_4$, pH 6.8, 300 mM NaCl, and 1 mM EDTA) was used for lysis, incubation, and washing of the beads. Bim1 protein was finally cleaved off the GST moiety after overnight incubation at 8°C with 0.01 mg/ml TEV protease in buffer B (25 mM NaH$_2$PO$_4$/Na$_2$HPO$_4$, pH 6.8, 150 mM NaCl, 1 mM EDTA, 0.1% Tween 20, and 1 mM DTT). The eluate was subjected to anion exchange chromatography using a HiTrapQ 1-ml column (GE Healthcare) and developed with a linear gradient. Protein concentration was determined with D$_C$ Protein Assay kit (Bio-Rad Laboratories), and samples were frozen in the presence of 5% (vol/vol) glycerol at –80°C.

7.2.3.2. Purification of 6xHis-tagged Bim1 and Ipl1-Sli15 variants from *E. coli*

6x His-tagged at N-terminus: Bim1-, Ipl1-, or Sli15 individually or EGFP fusion proteins, were expressed overnight at 18°C after induction with 0.1 mM IPTG and purified using buffer C (25 mM NaH$_2$PO$_4$/Na$_2$HPO$_4$, pH 7.5, 400 mM NaCl, and 15 mM imidazole) and Ni–nitrilotriacetic acid agarose $^{Ni-NTA}$ (QIAGEN). Elution of proteins was performed with 200 mM imidazole followed

by buffer exchange (25 mM NaH_2PO_4/Na_2HPO_4, pH 7.5, 150 mM NaCl, and 1 mM EDTA) using PD-10 columns (GE Healthcare).

7.2.4. Kinase assays

Recombinant Ipl1p–Sli15p complex at a concentration of 0.1 mg/ml was incubated with Bim1p substrates in kinase buffer (25 mM Hepes, pH 7.5, 150 mM KCl, 1 mM EDTA, 4 mM $MgCl_2$, 10% glycerol, and 1 mM DTT) in the presence of γ-$[P^{32}]$ATP.

Clb2-TAP tag purified Cdc28 (5 µl) was incubated with substrates (5 µg) in the Cdk1 buffer (25 mM Hepes pH 7.6, 100 mM KCl, 2 mM $MgCl_2$, 1 mM DTT, 1 mM EGTA, 5% glycerol, 20 mM β-glycerolophosphate). The reaction was performed at 30°C for 30 min, and products were separated by SDS-PAGE and analyzed by autoradiography.

7.2.5. In vitro binding assays

5 µg of purified GST- Bim1p variants was added to 30 µl glutathione-Sepharose and 10 µg of the individual proteins or Ipl1p–Sli15p complex (precleared with the same amount of beads) in a final volume of 500 µl of binding buffer (25 mM Hepes, pH 7.5, 135 mM KCl, 3 mM $MgCl_2$, 1 mM EDTA, 10% glycerol, 0.1% NP-40, and 1 mM DTT). After incubation for 1 h at 8°C, beads were washed three times with 0.5 ml of binding buffer and analyzed by SDS-PAGE and Coomassie staining or Western blotting. Kinase complex was detected with anti–5x His antibodies (QIAGEN).

7.2.6. Analytical SEC

Bim1p alone or together with Ipl1p was diluted into gel filtration buffer (25 mM NaH_2PO_4/Na_2HPO_4, pH 7.5, 150 mM NaCl, and 1 mM EDTA) on ice for 10 min before loading onto a Superdex 200 PC 3.2/30 (GE Healthcare) equilibrated in gel filtration buffer. Fractions of 75 µl were collected and separated by SDS-PAGE. Proteins were stained with Coomassie Brilliant blue R250.

Material and methods

7.2.7. MT-binding assays (conventional/fluorescence based)

Precleared at 60 k rpm Bim1[WT], Bim1[WT] phosphorylated preparatively by Ipl1p, and Bim1[6D] (at 1 µM) were incubated with increasing concentrations of taxol-stabilized MTs (0–10 µM) in 25 mM Hepes, pH 7.5, 150 mM KCl, 4 mM $MgCl_2$, 1 mM EGTA, and 10% glycerol. Bim1p bound to MTs was separated from unbound fraction by ultracentrifugation (60 k rpm 30-min 25°C). The amount of Bim1p in supernatant and pellet was quantified by densitometry of Coomassie-stained SDS-PAGE gels using ImageJ software (National Institutes of Health). To determine apparent K_d of Bim1p for MTs, data points from three independent experiments were fitted into the equation $Y = 0.5 \times \{(K_d + B_{max} + X) - [(K_d + B_{max} + X)^2 - (4B_{max}X)]^{1/2}\}$ using Prism 4.0 (GraphPad Software, Inc.), where Y is the concentration of Bim1p partitioning to the pellet with the MTs, B_{max} is the maximal fractional Bim1p–MTs complex, K_d is the dissociation constant, and X is the concentration of polymeric tubulin.

In the fluorescent-based MT-binding assay, 1 µM of purified Bim1p-EGFP constructs, Ipl1p-EGFP alone or with 1 µM unlabelled Bim1p was subjected to MT binding as described above and centrifuged. Supernatant and pellet were separately distributed to black 96-well plate and the amount of Bim1p bound to MTs was measured fluorometrically using plate reader (Synergy 2; BioTek). The averaged data from three individual experiments were similarly plotted as binding affinity curves.

7.2.8. Light-scattering assay

1 µM of Bim1 variants were incubated together with 8 mg/ml tubulin on ice in BRB80 buffer containing 1 mM GTP (in a total volume of 60 µl) and transferred into 3-mm quartz cuvettes. Right-angle light scattering of the solution was recorded every 10 s for a period of 30 min at 350 nm in a spectrofluorometer (FluoroMax4; Horiba Scientific) equilibrated to 30°C.

7.2.9. Isothermal titration calorimetry

ITC experiments were performed in 25 mM NaH_2PO_4/Na_2HPO_4, pH 7.5, 150 mM NaCl at 30°C using a VP-ITC calorimeter (Microcal Inc., Northampton, MA). Approximately 1.4 ml of 0.01 mM Bim1p coiled-coil dimerizatin domain (residues 197-283) in temperature controlled sample cell was titrated by 0.1 mM Ipl1 N-terminal fragments loaded in 300 µl mixing syringe. 29

of 10 µl sample injections were carried out with 120-s equilibration time between events and stirring at 300 rpm. The reference cell contained water. To obtain K_d value, binding isotherms were fitted with non-linear method assuming one set of binding sites per protomer provided by Origin 7 (OriginLab Corp.) software.

7.2.10. Glycerol gradient sedimentation

For glycerol gradient sedimentation, 0.1 mg of the purified recombinant Bim1p was layered to the top of a 2 ml 5–25% glycerol gradient diluted in 25 mM NaH_2PO_4/Na_2HPO_4, pH 7.5, 150 mM NaCl buffer and centrifuged at 100 k rpm for 12 h at 4°C. Next, 20 of 100 µl fractions were collected from the top (5% glycerol) to the bottom (25% glycerol) of the gradient, and samples analyzed by SDS-PAGE. Molecular weight of Bim1p was estimated from s-values of standard proteins from parallel experiment.

7.2.11. In vitro reconstitution of plus end tracking using TIRF microscopy

The preparation of perfusion chambers for microscopy was previously described (Westermann et al., 2006). Assay chambers were constructed using acid-washed cover glasses and silanized glass slides separated by double-sided tape (Scotch). Assembled chambers were first washed with miliQ water. A solution of 5 mg/ml biotinylated BSA (Vector Laboratories) was flowed in for 1 h and exchanged afterward with blocking solution containing 80 µg/ml casein, 0.1% pluronic F-127 (Sigma-Aldrich), and 1% polyethylene-block poly(ethylene glycol) (Sigma-Aldrich) in BRB80 buffer for 30 min. The chamber was then incubated with 0.3 mg/ml avidin DN (Vector Laboratories) in blocking buffer for at least 30 min. Reaction chambers were equilibrated with assay buffer (BRB80 supplemented with 150 mM KCl, 0.33 mg/ml casein, 0.5% β-mercaptoethanol, 4.5 µg/ml glucose, 200 µg/ml glucose oxidase, and 35 µg/ml catalase) and incubated with rhodamine-labeled, GMPCPP-stabilized short MT seeds for 1 min. Dynamic MT growth was initiated by flowing 15 µM of tubulin solution (containing 1 µM rhodamine-labeled tubulin) in assay buffer and visualized at 30°C using the TIRF3 microscopy system (Carl Zeiss, Inc.) operated with Axiovisiosoftware (Carl Zeiss, Inc.) and a 100x α Plan-Apochromat 1.46 NA objective. Time-lapse recordings were acquired every 5 s using an electron-multiplying charge-coupled device camera (C9100-02; Hamamatsu Photonics). For the observation of Bim1 plus end tracking, 70 nM EGFP-tagged Bim1 protein or 150 nM Bim1–Alexa Fluor 488 was included in the tubulin mix. In phosphoregulation assays, recombinant Ipl1–Sli15 complex at 0.1 mg/ml and 0.1 mM ATP were additionally included.

Material and methods

7.2.12.   Live cell imaging

To quantify spindle elongation kinetics, cells were arrested with α-factor, released into synthetic medium, and imaged at 30°C on concanavalin A–coated culture dishes (Matek). Eight z stacks 0.4 µm apart were acquired at 1-min intervals on a microscope (Axiovert 200M; Carl Zeiss, Inc.) equipped with a 100x α Plan-Apochromat 1.46 NA objective and a CoolSNAP HQ camera (Photometrics) controlled by MetaMorph software (MDS Analytical Technologies). Spindle length measurements were performed using ImageJ. Strains expressing *Bim1–3x GFP* and *mCherry-Tub1* were visualized by live cell Deltavision deconvolution microscopy (Applied Precision, LLC) on a microscope (IX-71; Olympus) controlled by SoftWoRx (Applied Precision, LLC). Images were acquired using a 100x Plan-Apochromat 1.4 NA objective (Olympus) and a CoolSNAP HQ camera at 25°C. Eight z stacks 0.35 µm apart were acquired at 15-s intervals, deconvoluted, and projected into 2D images.

8. Appendix

8.1. Zimniak, T., Stengl, K., Mechtler, K., Westermann, S. (2009). Phosphoregulation of the budding yeast EB1 homologue Bim1p by Aurora/Ipl1p. *J Cell Biol.* **186(3):379-91**

Phosphoregulation of the budding yeast EB1 homologue Bim1p by Aurora/Ipl1p

Tomasz Zimniak, Katharina Stengl, Karl Mechtler, and Stefan Westermann

Research Institute of Molecular Pathology, 1030 Vienna, Austria

EB1 (end binding 1) proteins have emerged as central regulators of microtubule (MT) plus ends in all eukaryotes, but molecular mechanisms controlling the activity of these proteins are poorly understood. In this study, we show that the budding yeast EB1 protein Bim1p is regulated by Aurora B/Ipl1p-mediated multisite phosphorylation. Bim1p forms a stable complex with Ipl1p and is phosphorylated on a cluster of six Ser residues in the flexible linker connecting the calponin homology (CH) and EB1 domains. Using reconstitution of plus end tracking in vitro and total internal reflection fluorescence microscopy, we show that dimerization of Bim1p and the presence of the linker domain are both required for efficient tip tracking and that linker phosphorylation removes Bim1p from static and dynamic MTs. Bim1 phosphorylation occurs during anaphase in vivo, and it is required for normal spindle elongation kinetics and an efficient disassembly of the spindle midzone. Our results define a mechanism for the use and regulation of CH domains in an EB1 protein.

Introduction

Microtubules (MTs) are highly dynamic polymers formed by a cylindrical assembly of $\alpha\beta$-tubulin subunits that have essential functions for intracellular transport, chromosome segregation, and cellular architecture. Several MT-associated proteins regulate their dynamics and interactions and help to organize the MT cytoskeleton. An important subgroup among MT-associated proteins is constituted by the plus end–tracking proteins (+TIPs), which are characterized by their preferential association with growing MT plus ends in vivo. +TIPs are highly conserved among all eukaryotes and they can be divided into different subfamilies, including the DIS/chTOG family of XMAP215-like proteins, the CLIP-170 or CLASP-related families, spectraplakins, and, finally, the EB1 (end binding 1) family of MT end–binding proteins (for reviews see Akhmanova and Hoogenraad, 2005; Akhmanova and Steinmetz, 2008). EB1 proteins have emerged as key regulators of MT plus ends in all eukaryotes (Vaughan, 2005). They contain an N-terminal calponin homology (CH) domain, which displays MT-binding activity and is part of various tubulin- or actin-binding molecules (Hayashi and Ikura, 2003; Slep and Vale, 2007). The following C-terminal coiled-coil mediates homodimerization and is followed by a four-helix bundle (EB1 homology domain), which is critical for

the tethering of cargo proteins to EB1 (Honnappa et al., 2005; Slep et al., 2005). Although crystal structures of the individual CH domain and the C-terminal cargo-binding domain have been solved, the spatial organization of these domains in the context of a full-length EB1 molecule remains unknown. Two recent studies of the *Schizosaccharomyces pombe* EB1 homologue Mal3 have provided some basic insights into the function of EB1 proteins. Using an EM approach, Sandblad et al. (2006) have investigated the decoration of stabilized MTs by Mal3 and found that the protein preferentially associates with the lattice seam of the MTs, the structurally most labile part of the polymer. Thus, it may act as a "molecular zipper" supporting the stabilization of the closing lattice seam (Sandblad et al., 2006; Vitre et al., 2008). In a different approach, Bieling et al. (2007) have reconstituted the interaction of three *S. pombe* +TIPs with dynamic MTs in vitro. Notably, only the EB1 homologue Mal3p had an intrinsic ability to track the MT end and was sufficient to localize the kinesin Tea1p and the CLIP-170 protein Tip1p to growing ends in vitro (Bieling et al., 2007). Despite this progress, important questions concerning EB1-related proteins have remained unanswered. For example, what is the molecular mechanism by which these proteins bind to the MT lattice and to the growing end? Moreover, how does the cell

Correspondence to Stefan Westermann: westermann@imp.ac.at

Abbreviations used in this paper: CH, calponin homology; MT, microtubule; SEC, size exclusion chromatography; TEV, tobacco etch virus; +TIP, plus end–tracking protein; TIRF, total internal reflection fluorescence; WT, wild type.

Supplemental Material can be found at:
http://jcb.rupress.org/content/suppl/2009/08/10/jcb.200901036.DC1.html

regulate EB1 activity to control the dynamics and transport of proteins to plus ends? Because EB1 proteins constitute the center of extensive +TIP networks and control the association of many proteins with plus ends, they are particularly important targets for regulatory mechanisms (Lansbergen and Akhmanova, 2006).

Plus ends establish the contact of MTs to various cellular structures, among them the kinetochore, a complex assembly of proteins on centromeric DNA which mediates the attachment of chromosomes to the mitotic and meiotic spindle (Westermann et al., 2007; Cheeseman and Desai, 2008; Tanaka and Desai, 2008). Regulation of kinetochore–MT attachments is particularly important in the process of biorientation, i.e., the pathway by which the cell ensures that duplicated sister chromatids are connected to opposite spindle poles (Tanaka et al., 2005). In addition, the MT plus ends of interpolar MTs are bundled to form the spindle midzone, which is required for proper spindle elongation (Khmelinskii et al., 2007) and cytokinesis (Norden et al., 2006). The mitotic kinase Aurora B is thought to be critical for the regulation of MT plus ends in both of these cellular situations. In the process of kinetochore biorientation, Aurora B phosphorylates kinetochore components to release improper attachments (Cheeseman et al., 2002; Ciferri et al., 2008), and during anaphase, Aurora B localizes to the spindle midzone, where it is involved in timely spindle disassembly (Buvelot et al., 2003). To understand how Aurora B performs its critical functions, it is essential to identify all relevant downstream targets and elucidate their mechanism of regulation.

In this study, we identify the budding yeast EB1 homologue Bim1p as Ipl1 substrate and provide molecular insights into its regulation. Biochemical analysis has revealed that Bim1p directly associates with the Ipl1p kinase and, upon activation by Sli15p, becomes phosphorylated on a cluster of six sites in the flexible linker domain. Our analysis indicates that the Bim1p linker domain is critical for MT binding, autonomous plus end tracking, and phosphoregulation of this EB1 family member.

Results

Bim1p is phosphorylated by the Ipl1–Sli15 complex at the linker domain

To analyze the protein–protein interactions and posttranslational modifications of the budding yeast EB1 homologue Bim1p, we constructed a strain in which the endogenous *BIM1* gene was tagged at the C terminus with a tandem affinity tag. The protein was purified from yeast extracts of logarithmically growing cells, and the preparation was analyzed after in-solution digest by mass spectrometry (Fig. 1 A). Under our stringent purification conditions (300 mM KCl), the budding yeast adenomatous polyposis coli homologue Kar9p, a known interaction partner of Bim1p with a role in orienting the yeast spindle (Hwang et al., 2003), was copurified. In addition, we mapped a total of six Bim1 phosphorylation sites. Interestingly, the identified sites (Ser139, -148, -149, -165, -166, and -176) were not randomly distributed throughout the molecule but clustered in a region of 40 aa in the flexible linker region connecting the

well-conserved CH and EB1-like domains (Fig. 1 B). Closer inspection of the phosphorylation sites revealed that most of them contained a consensus sequence targeted by the Aurora B kinase (Cheeseman et al., 2002), suggesting that Bim1p may be an Ipl1p substrate. To determine whether Bim1p is indeed phosphorylated by Ipl1/Aurora B, we expressed and purified full-length Bim1p from *Escherichia coli*, phosphorylated the protein with bacterially expressed Ipl1p in complex with its activator protein Sli15p, and analyzed the products of the kinase reaction by mass spectrometry. We found that precisely the same six phosphorylation sites we mapped in vivo were phosphorylated by purified Ipl1–Sli15 complex in vitro (Fig. 1 B). To further validate the phosphorylation sites, Bim1p variants in which the six mapped phosphorylation sites were either mutated to Ala to prevent phosphorylation (*Bim1^{6A}*) or mutated to aspartate to mimic constitutive phosphorylation (*Bim1^{6D}*) were expressed and purified from bacteria. Although wild-type (WT) Bim1p (Bim1p^{WT}) was an excellent substrate for Ipl1–Sli15 in vitro, changing the mapped phosphorylation sites to Ala or Asp prevented phosphorylation almost completely, demonstrating that the phosphorylation is highly specific for the mapped residues (Fig. 1 C). We also compared the efficiency of Bim1p phosphorylation either by Ipl1p alone or by Ipl1p and Sli15p. Although phosphorylation of Bim1p by Ipl1 alone was barely detectable under standard kinase assay conditions, the addition of Sli15p led to rapid phosphorylation (Fig. S1). Thus, effective phosphorylation of Bim1p by Ipl1p depends on the presence of Sli15p. Collectively, these results establish that Bim1p is a target of Ipl1p and that phosphorylation occurs on a cluster of six Ser residues located in the flexible linker region.

Bim1p forms a stable complex with Ipl1p via its C-terminal domain

Because Bim1p is phosphorylated by Ipl1p, we next explored which protein segments are important for mediating kinase–substrate interactions. A series of Bim1p N- and C-terminal truncation mutants were expressed, purified as GST fusion proteins, and tested for interaction with purified Ipl1–Sli15 complex in pull-down assays. We found that Ipl1–Sli15 could bind to Bim1p and that the interaction required the presence of the C-terminal residues 185–344 encompassing the EB1 homology domain, which is required for the binding of other cargo molecules to EB1 family members (Fig. 1 D and Fig. S2). The association between Bim1p and the Ipl1 complex was not affected by the phosphorylation status of Bim1p, as the phosphomimicking *Bim1^{6D}* mutant could interact effectively with Ipl1–Sli15. Furthermore, we observed that Bim1p can interact with Ipl1p also in the absence of Sli15p (Fig. S2). The Bim1–Ipl1 interaction was very robust and could be detected by analytical size exclusion chromatography (SEC) under physiologically relevant salt concentrations of 100 mM KCl (Fig. 1 E). Interestingly, upon Ipl1p binding, the elution position of Bim1p was shifted toward a smaller Stokes radius, suggesting that interaction with Ipl1p stabilized a more compact conformation of the Bim1 molecule. In further support of a direct association, a recent genome-wide two-hybrid analysis
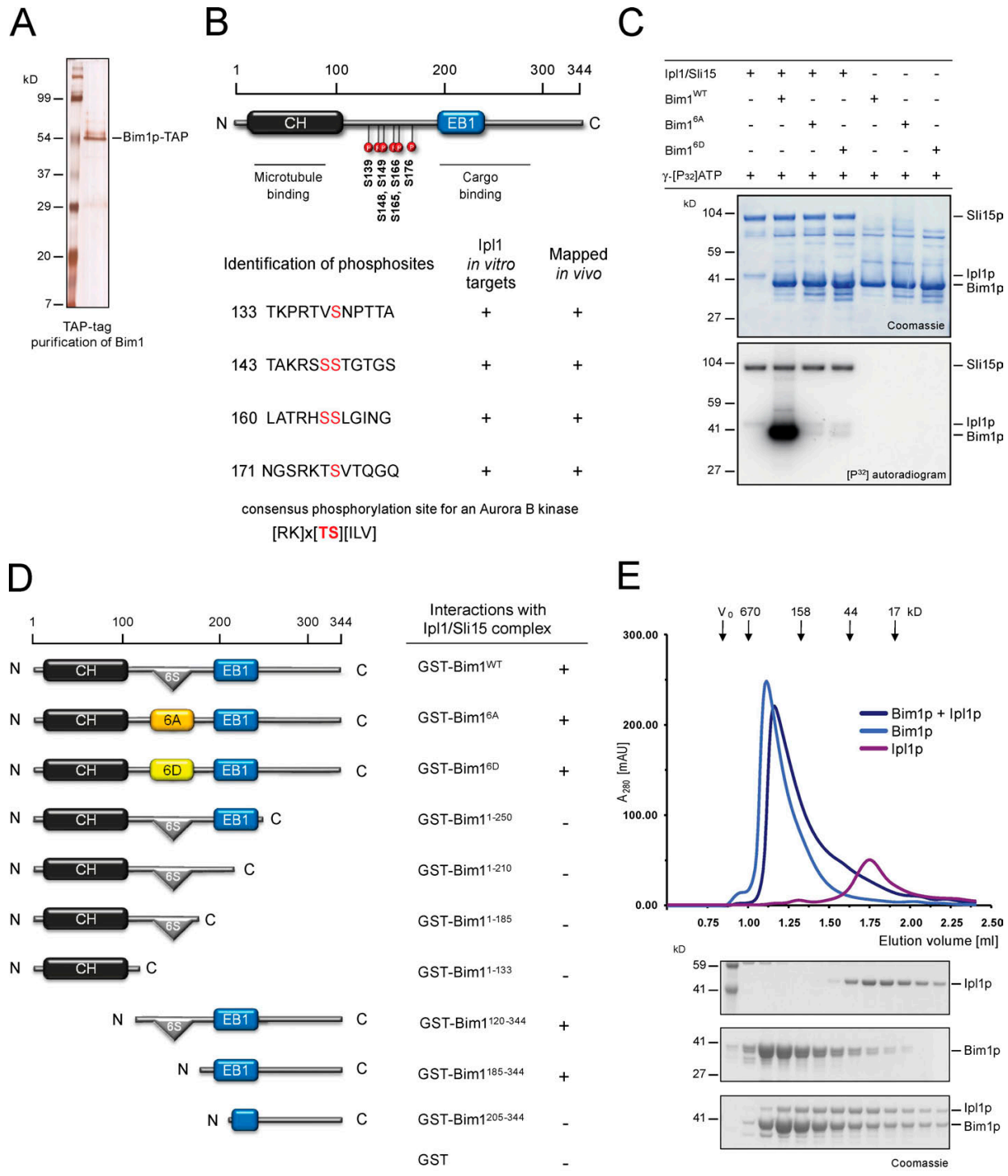
Figure 1. **Bim1p is phosphorylated by the Ipl1–Sli15 complex.** (A) Silver-stained gel of purified *Bim1–S-Tag-TEV-ZZ* from yeast extracts. TAP, tandem affinity purification. (B) Schematic representation of phosphorylation sites found after purification of Bim1p from yeast extracts and after in vitro phosphorylation of recombinant Bim1p with purified Ipl1–Sli15 complex. The phosphorylation sites cluster in the flexible linker region connecting the conserved CH and EB1 domains. (C) Validation of the mapped Bim1p phosphorylation sites. Recombinant Bim1p[WT] and mutants either preventing (6A) or mimicking (6D) Ipl1 phosphorylation were phosphorylated with the Ipl1–Sli15 complex in vitro. Note the elimination of phosphorylation upon changing the mapped phosphorylation sites. (D) Mapping the Bim1 interaction with the Ipl1–Sli15 complex. Different N- and C-terminal truncations of Bim1p were expressed as GST fusion proteins in *E. coli* and used in pull-down assays with His6-tagged recombinant Ipl1–Sli15 complex in vitro. Binding to Ipl1–Sli15 depends on the C-terminal domain of Bim1p. (E) Analytical SEC of Bim1p and Ipl1p alone or in combination indicates the formation of a stable complex between the two proteins.

Figure 2. **Bim1 phosphorylation occurs during anaphase in vivo.** (A) Western blot analysis of Bim1 phosphorylation in a WT and in an *ipl1-2* background. SDS-PAGE was performed in the presence of 30 μM Mn²⁺ Phos-tag. Note the elimination of the slower migrating form after the shift to the restrictive temperature of an *ipl1-2* mutant. (B) Time course of Bim1 phosphorylation in an α factor arrest/release experiment. Note that the slower migrating Bim1 forms are detected after degradation of the yeast securin Pds1p. The circled P represents the phosphorylated form of the protein.
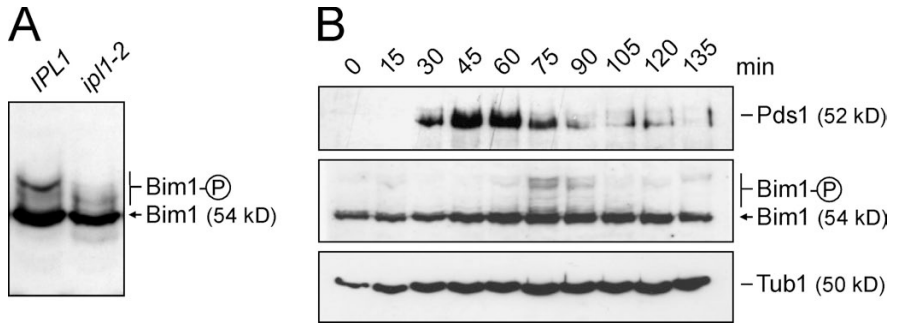
identified interactions between Bim1 and Ipl1–Sli15 (Wong et al., 2007).

We tested the effect of the multisite phosphorylated linker on the overall structure of Bim1p. We first compared the hydrodynamic properties of WT and phosphomimicking Bim1p proteins. Bim1p^{WT} elutes remarkably early during SEC with a Stokes radius of 58 Å, suggesting a highly elongated shape of the dimeric molecule. However, the elution peak of the phosphomimicking Bim1^{6D} mutant was shifted to a later elution volume (Fig. S3 A). This different migration behavior in SEC did not correspond to the presence of dimeric versus monomeric forms, as a Bim1p variant lacking the coiled-coil dimerization motif eluted later than the 6D mutant, reflecting its monomeric nature (Fig. S4). Thus, phosphorylation of the linker domain may lead to a conformational change of the dimeric Bim1 molecule, which results in a compaction. To further analyze the consequences of linker phosphorylation, we subjected Bim1^{WT}, Bim1^{6A}, and Bim1^{6D} variants to limited proteolysis using the protease chymotrypsin. Although WT and the 6A mutant showed similar degradation patterns, the digestion pattern for the 6D mutant was significantly altered, arguing for a profound conformational change exposing different cleavage sites (Fig. S3 B). Thus, full-length Bim1p is a highly elongated molecule, and linker phosphorylation by the Ipl1–Sli15 complex may trigger a conformational change that results in a more compact dimeric molecule.

Bim1p phosphorylation occurs during anaphase in vivo

To study the phosphorylation status of Bim1p in vivo, we analyzed the pattern of epitope-tagged Bim1p by Western blotting. To enhance a potential phospho shift, SDS-PAGE was performed in the presence of the Phos-tag reagent (Kinoshita et al., 2006). In extracts derived from WT cells, Bim1p displayed slower migrating forms, which were eliminated after shifting the cells to the restrictive temperature in an *ipl1-2* mutant (Fig. 2 A). To study the timing of Bim1 phosphorylation in vivo, we synchronized cells expressing Bim1-myc and the yeast securin Pds1-myc in G1 phase of the cell cycle with α factor, released the cells, and analyzed the phosphorylation pattern by Western blotting. Interestingly, Bim1 phosphorylation was detected in a narrow time window of 15–30 min after the beginning of Pds1 degradation (Fig. 2 B). Thus, Bim1 phosphorylation depends on Ipl1 and is detected specifically during anaphase in vivo.

Multisite linker phosphorylation reduces the affinity of Bim1p for MTs

As the principal function of EB1 proteins relies on their ability to bind MTs, we next analyzed how linker phosphorylation by the Ipl1–Sli15 complex would influence the MT-binding activity of Bim1p. We compared the binding affinities of Bim1p^{WT}, Bim1p phosphorylated in vitro with the Ipl1–Sli15 complex, and the phosphomimicking Bim1^{6D} mutant for taxol-stabilized MTs in cosedimentation assays. Bim1p^{WT} displayed a robust affinity for MTs with an apparent dissociation constant (K_d) of 0.44 μM. MT binding of Bim1p phosphorylated by Ipl1–Sli15 was markedly decreased, and the apparent K_d was raised about fivefold. The phosphomimicking Bim1^{6D} mutant displayed an even lower affinity for taxol-stabilized MTs (Fig. 3 A). We next asked whether Ipl1–Sli15 phosphorylation could also release Bim1p from the lattice after it had been prebound to taxol-stabilized MTs. We loaded MTs with Bim1p, incubated them with different amounts of purified Ipl1–Sli15 complex either in the absence or presence of ATP, and separated supernatant and pellet fractions after centrifugation. Only in the presence of ATP, Bim1p was removed by Ipl1–Sli15 from the pellet fraction into the supernatant (Fig. 3 B). Thus, Ipl1–Sli15-mediated phosphorylation of the Bim1p linker domain decreases the affinity for taxol-stabilized MTs in vitro and removes prebound Bim1p from the MT lattice.

To analyze the consequences of phosphorylation on Bim1p binding to MTs in vivo, we integrated Bim1^{WT}, Bim1^{6A}, and Bim1^{6D} variants fused with their C termini to 3× GFP into yeast. We expressed these Bim1p variants under their own promoter in a strain lacking endogenous *BIM1* and visualized them by fluorescence live cell microscopy. Western blotting indicated that the Bim1 variants were expressed in similar amounts (Fig. 3 D). Bim1^{WT}–3× GFP showed a typical localization pattern with individual dots corresponding to MT plus ends and a prominent localization to the spindle midzone. The localization pattern of the 6A mutant appeared similar, although the spindle midzone seemed to be more prominently stained than in the WT control. However, the phosphomimicking 6D mutant displayed only very weak spindle staining, the cytoplasmic background signal was stronger, and only weakly fluorescent Bim1p dots remained visible (Fig. 3 C), suggesting that constitutive phosphorylation of the linker domain also impairs binding of Bim1p to MTs in vivo.
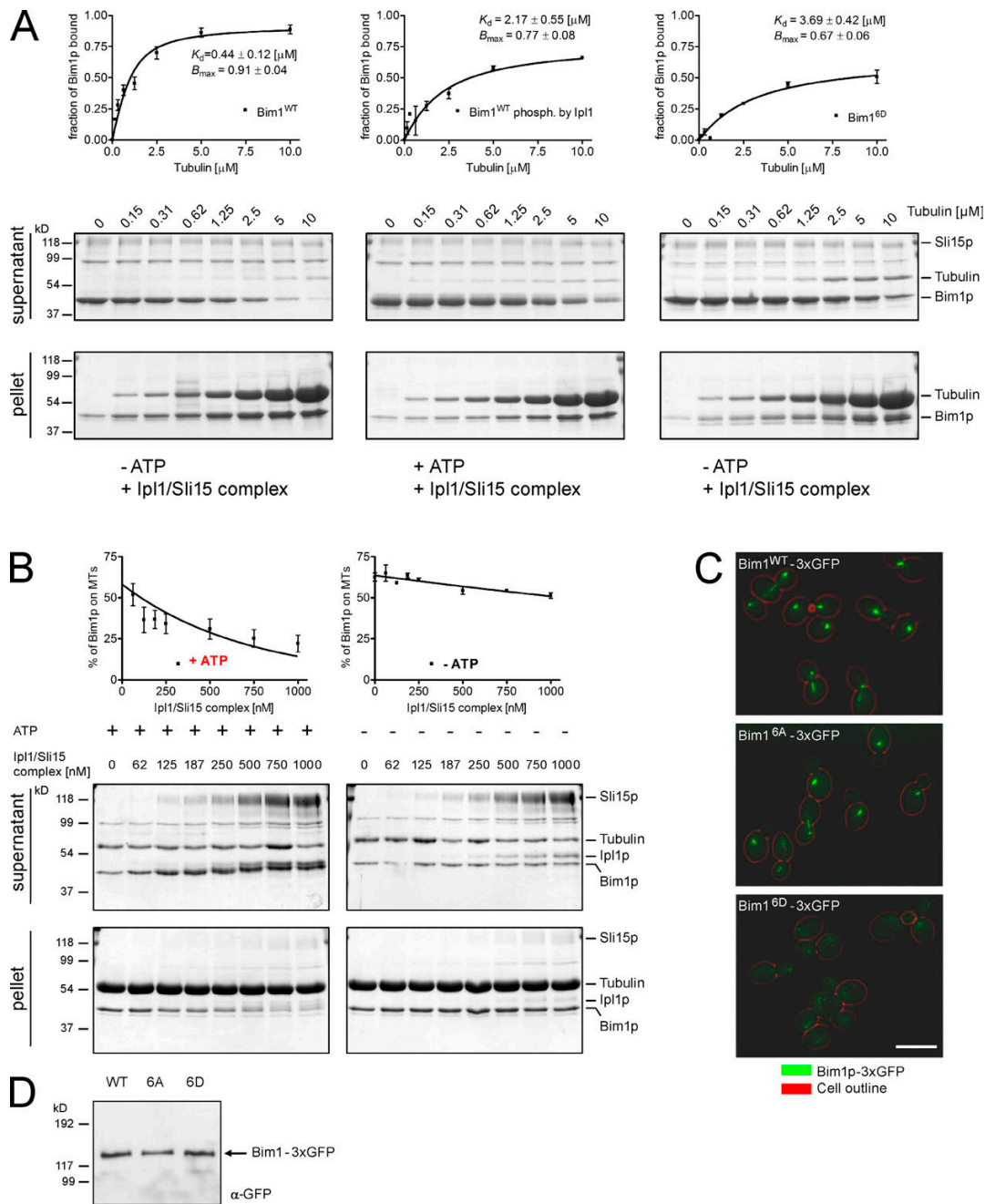
Figure 3. **Regulation of Bim1p MT binding by multisite linker phosphorylation.** (A) Equal amounts (1 μM) of Bim1[WT], Bim1[WT] phosphorylated with Ipl1–Sli15, and the phosphomimicking Bim1[6D] mutant were incubated with increasing amounts of taxol-stabilized MTs (0–10 μM). Bim1p bound to MTs was separated from the unbound fraction by ultracentrifugation, and the amount of Bim1p in the supernatant and pellet was quantified. The binding affinity curves represent averaged data from three independent experiments. (B) Bim1[WT] was bound to 2.5 μM MTs in the presence or absence of ATP. Increasing concentrations of the Ipl1–Sli15 complex were added, the binding reaction was centrifuged, and the supernatant and pellet fractions were separated and analyzed by SDS-PAGE. The top panel displays the quantification from two independent experiments. (A and B) Error bars denote standard error of the mean. (C) Bim1[WT], Bim1[6A], and Bim1[6D] variants were fused to 3× GFP, expressed as the sole source of Bim1p in yeast, and visualized by live cell microscopy. Examples of large-budded yeast cells are shown. Note the faint spindle staining of the 6D mutant. (D) Bim1[WT], Bim1[6A], and Bim1[6D] mutants are expressed at similar levels, as indicated by anti-GFP Western blotting. Bar, 6 μm.

CH and linker domains synergistically enhance MT binding of Bim1p

The MT-binding activity of EB1-like proteins had previously been assigned to the CH domain (Hayashi and Ikura, 2003). However, our surprising finding that phosphorylation of the linker region substantially influences the binding of Bim1p to MTs prompted us to further investigate the mechanism of MT binding by Bim1p. To establish the molecular requirements for MT binding more rigorously, we constructed, expressed, and purified eight Bim1p variants encompassing different combinations of CH, linker, and dimerization domains as C-terminal EGFP fusion proteins (Fig. 4, A and B; and Fig. S5). This
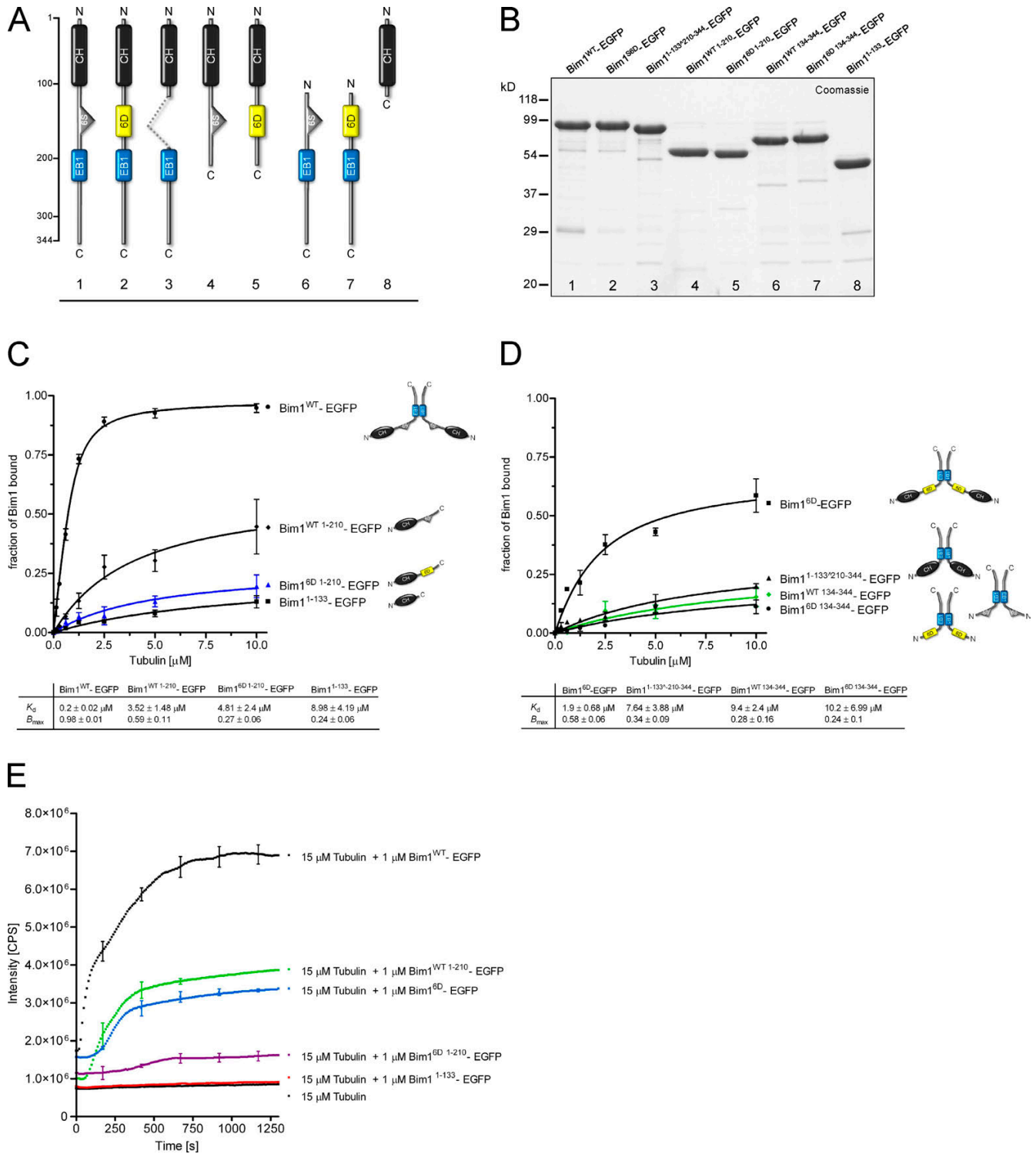
Figure 4. Molecular dissection of MT binding by Bim1p. (A) Cartoons of Bim1 variants (WT or mutants lacking the CH, flexible linker, or dimerization domain) expressed as EGFP fusion proteins in *E. coli*. (B) Coomassie-stained gel of the respective Bim1 variants. (C) 1 μM of purified Bim1p constructs was subjected to MT binding and centrifuged. The amount of Bim1p bound to MTs was measured fluorometrically, and averaged data from three experiments were plotted as binding affinity curves. The graph compares the binding affinities of dimeric versus monomeric Bim1p variants. (D) The binding affinities of different dimeric Bimp1 constructs are compared. K_d and B_{max} values for the different constructs are summarized in the table. (E) Light-scattering experiment showing the effects of Bim1 variants on the kinetics of tubulin polymerization. (C–E) Error bars denote standard error of the mean.

allowed us to analyze the MT-binding activities in a fluorescence-based cosedimentation assay (see Materials and methods). We first tested the MT-binding activities of monomeric versus dimeric Bim1 variants (Fig. 4 C). Full-length Bim1-EGFP

(residues 1–344) bound to MTs with an apparent K_d of 0.2 μM. In contrast, a monomeric construct encompassing the CH and the linker domain but lacking the coiled-coil dimerization motif (residues 1–210) showed a much lower affinity for

taxol-stabilized MTs, and the K_d was raised nearly 20-fold to 3.5 μM. Multisite phosphorylation by Ipl1p further lowered the affinity of this construct for MTs to 4.8 μM (Bim1$^{6D\ 1–210}$). Finally, a construct containing only the CH domain fused to EGFP (Bim1$^{1–133}$) bound to MTs but only weakly, with an apparent K_d of 8.9 μM.

In the next series of experiments, we compared the MT-binding activities of different dimeric Bim1 constructs (Fig. 4 D). Compared with full-length Bim1p, a variant lacking the CH domains (Bim1$^{134–344}$) displayed an ∼40-fold lower MT-binding activity. Multisite phosphorylation of the linker domain further reduced the MT affinity of this construct. Interestingly, a dimeric Bim1 variant that contained both CH domains but lacked the flexible linker residues (Bim1$^{1–133^210–344}$) displayed an MT-binding activity that was as low as the construct missing the CH domains.

We tested the effects of our engineered Bim1p constructs on tubulin polymerization using a light-scattering assay. As expected, full-length Bim1p strongly promoted MT assembly in vitro. Under the same experimental conditions, the phospho-mimicking 6D mutant and the monomeric Bim1 variant containing the CH and linker domain both displayed a strongly reduced ability to promote tubulin polymerization. A construct encompassing the CH domain alone was completely ineffective in promoting polymerization (Fig. 4 E). To exclude the possibility that the observed effects are caused by the fusion with EGFP, we repeated these experiments with an additional set of constructs that contained EGFP connected by a C-terminal flexible 36-aa linker and did not see any significant changes in protein behavior (unpublished data).

Collectively, these results demonstrate that the CH domain of Bim1p is necessary but not sufficient for MT binding of the molecule. The flexible linker region contributes significantly to MT binding, and CH and linker domains synergistically allow MT binding of the full-length Bim1p molecule.

In vitro reconstitution of Bim1p plus end tracking and regulation

In the cell, Bim1p exerts its functions on dynamic MTs. Thus, we aimed to reconstitute and directly visualize the interaction of Bim1p with dynamic MTs in vitro. To this end, we modified a microscopy flow cell assay, which was previously used to analyze the dynamics of the Dam1 ring complex (Westermann et al., 2006). We adhered short, brightly labeled, biotinylated MT seeds that had been stabilized with the slowly hydrolyzing GTP analogue GMPCPP (guanosine 5′-[α,β-methylene]triphosphate) to the surface of a coverslip via a biotin–streptavidin interaction (Fig. 5 A). After washing away any unbound seeds, dimly labeled free tubulin at a concentration of 15 μM was introduced. MTs were visualized at 30°C using total internal reflection fluorescence (TIRF) microscopy to eliminate the background fluorescence generated by unincorporated labeled tubulin dimers. Under these conditions, individual MTs grew from the stable seeds and displayed dynamic instability; i.e., phases of growth were followed by rapid disassembly before another growth phase started. A similar experimental setup has recently been used by Bieling et al. (2007) to investigate the properties of the *S. pombe* EB1 homologue Mal3p.

We first analyzed the behavior of full-length Bim1p^{WT} in the in vitro tracking assay: 70 nM Bim1-EGFP was added together with free tubulin into the flow chamber. Two-color time-lapse imaging demonstrated that Bim1-EGFP preferentially accumulated at MT ends during phases of growth but was rapidly lost from the MT upon disassembly (Fig. 5 C and Videos 1 and 2). Although the majority of Bim1p accumulated at growing plus ends, there was always a significant amount of Bim1p also bound to the MT lattice, which increased upon lowering the ionic strength of the solution or raising the Bim1p concentration in the assay (unpublished data). In alternative experiments, we followed the plus end tracking with Bim1p covalently conjugated to Alexa Fluor fluorophores, either via Cys or amine linkages (unpublished data). We did not observe significant differences between the Alexa Fluor conjugates and the EGFP fusion protein. Thus, we conclude that the budding yeast EB1 homologue Bim1p autonomously tracks growing MT ends in vitro.

The molecular requirements for autonomous plus end tracking have not been established in a defined in vitro system. Therefore, we tested our engineered Bim1 constructs in the in vitro tracking assay and asked whether they could associate with the MT lattice or with growing ends (Fig. 5 B). Under conditions in which Bim1p^{WT} displayed robust plus end tracking (70 nM final Bim1p concentration), the monomeric variant (Bim1$^{1–210}$) only weakly associated with dynamic MTs. Raising the final concentration of Bim1p$^{1–210}$ to 1 μM yielded a faint staining all along the MT lattice, whereas a substantial Bim1 accumulation at growing ends could not be observed (Fig. 5 C and Video 3). Thus, a monomeric Bim1p variant containing the CH and the linker domain failed to plus end track in vitro. In agreement with its low MT-binding affinity in the cosedimentation assay, the dimeric Bim1 variant lacking the linker domain (Bim1$^{1–133^210–344}$) was barely visible on MTs under our imaging conditions and did not display tip-tracking activity. Thus, dimerized CH domains and the presence of the linker are both necessary for the autonomous plus end–tracking activity of Bim1p.

To visualize the effect of Ipl1–Sli15 phosphorylation, we first analyzed the interaction of Bim1p with stable MT substrates. We incubated rhodamine-labeled, taxol-stabilized MTs with Bim1p–Alexa Fluor 488 and observed the binding reaction by TIRF microscopy. Bim1p–Alexa Fluor 488 decorated taxol-stabilized MTs along their length without any observable preference for MT ends. We included purified Ipl1–Sli15 complex in the binding reaction, and during recording, we introduced ATP into the flow chamber. Within seconds after ATP addition but not after a buffer control, the Bim1p–Alexa Fluor 488 signal disappeared from taxol-stabilized MTs (Fig. 5 D and Video 4). Finally, we investigated the effect of Ipl1 phosphorylation on plus end tracking in vitro. We performed the tip-tracking assay as described in this section but now added purified Ipl1–Sli15 complex either in the presence or absence of ATP. After initial association with growing plus ends, the Bim1 signal disappeared from the plus ends as well as from the lattice. This was not the case in control assays in which either the Ipl1–Sli15 complex or ATP was omitted from the reaction (Fig. 5 E and Video 5). These results demonstrate that linker phosphorylation by Ipl1p removes Bim1p from dynamic MTs in vitro.
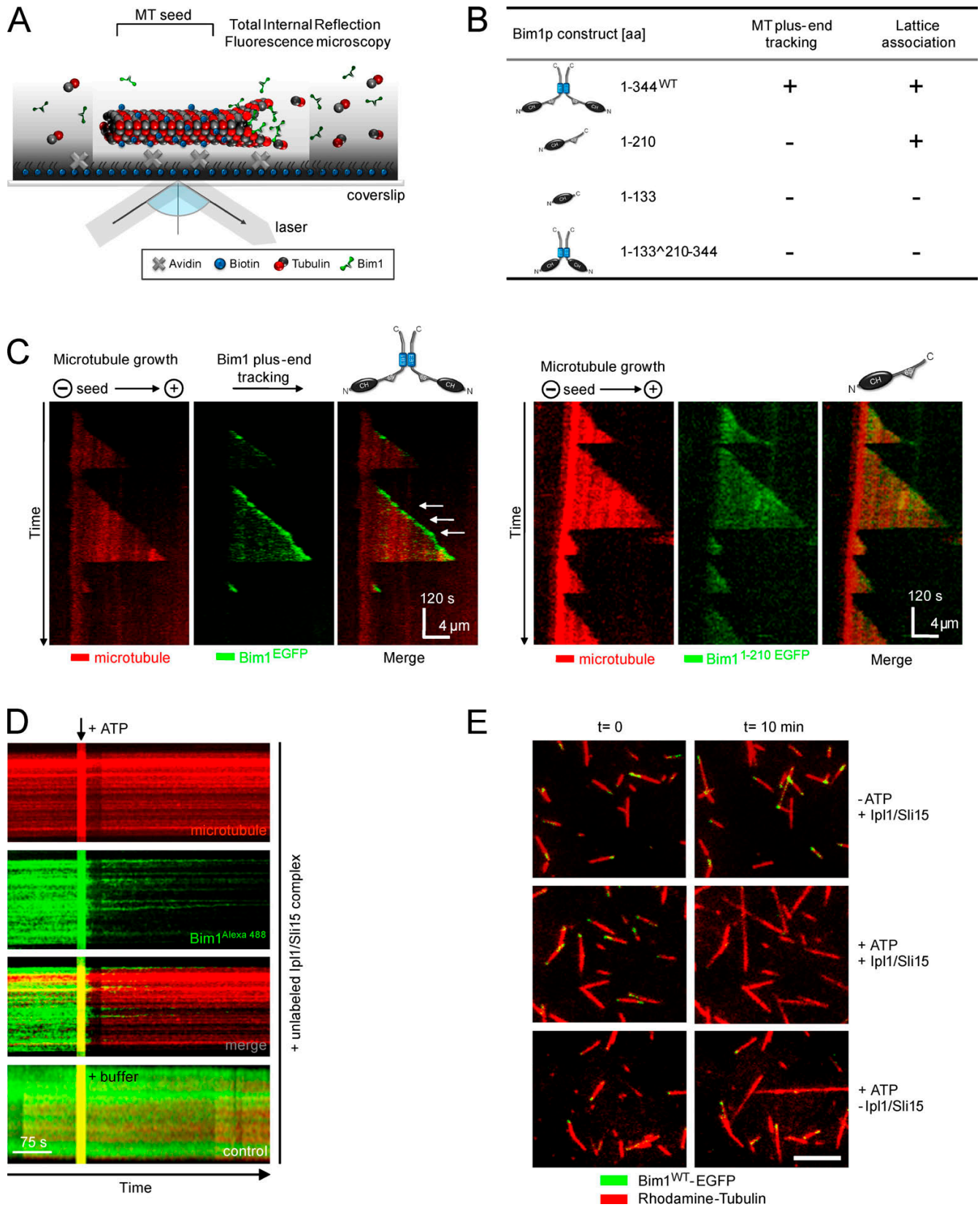
Figure 5. **Reconstitution of Bim1p MT plus end tracking in vitro using TIRF microscopy.** (A) Scheme of the experimental setup. (B) Table summarizing the ability of different Bim1 constructs for MT plus end tacking or lattice association. (C) Full-length Bim1-EGFP autonomously tracks a growing MT plus end in vitro. A kymograph representation demonstrating 70 nM Bim1p tip tracking is shown. Note that Bim1p is not found on the tips of depolymerizing MTs (left; Videos 1 and 2). Association of 1 µM of a Bim1p variant lacking the dimerization domain (Bim1p[1–210]) with dynamic MTs. Note that this variant faintly stains the MT lattice but fails to accumulate at growing ends (right; Video 3). Arrows show enrichment of Bim1 on the growing MT end. (D) In a microscopy flow cell, Alexa Fluor 488–labeled Bim1p (green) was bound to rhodamine-labeled, taxol-stabilized MTs. At the indicated time, ATP was added into the

Bim1p phosphorylation affects spindle dynamics and is critical for proper midzone disassembly in vivo

As Bim1p phosphorylation occurred preferentially in anaphase, we compared the spindle elongation kinetics of WT and mutant *bim1* cells using time-lapse live cell microscopy in strains expressing GFP-tubulin. Spindle elongation in WT cells occurred with typical biphasic kinetics consisting of an initial fast and a subsequent slow phase (Fig. 6 A). In a *bim1* deletion mutant, elongation started from a shortened metaphase spindle, the rate of elongation in anaphase was reduced, and the final spindle length was decreased. The *bim1* mutant mimicking Ipl1 phosphorylation (*Bim1^6D*) displayed spindle elongation kinetics very similar to WT cells. In contrast, the mutant preventing Ipl1 phosphorylation (*Bim1^6A*) showed a faster rate of spindle elongation in both phases of anaphase B and reached an increased maximum spindle length. These results suggest that Bim1 phosphorylation is required for spindle elongation to occur with normal kinetics. As the spindles in the phosphorylation-deficient *bim1* mutant grew faster and overextended, we also analyzed the mode of spindle disassembly by following the dynamic behavior of GFP-tagged Bim1^WT or Bim1 phosphorylation mutants in strains expressing mCherry-tubulin. Bim1^WT was prominently localized to the spindle midzone in anaphase cells, and during spindle disassembly, the length of the Bim1 zone gradually decreased until only a small amount of Bim1p remained on the ends of depolymerizing spindle MTs (Fig. 6 B and Video 6). The Bim1 phosphorylation-deficient mutant displayed a different behavior: upon spindle disassembly, the length of the Bim1 midzone decreased slightly, but in contrast to WT cells, a significant amount of *Bim1^6A* remained on the spindle. Instead of disassembling by depolymerization, the spindle then broke, and Bim1p remained on the ends of the MTs (Fig. 6 B, right; and Video 7). In extreme cases, instead of disassembling, the spindle even started to polymerize again and was bent before finally separating (Video 8). The *Bim1^6D* mutant displayed only a weak signal on the spindle MTs, and the spindle disassembled efficiently (Video 9). Collectively, these results demonstrate that Bim1 phosphorylation by Ipl1 is required for efficient disassembly of the spindle midzone in vivo.

Discussion

The mitotic kinase Aurora B has an important role in regulating MT plus ends in the process of kinetochore biorientation and at the spindle midzone, but only few relevant substrates have been identified. In this study, we show that Bim1p, a member of the evolutionary conserved family of EB1 proteins, is a physiological substrate of the yeast Aurora kinase Ipl1p. In addition to characterizing Bim1's role in spindle dynamics, our study provides insights into the molecular mechanism and regulation of autonomous plus end tracking by EB1 proteins.

Functional organization of EB1 proteins

The molecular mechanisms regulating the activity of EB1 proteins have so far remained elusive. In this study, we identify the flexible linker region as the critical regulatory domain of the budding yeast EB1 homologue Bim1p (Fig. 7 A). This was unexpected, as previous work had assigned the MT-binding activity to the CH domain, and it has been speculated that the regulatory mechanisms may target this region of the molecule (Hayashi and Ikura, 2003). Among EB1 homologues, the sequence of the linker region is less well conserved than the CH and dimerization domains. However, the approximate length of the linker, its predicted unstructured nature, and its overall basic electrostatic character are common features of all EB1 proteins. A recent study suggests that the linker region may also be of critical importance for the *S. pombe* EB1 homologue Mal3, as C-terminal truncations of a monomeric Mal3 construct abolished its polymerization-promoting activity (des Georges et al., 2008). There is further evidence that the observed interaction between Bim1p and Ipl1p may be evolutionary conserved: using two-hybrid and coimmunoprecipitation analyses, a recent study identifies human Aurora B as an interaction partner of EB1 (Sun et al., 2008). Although a direct phosphorylation of EB1 by Aurora B could not be detected in vitro, which may be caused by the absence of an activator protein, there remains the possibility that either EB1 or the related proteins EB2 and -3 may be relevant physiological Aurora B targets. Furthermore, we did not obtain experimental evidence that Bim1p is regulated by autoinhibition between the CH domains and the extreme C termini, as has been proposed for EB1 (Hayashi et al., 2005). The reason may be that Bim1p is significantly larger than EB1 (344 residues compared with 268 for EB1) or that the C-terminal residues (ETF for Bim1p) differ from the sequence found in EB1 (EEY).

A common mechanism for the function and regulation of CH domains as MT–binding interfaces

With the identification of Bim1p as an Ipl1 target, it is noteworthy to point out striking similarities between its regulation of MT binding and that of the Ndc80 kinetochore complex. Both molecules exploit CH domains as part of their MT-binding interfaces (Cheeseman et al., 2006; Wei et al., 2007), yet in both cases, unstructured regions located adjacent to the globular CH domain contribute significantly to MT binding and are the target of Aurora B phosphorylation at a cluster of neighboring residues (Ciferri et al., 2008; Guimaraes et al., 2008; Miller et al., 2008). Recent cryo-EM studies describing the decoration of MTs by Ndc80/Nuf2 (Wilson-Kubalek et al., 2008) or by the *S. pombe* EB1 homologue Mal3 (des Georges et al., 2008) suggest that the CH domain nestles into a groove at the interface between tubulin dimers on the MT lattice. The N-terminal tail domain of Ndc80 and the linker domain of EB1 proteins may

---

flow cell. In the kymograph representation, the Bim1p signal disappears rapidly from the stable MTs; in contrast, it persists in a buffer control (Video 4). (E) In vitro tracking of Bim1p in the presence of the Ipl1–Sli15 complex. Bim1p is removed from growing MT ends when the Ipl1–Sli15 complex and ATP are present (Video 5). Bar, 5 μm.
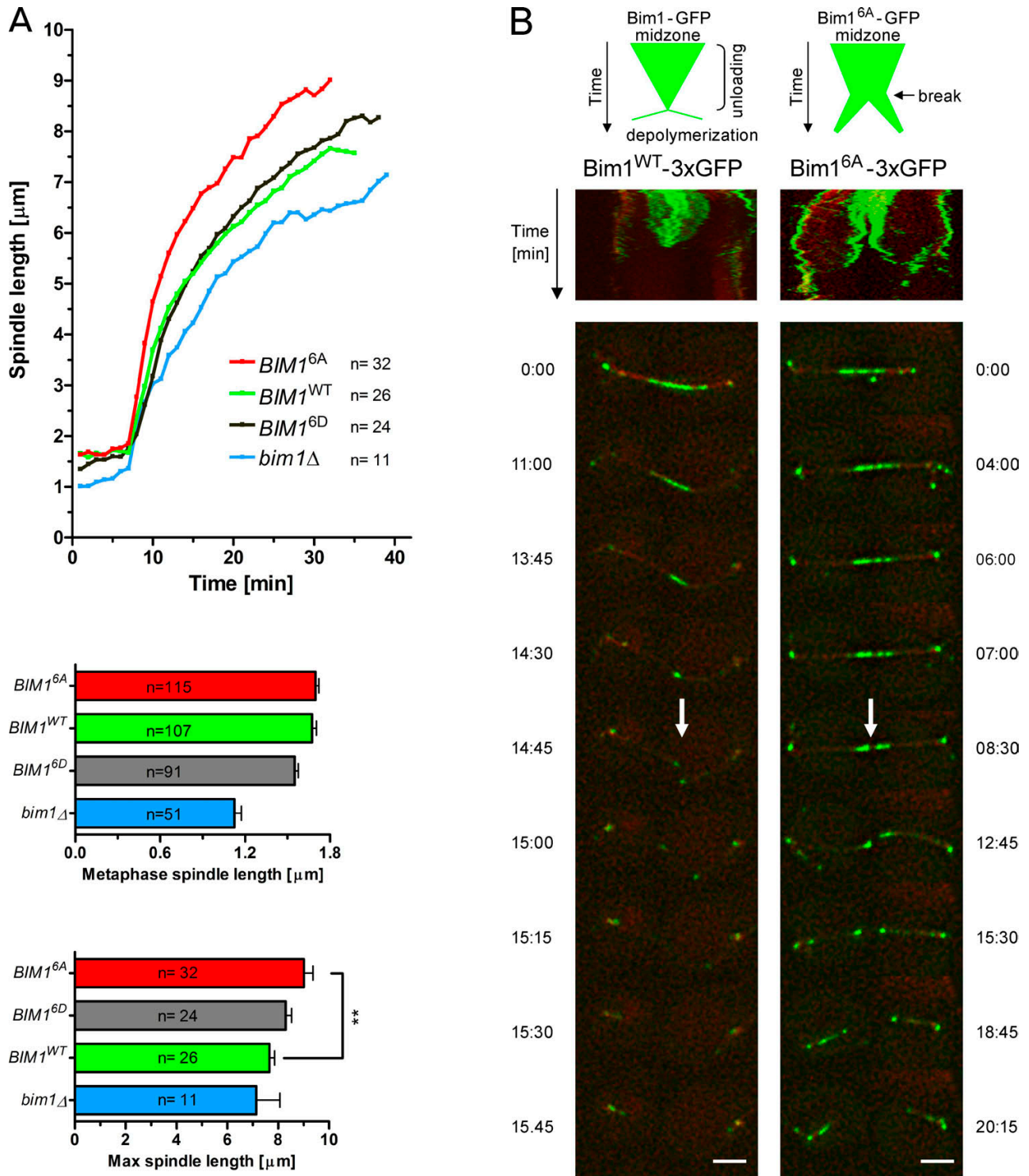
Figure 6. **Bim1 phosphorylation affects spindle dynamics and midzone disassembly in vivo.** (A) Averaged kinetics of anaphase spindle elongation in WT, *BIM1^6A*, *BIM1^6D*, and *bim1Δ* cells followed by live cell microscopy of strains expressing *GFP-TUB1*. (middle and bottom) Quantification of maximum anaphase spindle length and metaphase spindle length in the different *bim1* mutants. Error bars denote standard error of the mean. **, P = 0.0011. (B) Live cell microscopy of *BIM1–3× GFP* and *BIM1^6A–3× GFP* during spindle disassembly in strains expressing *mCherry-TUB1*. The middle panels show kymographs (space–time plots) of midzone disassembly in the WT and in the *BIM1^6A* background. The bottom panels show individual frames from the corresponding videos for a WT spindle (Video 6) and for the 6A mutant (Video 7). Arrows show separation of the Bim1 signal on the spindle. Bars, 3 µm.

contribute to binding by interacting with the negatively charged C-terminal tails of αβ-tubulin (E-hook). CH domains are used by a variety of molecules with very different binding partners. It seems that a general theme for their usage in MT binding is

to combine them with adjacent flexible regions that have an overall positive charge. Modulating the electrostatic properties of the linker domain may be a very effective way to control the affinity for MTs. Mechanistically, there are different possibilities
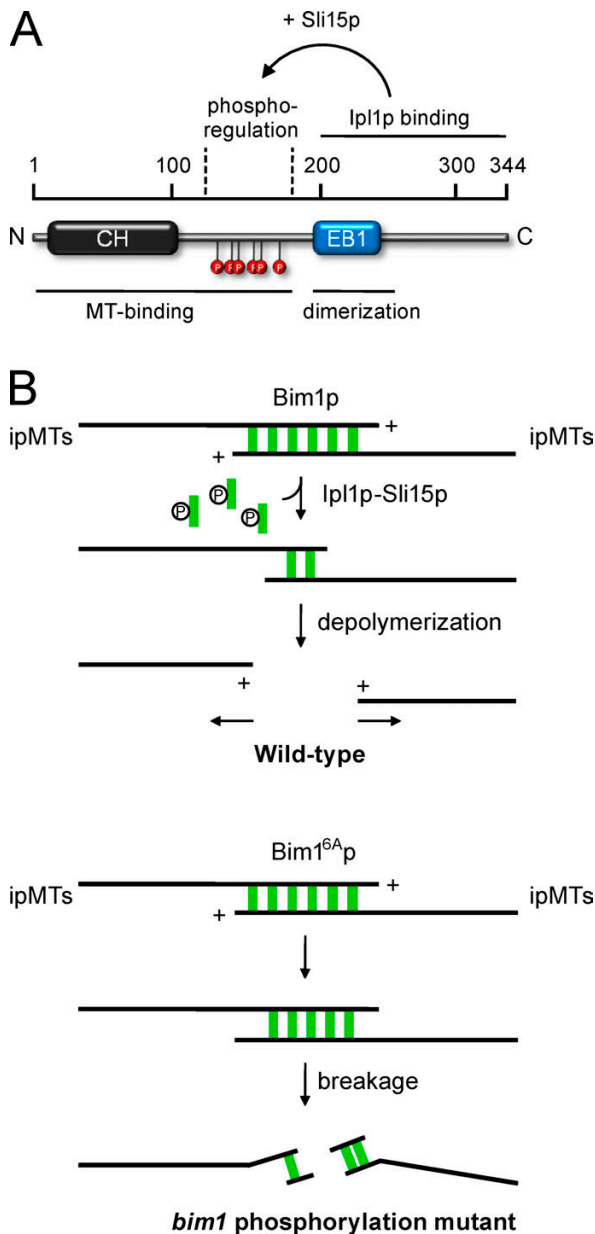
Figure 7. **Model for Bim1 phosphoregulation.** (A) Functional domains and regulation of the EB1 family member Bim1p. (B) Model for the role of Bim1 phosphorylation by Ipl1–Sli15 in the process of midzone disassembly. In a WT cell, Ipl1 phosphorylation facilitates the removal of Bim1p from the midzone and allows spindle disassembly. In a phosphorylation mutant, Bim1p persists at the spindle midzone, leading to defects in disassembly and spindle breakage. ipMT, interpolar MT.

Establishing molecular requirements for plus end tracking

The reconstitution of MT plus end tracking in vitro using a purified system in combination with the engineering of fluorescently labeled Bim1p variants has allowed us to address the basic molecular requirements for autonomous tip tracking. We demonstrate that Bim1p, like Mal3 (Bieling et al., 2007), autonomously tracks growing MT ends in a purified system. Given the high degree of evolutionary conservation and a recent study demonstrating end tracking of *Xenopus laevis* EB1 (Bieling et al., 2008), we expect autonomous tip tracking to be a general, defining feature of all EB1 proteins. Furthermore, we show that MT-binding CH domains and even dimerized CH domains alone are not sufficient to allow effective plus end tracking of Bim1p in vitro. Instead, our results indicate that the flexible linker region has an essential role in providing full MT-binding and tip-tracking activity. The failure of a monomeric Bim1p construct to display tip tracking is not just caused by its overall lower binding affinity for MTs because even raising its concentration in the assay does not lead to a specific accumulation at MT ends. Instead, it seems that the dimeric arrangement of CH and linker domains is essential for the effective recognition of a specific structure at assembling MT ends (Bieling et al., 2007). This result agrees with in vivo observations demonstrating that artificial dimerization allows plus end tracking of various +TIPs (Slep and Vale, 2007). However, it is in contrast to a recent study demonstrating that an isolated CH domain of the human EB3 protein shows specific accumulation on growing plus ends in vitro (Komarova et al., 2009). Different properties of Bim1p versus EB3 may explain the contrasting experimental outcomes. In the future, the minimal requirements for plus end tracking will have to be investigated in more detail, and it will be interesting to see whether MT-binding proteins that have different arrangements of CH domains can display autonomous tip tracking. For example, in the Ndc80/Nuf2 head of the Ndc80 complex, the two CH domains reside very close together (Ciferri et al., 2008) and provide one common rather than two spatially separated MT-binding interfaces.

The role of Bim1 phosphorylation in vivo

What is the physiological role of Bim1 phosphorylation by Ipl1p? As judged from a mobility shift in SDS-PAGE, a fraction of Bim1p becomes phosphorylated in a narrow time window after securin degradation in mid to late anaphase. At this time, Bim1p localizes to the midzone of the anaphase spindle and is critical for its structural integrity by stabilizing the zone of overlapping MT plus ends (Gardner et al., 2008). Our results suggest that phosphorylation by Ipl1 regulates the interaction of Bim1p with the anaphase spindle. The Ipl1–Sli15 complex colocalizes with Bim1p to the spindle midzone (Khmelinskii et al., 2007), and Ipl1 kinase activity increases before spindle disassembly (Buvelot et al., 2003). Although a stable midzone is essential for proper spindle elongation, the zone of overlapping MT plus ends needs to be destabilized to allow efficient spindle disassembly in telophase. In a WT cell, the majority of Bim1 is unloaded from the spindle just before disassembly, but in the Bim1 phosphorylation mutant, this unloading process is inefficient, the midzone is hyperstable, and the spindle disassembles

by which this can be achieved. First, multisite phosphorylation may down-regulate the MT-binding activity that is intrinsic to the unstructured region by changing its bulk electrostatic properties (Serber and Ferrell, 2007). Second, it may change the conformation of the flexible linker region with the consequence that the CH domains are not in the optimal position for cooperative MT binding anymore. Third, cluster phosphorylation may create a negatively charged domain that could compete with tubulin for binding to the CH domains (Fig. 7 A). The observed conformational compaction of the Bim1 molecule upon multisite phosphorylation of the linker domain supports the latter two possibilities.

by breakage rather than plus end depolymerization (Fig. 7 B). A constitutively high level of Bim1p on the spindle would also explain why the spindle overextends in the phosphorylation-deficient mutant. With an extended overlap zone, motors can act more efficiently in the fast phase of elongation, and sustained plus end polymerization will allow further extension in the slow phase. It is important to note that the *bim1* phosphorylation-deficient mutant does not precisely phenocopy the *ipl1-2* mutant, as this allele is not reported to have an effect on anaphase B kinetics (Buvelot et al., 2003). This may be explained by the presence of additional Ipl1 substrates relevant for spindle elongation such as the bundling protein Ase1p (Kotwaliwale et al., 2007). We also do not exclude additional functions for Bim1 phosphorylation and for the Bim1–Ipl1 interaction, particularly in the process of kinetochore biorientation. Additional mutants that specifically affect the interaction between Bim1p and Ipl1 will be required to clarify whether this association is critical for the regulation of MT plus ends in other cellular situations.

Materials and methods

Yeast strain construction, purification of Bim1–S-Tag–tobacco etch virus (TEV)–ZZ from yeast extracts, and mass spectrometry analysis
Yeast strains (Table S1) were constructed using standard procedures. C-terminal S-Tag-TEV-ZZ (tandem affinity purification) tags, deletions, and conditional alleles of Bim1 were constructed by PCR as described previously (Cheeseman et al., 2002). Phosphorylation site mutants were generated using QuikChange Multi Site-Directed Mutagenesis (Agilent Technologies), cloned into modified pRS303–3× GFP, and integrated into a *bim1Δ* strain. All growth experiments were conducted in YPD (YP + 2% dextrose), and tandem affinity purification tag purification was performed as described previously (Cheeseman et al., 2002). Mass spectrometry analysis was performed after in-solution digest of purified Bim1p from two independent preparations.

Cloning, expression, and purification of Bim1p variants
PCR amplified *Saccharomyces cerevisiae BIM1* ORF was ligated into pBSIIKS, modified pGEX-4T-TEV, or modified pET28a(+)-EGFP plasmids. QuikChange Multi Site-Directed Mutagenesis was used to selectively mutate serines on pBSII KS-Bim1^{WT} full length (Ser139, -148, -149, -165, -166, and -176) into alanines or aspartic acids, and mutations were verified by sequencing. GST-TEV-Bim1^{WT}, -Bim1^{6A}, and -Bim1^{6D} variants were expressed overnight at 18°C after induction with 0.1 mM IPTG. Bacteria were disrupted by sonication in the presence of protease inhibitors (Roche), and fusion proteins were purified from cell lysates using glutathione-Sepharose (GE Healthcare). Phosphate buffer A (25 mM NaH$_2$PO$_4$/Na$_2$HPO$_4$, pH 6.8, 300 mM NaCl, and 1 mM EDTA) was used for lysis, incubation, and washing of the beads. Bim1 protein was finally cleaved off the GST moiety after overnight incubation at 8°C with 0.01 mg/ml TEV protease in buffer B (25 mM NaH$_2$PO$_4$/Na$_2$HPO$_4$, pH 6.8, 150 mM NaCl, 1 mM EDTA, 0.1% Tween 20, and 1 mM DTT). The eluate was subjected to anion exchange chromatography using a HiTrapQ 1-ml column (GE Healthcare) and developed with a linear gradient. Protein concentration was determined with D$_C$ Protein Assay kit (Bio-Rad Laboratories), and samples were frozen in the presence of 5% (vol/vol) glycerol at −80°C. 6× His–tagged Bim1-, Ipl1-, or Sli15-EGFP fusion proteins, either individually or with a flexible 36-aa linker at the fusion site (QQFFGDDSPFCQEGSPFQSSPFC-QGGQGGNGGGQQQ), were expressed under the aforementioned conditions but purified using buffer C (25 mM NaH$_2$PO$_4$/Na$_2$HPO$_4$, pH 7.5, 400 mM NaCl, and 15 mM imidazole) and Ni–nitrilotriacetic acid agarose (QIAGEN). Elution of proteins was performed with 200 mM imidazole followed by buffer exchange (25 mM NaH$_2$PO$_4$/Na$_2$HPO$_4$, pH 7.5, 150 mM NaCl, and 1 mM EDTA) using PD-10 columns (GE Healthcare).

Kinase assays
Recombinant Ipl1–Sli15 complex at a concentration of 0.1 mg/ml was incubated with Bim1p substrates in kinase buffer (25 mM Hepes, pH 7.5, 150 mM KCl, 1 mM EDTA, 4 mM MgCl$_2$, 10% glycerol, and 1 mM DTT) in the presence of γ-[P^{32}]ATP. The reaction was performed at 25°C for 30 min, and products were separated by SDS-PAGE and analyzed by autoradiography.

In vitro binding assays
5 µg of purified GST fusion Bim1 proteins was added to 30 µl glutathione-Sepharose and 10 µg of the Ipl1–Sli15 complex (precleared with the same amount of beads) in a final volume of 400 µl of binding buffer (25 mM Hepes, pH 7.5, 100 mM KCl, 3 mM MgCl$_2$, 1 mM EDTA, 10% glycerol, 0.1% NP-40, and 1 mM DTT). After incubation for 1 h at 8°C, beads were washed three times with 0.5 ml of binding buffer and analyzed by Western blotting, and kinase complex was detected with anti–5× His antibodies (QIAGEN).

Analytical SEC
The indicated Bim1 variants were diluted into gel filtration buffer (25 mM NaH$_2$PO$_4$/Na$_2$HPO$_4$, pH 6.8, 150 mM NaCl, and 1 mM EDTA) on ice for 10 min before loading onto a Superdex 200 PC 3.2/30 (GE Healthcare) or Superose 6 PC 3.2/30 column (GE Healthcare) equilibrated in gel filtration buffer. Fractions of 50 µl were collected and separated by SDS-PAGE. Proteins were stained with Coomassie Brilliant blue R250.

MT-binding assays (conventional/fluorescence based)
Binding assays were performed essentially as previously described (Cheeseman et al., 2001). Precleared Bim1^{WT}, Bim1^{WT} phosphorylated preparatively by Ipl1, and Bim1^{6D} (at 1 µM) were incubated with increasing concentrations of taxol-stabilized MTs (0–10 µM) in 25 mM Hepes, pH 7.5, 150 mM KCl, 4 mM MgCl$_2$, 1 mM EGTA, and 10% glycerol. Bim1 bound to MTs was separated from unbound fraction by ultracentrifugation. The amount of Bim1p in supernatant and pellet was quantified by densitometry of Coomassie-stained SDS-PAGE gels using ImageJ software (National Institutes of Health). To determine apparent K_d of Bim1 for MTs, data points from three independent experiments were fitted into the equation $Y = 0.5 \times \{(K_d + B_{max} + X) - [(K_d + B_{max} + X)^2 - (4B_{max}X)]^{1/2}\}$ using Prism 4.0 (Graph-Pad Software, Inc.), where Y is the concentration of Bim1 partitioning to the pellet with the MTs, B_{max} is the maximal fractional Bim1–MTs complex, K_d is the dissociation constant, and X is the concentration of polymeric tubulin.

In the fluorescent-based MT-binding assay, 1 µM of purified Bim1 constructs was subjected to MT binding as described in the previous paragraph and centrifuged. The amount of Bim1 bound to MTs was measured fluorometrically using a plate reader (Synergy 2; BioTek), and averaged data from three individual experiments were similarly plotted as binding affinity curves.

Light-scattering assay
8 mg/ml tubulin and 1 µM of Bim1 variants were incubated on ice in BRB80 buffer containing 1 mM GTP (in a total volume of 60 µl) and transferred into 3-mm quartz cuvettes. Right-angle light scattering of the solution was recorded every 10 s for a period of 30 min at 350 nm in a spectrofluorometer (FluoroMax4; Horiba Scientific) equilibrated to 30°C.

In vitro reconstitution of plus end tracking using TIRF microscopy
The preparation of perfusion chambers for microscopy was previously described (Westermann et al., 2006). Assay chambers were constructed using acid-washed cover glasses and silanized glass slides. Assembled chambers were first washed with miliQ water. A solution of 5 mg/ml biotinylated BSA (Vector Laboratories) was flowed in for 1 h and exchanged afterward with blocking solution containing 80 µg/ml casein, 0.1% pluronic F-127 (Sigma-Aldrich), and 1% polyethylene-block poly(ethylene glycol) (Sigma-Aldrich) in BRB80 buffer for 30 min. The chamber was then incubated with 0.3 mg/ml avidin DN (Vector Laboratories) in blocking buffer for at least 30 min. Reaction chambers were equilibrated with assay buffer (BRB80 supplemented with 150 mM KCl, 0.33 mg/ml casein, 0.5% β-mercaptoethanol, 4.5 µg/ml glucose, 200 µg/ml glucose oxidase, and 35 µg/ml catalase) and incubated with rhodamine-labeled, GMPCPP-stabilized short MT seeds for 1 min. Dynamic MT growth was initiated by flowing 15 µM of tubulin solution (containing 1 µM rhodamine-labeled tubulin) in assay buffer and visualized at 30°C using the TIRF3 microscopy system (Carl Zeiss, Inc.) operated with Axiovision software (Carl Zeiss, Inc.) and a 100× α Plan-Apochromat 1.46 NA objective. Time-lapse recordings were acquired every 5 s using an electron-multiplying charge-coupled device camera (C9100-02; Hamamatsu Photonics). For the observation of Bim1 plus end tracking, 70 nM EGFP-tagged Bim1 protein or 150 nM Bim1–Alexa Fluor 488 was included in the tubulin mix. In phosphoregulation assays, recombinant Ipl1–Sli15 complex at 0.1 mg/ml and 0.1 mM ATP were additionally included.

Live cell imaging
To quantify spindle elongation kinetics, cells were arrested with α factor, released into synthetic medium, and imaged on concanavalin A–coated culture dishes (Matek) at 30°C. z stacks (eight stacks 0.4 µm apart) were acquired at 1-min intervals on a microscope (Axiovert 200M; Carl Zeiss,

Inc.) equipped with a 100× α Plan-Apochromat 1.46 NA objective and a CoolSNAP HQ camera (Photometrics) controlled by MetaMorph software (MDS Analytical Technologies). Spindle length measurements were performed using ImageJ. Strains expressing *Bim1–3× GFP* and *mCherry-Tub1* were visualized by live cell Deltavision deconvolution microscopy (Applied Precision, LLC) on a microscope (IX-71; Olympus) controlled by SoftWoRx (Applied Precision, LLC) and equipped with a 100× Plan-Apochromat 1.4 NA objective (Olympus) and a CoolSNAP HQ camera at 25°C. z stacks (eight stacks 0.35 µm apart) were acquired at 15-s intervals, deconvoluted, and projected into 2D images.

Online supplemental material
Fig. S1 demonstrates that phosphorylation of Bim1p by Ipl1p is dependent on the presence of Sli15p. Fig. S2 shows GST pull-down assays mapping the interaction of different Bim1 variants with Ipl1p and Sli15p. Fig. S3 documents a potential conformational change in Bim1p upon phosphorylation by Ipl1–Sli15. Fig. S4 shows SEC profiles of full-length and monomeric Bim1 variants. Fig. S5 shows SEC of Bim1 variants fused to EGFP. Videos 1 and 2 show plus end tracking of full-length Bim1-EGFP in vitro visualized by TIRF microscopy. Video 3 shows the behavior of the monomeric Bim1-EGFP protein. Video 4 shows the removal of Bim1–Alexa Fluor 488 from taxol-stabilized MTs upon phosphorylation by Ipl1–Sli15. Video 5 illustrates the release of Bim1-EGFP from dynamic MT ends upon phosphorylation. Video 6 is a live cell Deltavision video showing the behavior of Bim1^WT–3× GFP during spindle disassembly. Videos 7 and 8 show the behavior of nonphosphorylatable Bim1^6A–3× GFP during spindle disassembly. Video 9 shows the behavior of the phosphomimicking Bim1^6D–3× GFP mutant. Online supplemental material is available at http://www.jcb.org/cgi/content/full/jcb.200901036/DC1.

References

Akhmanova, A., and C.C. Hoogenraad. 2005. Microtubule plus-end-tracking proteins: mechanisms and functions. *Curr. Opin. Cell Biol.* 17:47–54.

Akhmanova, A., and M.O. Steinmetz. 2008. Tracking the ends: a dynamic protein network controls the fate of microtubule tips. *Nat. Rev. Mol. Cell Biol.* 9:309–322.

Bieling, P., L. Laan, H. Schek, E.L. Munteanu, L. Sandblad, M. Dogterom, D. Brunner, and T. Surrey. 2007. Reconstitution of a microtubule plus-end tracking system in vitro. *Nature.* 450:1100–1105.

Bieling, P., S. Kandels-Lewis, I.A. Telley, J. van Dijk, C. Janke, and T. Surrey. 2008. CLIP-170 tracks growing microtubule ends by dynamically recognizing composite EB1/tubulin-binding sites. *J. Cell Biol.* 183:1223–1233.

Buvelot, S., S.Y. Tatsutani, D. Vermaak, and S. Biggins. 2003. The budding yeast Ipl1/Aurora protein kinase regulates mitotic spindle disassembly. *J. Cell Biol.* 160:329–339.

Cheeseman, I.M., and A. Desai. 2008. Molecular architecture of the kinetochore-microtubule interface. *Nat. Rev. Mol. Cell Biol.* 9:33–46.

Cheeseman, I.M., C. Brew, M. Wolyniak, A. Desai, S. Anderson, N. Muster, J.R. Yates, T.C. Huffaker, D.G. Drubin, and G. Barnes. 2001. Implication of a novel multiprotein Dam1p complex in outer kinetochore function. *J. Cell Biol.* 155:1137–1145.

Cheeseman, I.M., S. Anderson, M. Jwa, E.M. Green, J. Kang, J.R. Yates III, C.S. Chan, D.G. Drubin, and G. Barnes. 2002. Phospho-regulation of kinetochore-microtubule attachments by the Aurora kinase Ipl1p. *Cell.* 111:163–172.

Cheeseman, I.M., J.S. Chappie, E.M. Wilson-Kubalek, and A. Desai. 2006. The conserved KMN network constitutes the core microtubule-binding site of the kinetochore. *Cell.* 127:983–997.

Ciferri, C., S. Pasqualato, E. Screpanti, G. Varetti, S. Santaguida, G. Dos Reis, A. Maiolica, J. Polka, J.G. De Luca, P. De Wulf, et al. 2008. Implications for kinetochore-microtubule attachment from the structure of an engineered Ndc80 complex. *Cell.* 133:427–439.

des Georges, A., M. Katsuki, D.R. Drummond, M. Osei, R.A. Cross, and L.A. Amos. 2008. Mal3, the *Schizosaccharomyces pombe* homolog of EB1, changes the microtubule lattice. *Nat. Struct. Mol. Biol.* 15:1102–1108.

Gardner, M.K., J. Haase, K. Mythreye, J.N. Molk, M. Anderson, A.P. Joglekar, E.T. O'Toole, M. Winey, E.D. Salmon, D.J. Odde, and K. Bloom. 2008. The microtubule-based motor Kar3 and plus end-binding protein Bim1 provide structural support for the anaphase spindle. *J. Cell Biol.* 180:91–100.

Guimaraes, G.J., Y. Dong, B.F. McEwen, and J.G. Deluca. 2008. Kinetochore-microtubule attachment relies on the disordered N-terminal tail domain of Hec1. *Curr. Biol.* 18:1778–1784.

Hayashi, I., and M. Ikura. 2003. Crystal structure of the amino-terminal microtubule-binding domain of end-binding protein 1 (EB1). *J. Biol. Chem.* 278:36430–36434.

Hayashi, I., A. Wilde, T.K. Mal, and M. Ikura. 2005. Structural basis for the activation of microtubule assembly by the EB1 and p150Glued complex. *Mol. Cell.* 19:449–460.

Honnappa, S., C.M. John, D. Kostrewa, F.K. Winkler, and M.O. Steinmetz. 2005. Structural insights into the EB1-APC interaction. *EMBO J.* 24:261–269.

Hwang, E., J. Kusch, Y. Barral, and T.C. Huffaker. 2003. Spindle orientation in *Saccharomyces cerevisiae* depends on the transport of microtubule ends along polarized actin cables. *J. Cell Biol.* 161:483–488.

Khmelinskii, A., C. Lawrence, J. Roostalu, and E. Schiebel. 2007. Cdc14-regulated midzone assembly controls anaphase B. *J. Cell Biol.* 177:981–993.

Kinoshita, E., E. Kinoshita-Kikuta, K. Takiyama, and T. Koike. 2006. Phosphate-binding tag, a new tool to visualize phosphorylated proteins. *Mol. Cell. Proteomics.* 5:749–757.

Komarova, Y., C.O. De Groot, I. Grigoriev, S.M. Gouveia, E.L. Munteanu, J.M. Schober, S. Honnappa, R.M. Buey, C.C. Hoogenraad, M. Dogterom, et al. 2009. Mammalian end binding proteins control persistent microtubule growth. *J. Cell Biol.* 184:691–706.

Kotwaliwale, C.V., S.B. Frei, B.M. Stern, and S. Biggins. 2007. A pathway containing the Ipl1/aurora protein kinase and the spindle midzone protein Ase1 regulates yeast spindle assembly. *Dev. Cell.* 13:433–445.

Lansbergen, G., and A. Akhmanova. 2006. Microtubule plus end: a hub of cellular activities. *Traffic.* 7:499–507.

Miller, S.A., M.L. Johnson, and P.T. Stukenberg. 2008. Kinetochore attachments require an interaction between unstructured tails on microtubules and Ndc80(Hec1). *Curr. Biol.* 18:1785–1791.

Norden, C., M. Mendoza, J. Dobbelaere, C.V. Kotwaliwale, S. Biggins, and Y. Barral. 2006. The NoCut pathway links completion of cytokinesis to spindle midzone function to prevent chromosome breakage. *Cell.* 125:85–98.

Sandblad, L., K.E. Busch, P. Tittmann, H. Gross, D. Brunner, and A. Hoenger. 2006. The *Schizosaccharomyces pombe* EB1 homolog Mal3p binds and stabilizes the microtubule lattice seam. *Cell.* 127:1415–1424.

Serber, Z., and J.E. Ferrell Jr. 2007. Tuning bulk electrostatics to regulate protein function. *Cell.* 128:441–444.

Slep, K.C., and R.D. Vale. 2007. Structural basis of microtubule plus end tracking by XMAP215, CLIP-170, and EB1. *Mol. Cell.* 27:976–991.

Slep, K.C., S.L. Rogers, S.L. Elliott, H. Ohkura, P.A. Kolodziej, and R.D. Vale. 2005. Structural determinants for EB1-mediated recruitment of APC and spectraplakins to the microtubule plus end. *J. Cell Biol.* 168:587–598.

Sun, L., J. Gao, X. Dong, M. Liu, D. Li, X. Shi, J.T. Dong, X. Lu, C. Liu, and J. Zhou. 2008. EB1 promotes Aurora-B kinase activity through blocking its inactivation by protein phosphatase 2A. *Proc. Natl. Acad. Sci. USA.* 105:7153–7158.

Tanaka, T.U., and A. Desai. 2008. Kinetochore-microtubule interactions: the means to the end. *Curr. Opin. Cell Biol.* 20:53–63.

Tanaka, T.U., M.J. Stark, and K. Tanaka. 2005. Kinetochore capture and bi-orientation on the mitotic spindle. *Nat. Rev. Mol. Cell Biol.* 6:929–942.

Vaughan, K.T. 2005. TIP maker and TIP marker; EB1 as a master controller of microtubule plus ends. *J. Cell Biol.* 171:197–200.

Vitre, B., F.M. Coquelle, C. Heichette, C. Garnier, D. Chrétien, and I. Arnal. 2008. EB1 regulates microtubule dynamics and tubulin sheet closure in vitro. *Nat. Cell Biol.* 10:415–421.

Wei, R.R., J. Al-Bassam, and S.C. Harrison. 2007. The Ndc80/HEC1 complex is a contact point for kinetochore-microtubule attachment. *Nat. Struct. Mol. Biol.* 14:54–59.

Westermann, S., H.W. Wang, A. Avila-Sakar, D.G. Drubin, E. Nogales, and G. Barnes. 2006. The Dam1 kinetochore ring complex moves processively on depolymerizing microtubule ends. *Nature.* 440:565–569.

Westermann, S., D.G. Drubin, and G. Barnes. 2007. Structures and functions of yeast kinetochore complexes. *Annu. Rev. Biochem.* 76:563–591.

Wilson-Kubalek, E.M., I.M. Cheeseman, C. Yoshioka, A. Desai, and R.A. Milligan. 2008. Orientation and structure of the Ndc80 complex on the microtubule lattice. *J. Cell Biol.* 182:1055–1061.

Wong, J., Y. Nakajima, S. Westermann, C. Shang, J.S. Kang, C. Goodner, P. Houshmand, S. Fields, C.S. Chan, D. Drubin, et al. 2007. A protein interaction map of the mitotic spindle. *Mol. Biol. Cell.* 18:3800–3809.
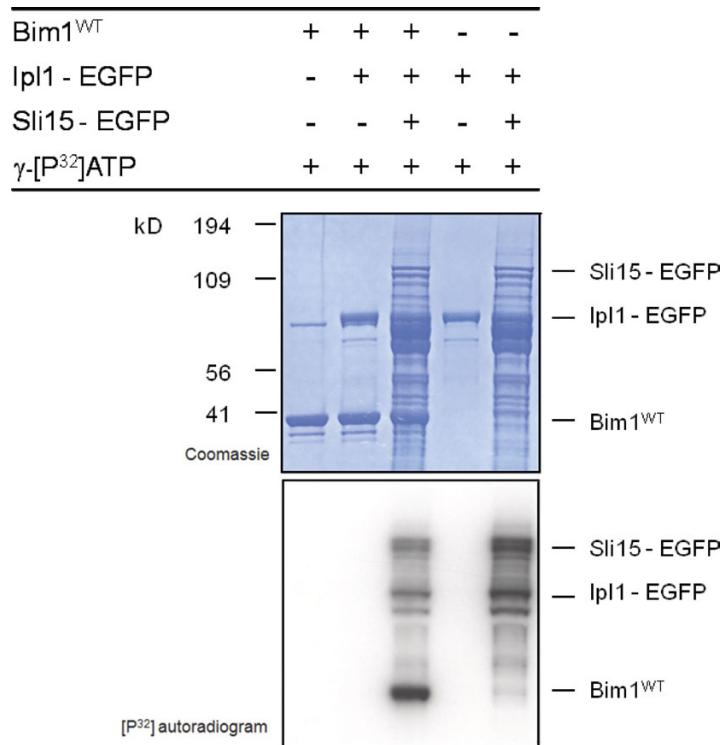
Supplemental material

Zimniak et al., http://www.jcb.org/cgi/content/full/jcb.200901036/DC1

Figure S1.   **Bim1p is phosphorylated by Ipl1p only in the presence of the activating protein Sli15p.** Coomassie-stained gel and autoradiography of kinase assay using Bim1p in combination with Ipl1-EGFP alone or after the addition of Sli15-EGFP. Ipl1 kinase alone is unable to phosphorylate either Bim1p or itself, but upon the addition of Sli15-EGFP, autophosphorylation of Ipl1p, phosphorylation of the activator Sli15p, and phosphorylation of Bim1p are detectable.
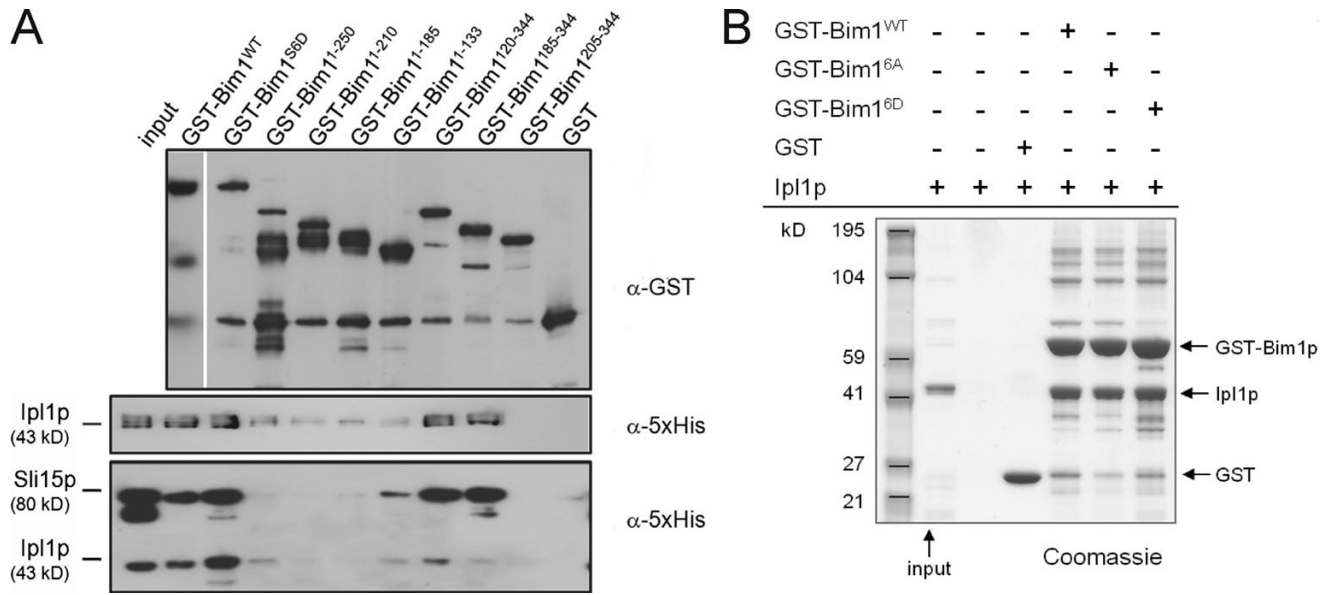
Figure S2. Mapping the Bim1p interaction with the Ipl1–Sli15 complex and Ipl1p. (A) Different N- and C-terminal truncations of Bim1p were expressed as GST fusion proteins in *E. coli* and used in pull-down assays either with His6-tagged recombinant Ipl1–Sli15 complex or with His6-tagged Ipl1p. Immobilized constructs were detected with an anti-GST antibody (top), and interacting proteins were detected with a 5× His antibody (bottom). The white line indicates that intervening lanes have been spliced out. (B) Coomassie-stained gel of the pull-down assay using GST-Bim1 phospho mutants and His6-tagged Ipl1p.
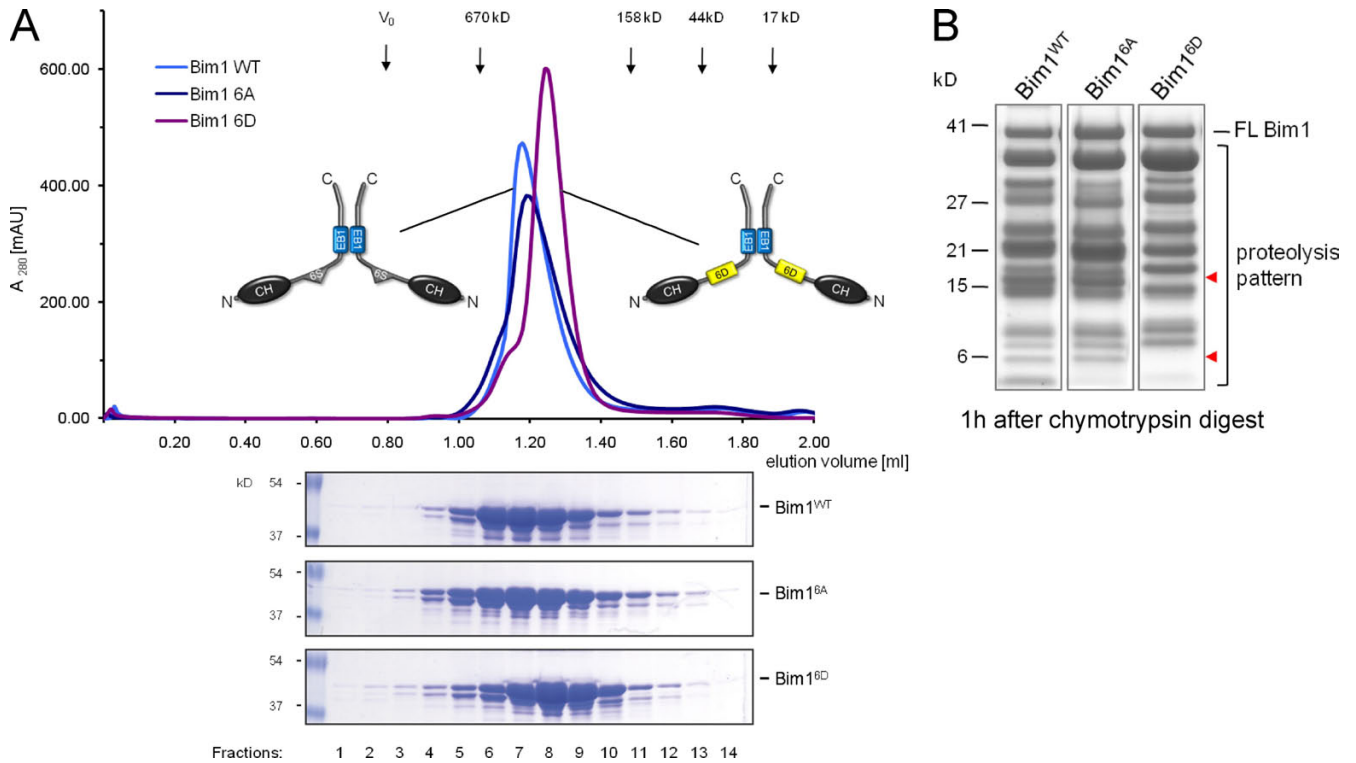

Figure S3. Characterization of WT and Ipl1-phosphorylated Bim1p in vitro. (A) SEC of different Bim1 variants on a Superdex 200 column. Coomassie-stained gels of the indicated fractions are shown below. Note the increased elution volume of the phosphomimicking Bim1^{6D} mutant. (B) Limited proteolysis of Bim1^{WT}, Bim1^{6A}, and Bim1^{6D} variants using chymotrypsin. A coomassie-stained gel showing products of limited proteolysis after 60 min is shown. Note the altered digestion pattern in the 6D mutant. Arrowheads point to altered proteolysis patterns of the Bim1^{6D} mutant. FL, full length.
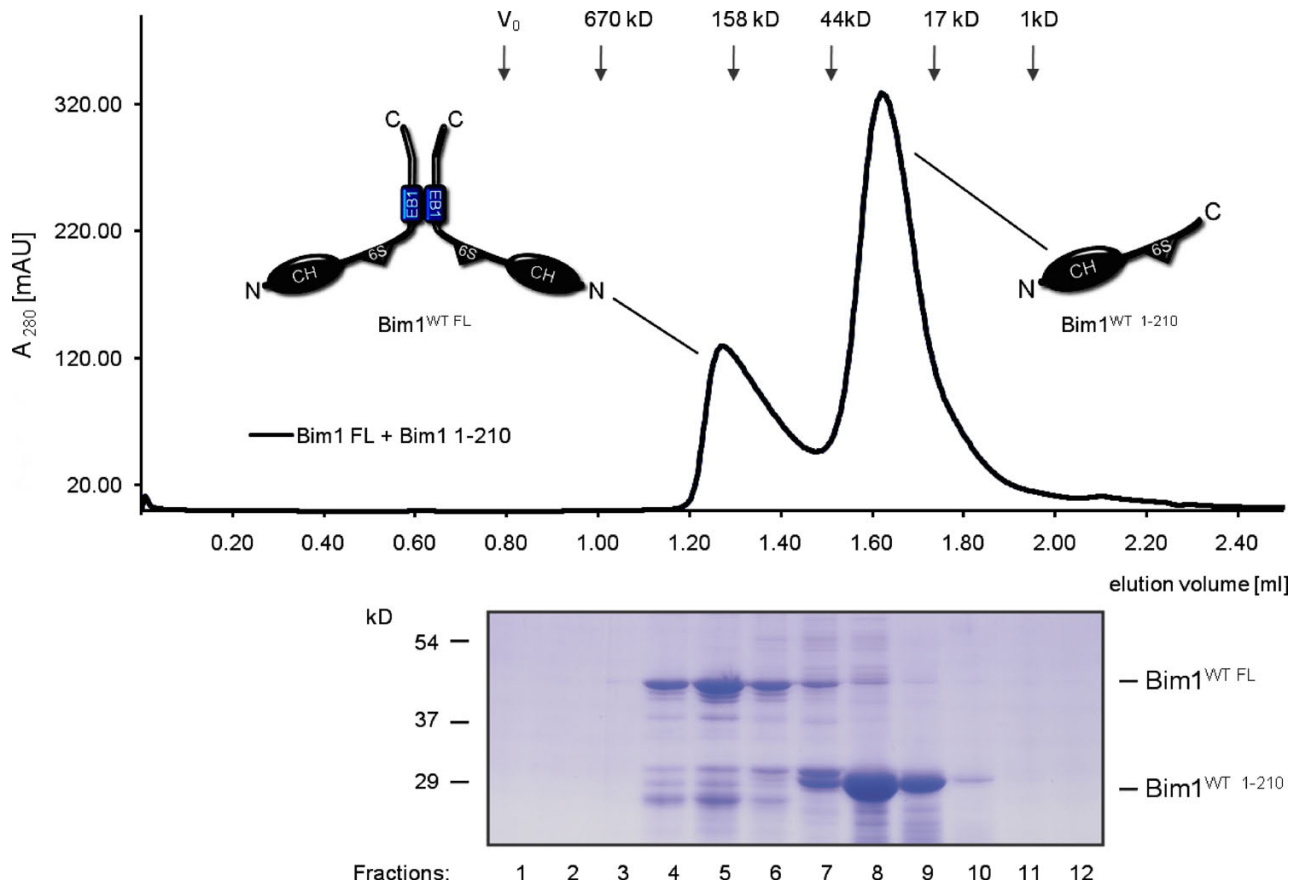
Figure S4.   **Analytical SEC of full-length Bim1p and monomeric Bim1$^{1-210}$.** Recombinant Bim1$^{1-344}$ and Bim1$^{1-210}$ were combined and separated together on a Superdex 200 PC 3.2/30 column. Bim1 full-length (FL) elutes early, suggesting an elongated dimeric shape, and elimination of the last 134 residues of Bim1p (Bim1$^{1-210}$) prevents dimerization. Note that these two variants elute separately, showing that they do not interact with each other.
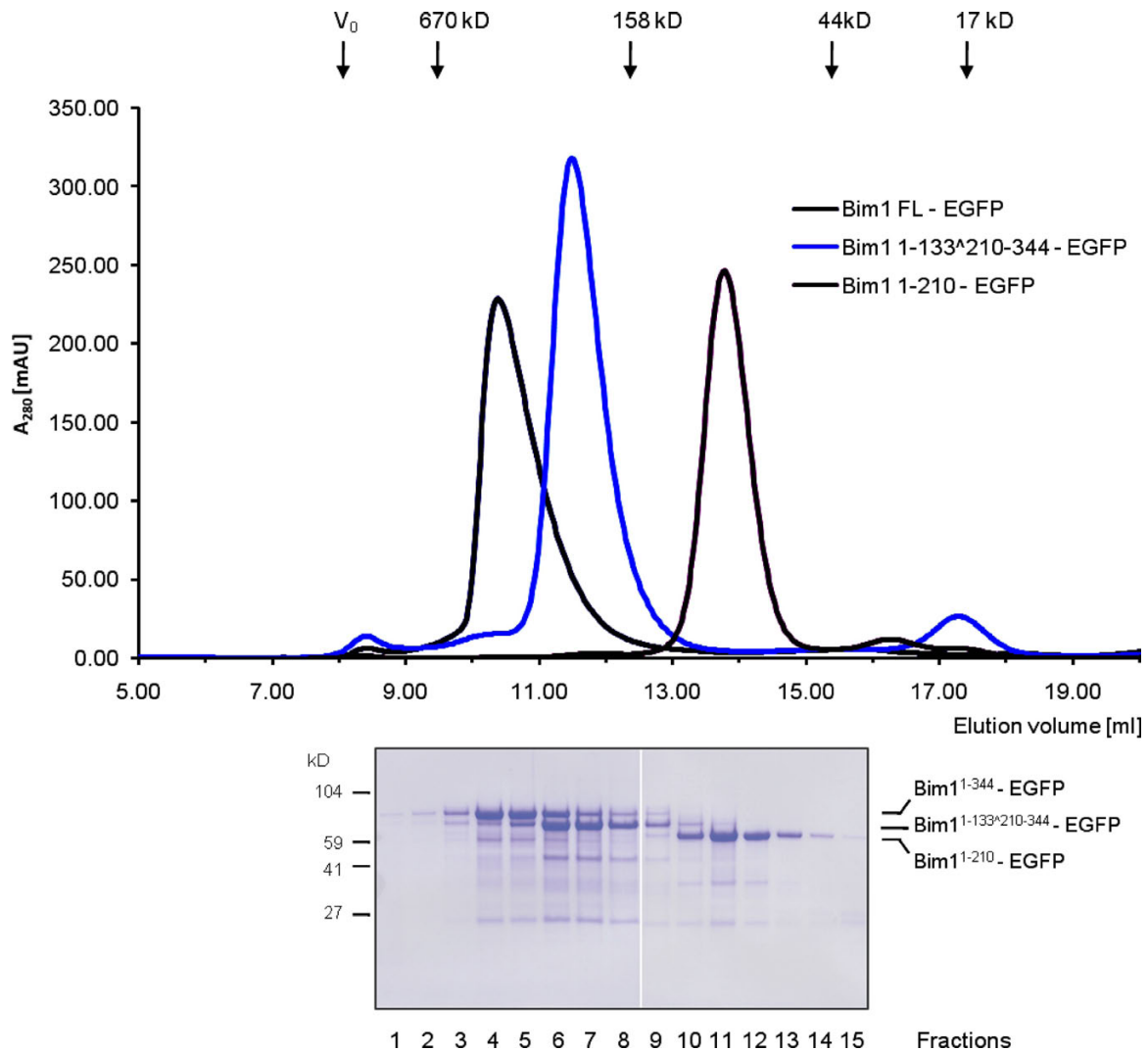
Figure S5. **Analytical SEC of the full-length Bim1-EGFP, Bim1[1–133^210–344]-EGFP, and Bim1[1–210]-EGFP.** Elution profiles and Coomassie-stained gel of the indicated proteins separated individually on a Superdex 200 PC 3.2/30 column. Elimination of the Bim1 linker region shifts the elution profile toward a smaller molecular mass but does not change its dimeric properties. The white line indicates that this blot is a composite of two gels. FL, full length.
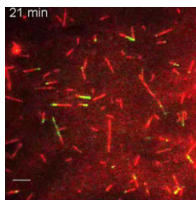
Video 1. **Autonomous MT plus end tracking of Bim1-EGFP in vitro.** Dynamic MT growth was induced from stable GMPCPP seeds in the presence of rhodamine-labeled tubulin (red) and 70 nM Bim1-EGFP (green). Dynamic MT polymerization and Bim1 plus end tracking was visualized using two-color TIRF microscopy. Images were recorded every 5 s. A kymograph from this video is shown in Fig. 5 C (left). The video is shown at 30 frames/s. Bar, 6 µm.
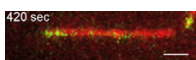
Video 2. **Plus end association of Bim1-EGFP on an individual dynamic MT.** GMPCPP MT seeds initiating MT growth were observed in the presence of rhodamine-labeled tubulin (red) and 70 nM Bim1-EGFP (green). TIRF images were recorded at 5-s intervals. A single MT from the experiment is shown. The video is shown at 20 frames/s. Bar, 4 µm.
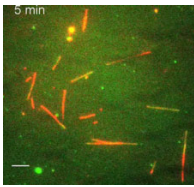
Video 3. **The monomeric Bim1$^{1–210}$–EGFP shows weak MT lattice binding.** MT growth is induced from stable GMPCPP MT seeds in the presence of rhodamine-labeled tubulin (red) and 1 µM Bim1$^{1–210}$-EGFP (green). TIRF images were recorded every 5 s, showing reduced Bim1$^{1–210}$-EGFP association with MTs. A kymograph from this video is shown in Fig. 5 C (right). The video is shown at 25 frames/s. Bar, 6 µm.
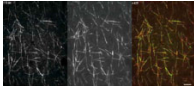

Video 4. **Ipl1–Sli15 phosphorylation removes Bim1–Alexa Fluor 488 from stable MTs.** Taxol-stabilized, rhodamine-labeled MTs (middle) were adhered to the coverslip, followed by incubation with Bim1–Alexa Fluor 488 and wash out of unbound protein. Under these conditions, Bim1p binds all along the MT lattice. Subsequently, reaction buffer containing 0.5 µM of the Ipl1–Sli15 complex was introduced into the flow chamber. TIRF images were recorded at 2-s intervals, and after ∼100 s, 0.5 mM ATP was injected into reaction chamber. The Bim1–Alexa Fluor 488 signal (left) is rapidly disappearing from MTs. The video is shown at 10 frames/s. Bar, 8 µm.
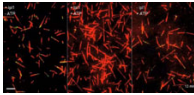
Video 5. **Ipl1–Sli15 phosphorylation removes Bim1-EGFP from dynamic MT plus ends.** MT growth is induced from stable GMPCPP seeds in the presence of rhodamine-labeled tubulin (red), 70 nM Bim1-EGFP (green), 1 µM of unlabeled Ipl1–Sli15 complex, and 0.5 mM ATP, as indicated at the top of the panels. The Bim1-EGFP signal is rapidly lost from MT tips in the presence of the kinase complex and ATP (middle). TIRF images were recorded at 5-s intervals. The video is shown at 30 frames/s. Bar, 6 µm.
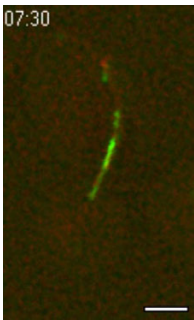
Video 6. **Dynamic localization of Bim1^{WT}–3× GFP on the anaphase spindle.** *BIM1* was C-terminally tagged with 3× GFP and visualized together with mCherry-Tub1 by live cell Deltavision microscopy. z stacks (eight stacks 0.35 µm apart) were acquired at 15-s intervals, deconvoluted, and projected into 2D images. Note the decreasing Bim1–3× GFP (green) signal at the spindle midzone before the spindle disassembly (red). The video is shown at 10 frames/s. Bar, 2 µm.
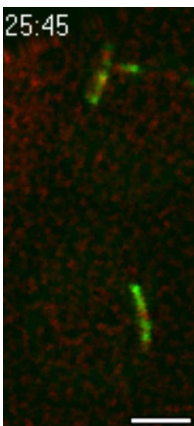
Video 7. **The Bim1^{6A}–3× GFP phospho mutant persists on the disassembling spindle.** The Bim1^{6A}–3× GFP phospho mutant and mCherry-Tub1 were visualized by live cell Deltavision microscopy. z stacks (eight stacks 0.35 µM apart) were acquired at 15-s intervals, deconvoluted, and projected into 2D images. Note the prominent Bim1^{6A}–3× GFP (green) signals remaining on the MTs after spindle disassembly (red). The video is shown at 10 frames/s. Bar, 2 µm.
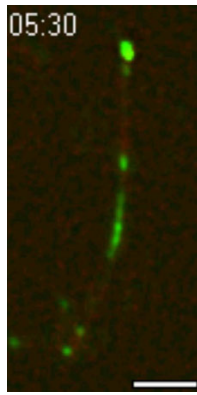
Video 8.   **The Bim1⁶ᴬ–3× GFP phospho mutant persists on the disassembling spindle.** The Bim1⁶ᴬ–3× GFP phospho mutant and mCherry-Tub1 were visualized by live cell Deltavision microscopy. z stacks (eight stacks 0.35 μM apart) were acquired at 15-s intervals, deconvoluted, and projected into 2D images. Note the example of polymerization and spindle bending. The video is shown at 10 frames/s. Bar, 2 μm.
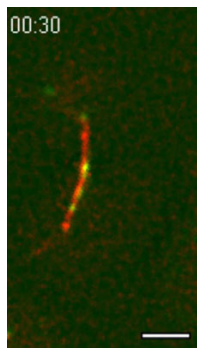
Video 9.   **The Bim1⁶ᴰ–3× GFP phospho mutant localizes weakly to the midzone and disassembles efficiently.** The Bim1⁶ᴰ–3× GFP phospho mutant and mCherry-Tub1 were visualized by live cell Deltavision microscopy. z stacks (eight stacks 0.35 μM apart) were acquired at 15-s intervals, deconvoluted, and projected into 2D images. The video is shown at 10 frames/s. Bar, 2 μm.

Table S1.   **Yeast strains used in this study**

Strain number	Genotype
SWY 167	*Mat a, leu2, ura3-52, trp1, prb1-1122, pep4-3, pre1-451, Bim1–S-Tag-TEV-ZZ::KanMX*
TZY 39	*Mat α, his3Δ200, leu2-Δ1, ura3-52, ade2-101, lys2-801, TUB1-LYS2, bim1Δ::URA3, BIM1–3× GFP::HISMX5*
TZY 40	*Mat α, his3Δ200, leu2-Δ1, ura3-52, ade2-101, lys2-801, TUB1-LYS2, bim1Δ::URA3, bim1⁶ᴬ–3× GFP::HISMX5*
TZY 41	*Mat α, his3Δ200, leu2-Δ1, ura3-52, ade2-101, lys2-801, TUB1-LYS2, bim1Δ::URA3, bim1⁶ᴰ–3× GFP::HISMX5*
TZY 114	*Mat a, his3Δ200, leu2-3,112, lys2-801, trp1-1, BIM1ᵂᵀ::KanMX, GFP-Tub1::URA*
TZY 115	*Mat a, his3Δ200, leu2-3,112, lys2-801, trp1-1, bim1⁶ᴬ::KanMX, GFP-Tub1::URA*
TZY 116	*Mat a, his3Δ200, leu2-3,112, lys2-801, trp1-1, bim1⁶ᴰ::KanMX, GFP-Tub1::URA*
TZY 143	*Mat α, his3Δ200, leu2-3,112, lys2-801, trp1-1, bim1Δ::KanMX, mCherry-Tub1::URA, BIM1ᵂᵀ–3× GFP::HISMX5*
TZY 144	*Mat α, his3Δ200, leu2-3,112, lys2-801, trp1-1, bim1Δ::KanMX, mCherry-Tub1::URA, bim1⁶ᴬ–3× GFP::HISMX5*
TZY 145	*Mat α, his3Δ200, leu2-3,112, lys2-801, trp1-1, bim1Δ::KanMX, mCherry-Tub1::URA, bim1⁶ᴰ–3× GFP::HISMX5*
TZY 146	*Mat a, his3Δ200, leu2-3,112, lys2-801, trp1-1, bim1Δ::KanMX, GFP-Tub1::URA*

9. Abbreviations

amp	ampicilin
ATP	adenosine tri-phosphate
a.u.	arbitrary units
bp	base pairs
BSA	bovine serum albumin
DMSO	dimethylsulfoxyde
DTT	dithiothreithol
EDTA	ethylenediamine tetraacetic acid
EGTA	ethylene glycol tetraacetic acid
FL	full length
GFP	green fluorescence protein
GMPCPP	guanosine 5'-[α,β-methylene]triphosphate
GST	gluthatione-S-transferase
GTP	guanosine tri-phosphate
h	hour
IPTG	isopropyl β-D-1-thiogalactopyranoside
kDa	kilo Dalton
LB	Luria-Bertani medium
min	minute
MTs	microtubules
Ni-NTA	nickel-nitrilotriacetic acid
PAGE	polyacrylamide gel electrophoresis
PBS	phosphate buffered saline
PCR	polymerase chain reaction
PEG	polyethylenglycole
rpm	revolutions per minute
SEM	standard error of the mean
SDS	sodium dodecyl sulphate
TBS	tris-buffered saline
TBS-T	tris-buffered saline with Tween 20

Abbreviations

TEV	tobacco etch virus
TIRF	total internal reflection fluorescence microscopy
WB	western blot
WT	wild type
YPD	yeast extract peptrone dextrose

10. References

Akhmanova, A., C.C. Hoogenraad, K. Drabek, T. Stepanova, B. Dortland, T. Verkerk, W. Vermeulen, B.M. Burgering, C.I. De Zeeuw, F. Grosveld, and N. Galjart. 2001. Clasps are CLIP-115 and -170 associating proteins involved in the regional regulation of microtubule dynamics in motile fibroblasts. *Cell*. 104:923-35.

Akhmanova, A., and M.O. Steinmetz. 2008. Tracking the ends: a dynamic protein network controls the fate of microtubule tips. *Nat Rev Mol Cell Biol*. 9:309-22.

Al-Bassam, J., N.A. Larsen, A.A. Hyman, and S.C. Harrison. 2007. Crystal structure of a TOG domain: conserved features of XMAP215/Dis1-family TOG domains and implications for tubulin binding. *Structure*. 15:355-62.

Amos, L., and A. Klug. 1974. Arrangement of subunits in flagellar microtubules. *J Cell Sci*. 14:523-49.

Andrews, P.D., Y. Ovechkina, N. Morrice, M. Wagenbach, K. Duncan, L. Wordeman, and J.R. Swedlow. 2004. Aurora B regulates MCAK at the mitotic centromere. *Dev Cell*. 6:253-68.

Badin-Larcon, A.C., C. Boscheron, J.M. Soleilhac, M. Piel, C. Mann, E. Denarier, A. Fourest-Lieuvin, L. Lafanechere, M. Bornens, and D. Job. 2004. Suppression of nuclear oscillations in Saccharomyces cerevisiae expressing Glu tubulin. *Proc Natl Acad Sci U S A*. 101:5577-82.

Ban, R., H. Matsuzaki, T. Akashi, G. Sakashita, H. Taniguchi, S.Y. Park, H. Tanaka, K. Furukawa, and T. Urano. 2009. Mitotic regulation of the stability of microtubule plus-end tracking protein EB3 by ubiquitin ligase SIAH-1 and Aurora mitotic kinases. *J Biol Chem*. 284:28367-81.

Beardmore, V.A., L.J. Ahonen, G.J. Gorbsky, and M.J. Kallio. 2004. Survivin dynamics increases at centromeres during G2/M phase transition and is regulated by microtubule-attachment and Aurora B kinase activity. *J Cell Sci*. 117:4033-42.

Bieling, P., S. Kandels-Lewis, I.A. Telley, J. van Dijk, C. Janke, and T. Surrey. 2008. CLIP-170 tracks growing microtubule ends by dynamically recognizing composite EB1/tubulin-binding sites. *J Cell Biol*. 183:1223-33.

Bieling, P., L. Laan, H. Schek, E.L. Munteanu, L. Sandblad, M. Dogterom, D. Brunner, and T. Surrey. 2007. Reconstitution of a microtubule plus-end tracking system in vitro. *Nature*. 450:1100-5.

Brouhard, G.J., J.H. Stear, T.L. Noetzel, J. Al-Bassam, K. Kinoshita, S.C. Harrison, J. Howard, and A.A. Hyman. 2008. XMAP215 is a processive microtubule polymerase. *Cell*. 132:79-88.

Bu, W., and L.K. Su. 2003. Characterization of functional domains of human EB1 family proteins. *J Biol Chem*. 278:49721-31.

Buvelot, S., S.Y. Tatsutani, D. Vermaak, and S. Biggins. 2003. The budding yeast Ipl1/Aurora protein kinase regulates mitotic spindle disassembly. *J Cell Biol*. 160:329-39.

Cassimeris, L., and C. Spittle. 2001. Regulation of microtubule-associated proteins. *Int Rev Cytol*. 210:163-226.

References

Cheeseman, I.M., S. Anderson, M. Jwa, E.M. Green, J. Kang, J.R. Yates, 3rd, C.S. Chan, D.G. Drubin, and G. Barnes. 2002. Phospho-regulation of kinetochore-microtubule attachments by the Aurora kinase Ipl1p. *Cell*. 111:163-72.

Cheeseman, I.M., J.S. Chappie, E.M. Wilson-Kubalek, and A. Desai. 2006. The conserved KMN network constitutes the core microtubule-binding site of the kinetochore. *Cell*. 127:983-97.

Ciferri, C., S. Pasqualato, E. Screpanti, G. Varetti, S. Santaguida, G. Dos Reis, A. Maiolica, J. Polka, J.G. De Luca, P. De Wulf, M. Salek, J. Rappsilber, C.A. Moores, E.D. Salmon, and A. Musacchio. 2008. Implications for kinetochore-microtubule attachment from the structure of an engineered Ndc80 complex. *Cell*. 133:427-39.

des Georges, A., M. Katsuki, D.R. Drummond, M. Osei, R.A. Cross, and L.A. Amos. 2008. Mal3, the Schizosaccharomyces pombe homolog of EB1, changes the microtubule lattice. *Nat Struct Mol Biol*. 15:1102-8.

Desai, A., and T.J. Mitchison. 1997. Microtubule polymerization dynamics. *Annu Rev Cell Dev Biol*. 13:83-117.

Dewar, H., K. Tanaka, K. Nasmyth, and T.U. Tanaka. 2004. Tension between two kinetochores suffices for their bi-orientation on the mitotic spindle. *Nature*. 428:93-7.

Djinovic Carugo, K., S. Banuelos, and M. Saraste. 1997. Crystal structure of a calponin homology domain. *Nat Struct Biol*. 4:175-9.

Dougherty, G.W., H.J. Adler, A. Rzadzinska, M. Gimona, Y. Tomita, M.C. Lattig, R.C. Merritt, Jr., and B. Kachar. 2005. CLAMP, a novel microtubule-associated protein with EB-type calponin homology. *Cell Motil Cytoskeleton*. 62:141-56.

Drechsel, D.N., and M.W. Kirschner. 1994. The minimum GTP cap required to stabilize microtubules. *Curr Biol*. 4:1053-61.

Dujardin, D., U.I. Wacker, A. Moreau, T.A. Schroer, J.E. Rickard, and J.R. De Mey. 1998. Evidence for a role of CLIP-170 in the establishment of metaphase chromosome alignment. *J Cell Biol*. 141:849-62.

Eckley, D.M., A.M. Ainsztein, A.M. Mackay, I.G. Goldberg, and W.C. Earnshaw. 1997. Chromosomal proteins and cytokinesis: patterns of cleavage furrow formation and inner centromere protein positioning in mitotic heterokaryons and mid-anaphase cells. *J Cell Biol*. 136:1169-83.

Endow, S.A., S.J. Kang, L.L. Satterwhite, M.D. Rose, V.P. Skeen, and E.D. Salmon. 1994. Yeast Kar3 is a minus-end microtubule motor protein that destabilizes microtubules preferentially at the minus ends. *EMBO J*. 13:2708-13.

Erickson, H.P., and E.T. O'Brien. 1992. Microtubule dynamic instability and GTP hydrolysis. *Annu Rev Biophys Biomol Struct*. 21:145-66.

Gadea, B.B., and J.V. Ruderman. 2006. Aurora B is required for mitotic chromatin-induced phosphorylation of Op18/Stathmin. *Proc Natl Acad Sci U S A*. 103:4493-8.

Gardner, M.K., J. Haase, K. Mythreye, J.N. Molk, M. Anderson, A.P. Joglekar, E.T. O'Toole, M. Winey, E.D. Salmon, D.J. Odde, and K. Bloom. 2008. The microtubule-based motor Kar3 and plus end-binding protein Bim1 provide structural support for the anaphase spindle. *J Cell Biol*. 180:91-100.

Geraldo, S., U.K. Khanzada, M. Parsons, J.K. Chilton, and P.R. Gordon-Weeks. 2008. Targeting of the F-actin-binding protein drebrin by the microtubule plus-tip protein EB3 is required for neuritogenesis. *Nat Cell Biol.* 10:1181-9.

Gimona, M., K. Djinovic-Carugo, W.J. Kranewitter, and S.J. Winder. 2002. Functional plasticity of CH domains. *FEBS Lett.* 513:98-106.

Goshima, G., F. Nedelec, and R.D. Vale. 2005. Mechanisms for focusing mitotic spindle poles by minus end-directed motor proteins. *J Cell Biol.* 171:229-40.

Gruneberg, U., R. Neef, R. Honda, E.A. Nigg, and F.A. Barr. 2004. Relocation of Aurora B from centromeres to the central spindle at the metaphase to anaphase transition requires MKlp2. *J Cell Biol.* 166:167-72.

Guimaraes, G.J., Y. Dong, B.F. McEwen, and J.G. Deluca. 2008. Kinetochore-microtubule attachment relies on the disordered N-terminal tail domain of Hec1. *Curr Biol.* 18:1778-84.

Gupta, M.L., Jr., P. Carvalho, D.M. Roof, and D. Pellman. 2006. Plus end-specific depolymerase activity of Kip3, a kinesin-8 protein, explains its role in positioning the yeast mitotic spindle. *Nat Cell Biol.* 8:913-23.

Hayashi, I., and M. Ikura. 2003. Crystal structure of the amino-terminal microtubule-binding domain of end-binding protein 1 (EB1). *J Biol Chem.* 278:36430-4.

Hayashi, I., M.J. Plevin, and M. Ikura. 2007. CLIP170 autoinhibition mimics intermolecular interactions with p150Glued or EB1. *Nat Struct Mol Biol.* 14:980-1.

Hayashi, I., A. Wilde, T.K. Mal, and M. Ikura. 2005. Structural basis for the activation of microtubule assembly by the EB1 and p150Glued complex. *Mol Cell.* 19:449-60.

Hestermann, A., and R. Graf. 2004. The XMAP215-family protein DdCP224 is required for cortical interactions of microtubules. *BMC Cell Biol.* 5:24.

Holt, L.J., B.B. Tuch, J. Villen, A.D. Johnson, S.P. Gygi, and D.O. Morgan. 2009. Global analysis of Cdk1 substrate phosphorylation sites provides insights into evolution. *Science.* 325:1682-6.

Honnappa, S., S.M. Gouveia, A. Weisbrich, F.F. Damberger, N.S. Bhavesh, H. Jawhari, I. Grigoriev, F.J. van Rijssel, R.M. Buey, A. Lawera, I. Jelesarov, F.K. Winkler, K. Wuthrich, A. Akhmanova, and M.O. Steinmetz. 2009. An EB1-binding motif acts as a microtubule tip localization signal. *Cell.* 138:366-76.

Honnappa, S., C.M. John, D. Kostrewa, F.K. Winkler, and M.O. Steinmetz. 2005. Structural insights into the EB1-APC interaction. *EMBO J.* 24:261-9.

Honnappa, S., O. Okhrimenko, R. Jaussi, H. Jawhari, I. Jelesarov, F.K. Winkler, and M.O. Steinmetz. 2006. Key interaction modes of dynamic +TIP networks. *Mol Cell.* 23:663-71.

Juang, Y.L., J. Huang, J.M. Peters, M.E. McLaughlin, C.Y. Tai, and D. Pellman. 1997. APC-mediated proteolysis of Ase1 and the morphogenesis of the mitotic spindle. *Science.* 275:1311-4.

Kang, J., I.M. Cheeseman, G. Kallstrom, S. Velmurugan, G. Barnes, and C.S. Chan. 2001. Functional cooperation of Dam1, Ipl1, and the inner centromere protein (INCENP)-related protein Sli15 during chromosome segregation. *J Cell Biol.* 155:763-74.

Kiermaier, E., S. Woehrer, Y. Peng, K. Mechtler, and S. Westermann. 2009. A Dam1-based artificial kinetochore is sufficient to promote chromosome segregation in budding yeast. *Nat Cell Biol.* 11:1109-15.

References

Kikkawa, M., T. Ishikawa, T. Nakata, T. Wakabayashi, and N. Hirokawa. 1994. Direct visualization of the microtubule lattice seam both in vitro and in vivo. *J Cell Biol*. 127:1965-71.

Kim, J.H., J.S. Kang, and C.S. Chan. 1999. Sli15 associates with the ipl1 protein kinase to promote proper chromosome segregation in Saccharomyces cerevisiae. *J Cell Biol*. 145:1381-94.

Kinoshita, E., E. Kinoshita-Kikuta, K. Takiyama, and T. Koike. 2006. Phosphate-binding tag, a new tool to visualize phosphorylated proteins. *Mol Cell Proteomics*. 5:749-57.

Komarova, Y., C.O. De Groot, I. Grigoriev, S.M. Gouveia, E.L. Munteanu, J.M. Schober, S. Honnappa, R.M. Buey, C.C. Hoogenraad, M. Dogterom, G.G. Borisy, M.O. Steinmetz, and A. Akhmanova. 2009. Mammalian end binding proteins control persistent microtubule growth. *J Cell Biol*. 184:691-706.

Kotwaliwale, C.V., S.B. Frei, B.M. Stern, and S. Biggins. 2007. A pathway containing the Ipl1/aurora protein kinase and the spindle midzone protein Ase1 regulates yeast spindle assembly. *Dev Cell*. 13:433-45.

Lampert, F., P. Hornung, and S. Westermann 2010. The Dam1 complex confers microtubule plus-end tracking actvity to the Ndc80 kinetochore complex. *Journal of Cell Biology*. In press.

Lampson, M.A., K. Renduchitala, A. Khodjakov, and T.M. Kapoor. 2004. Correcting improper chromosome-spindle attachments during cell division. *Nat Cell Biol*. 6:232-7.

Lan, W., X. Zhang, S.L. Kline-Smith, S.E. Rosasco, G.A. Barrett-Wilt, J. Shabanowitz, D.F. Hunt, C.E. Walczak, and P.T. Stukenberg. 2004. Aurora B phosphorylates centromeric MCAK and regulates its localization and microtubule depolymerization activity. *Curr Biol*. 14:273-86.

Lansbergen, G., Y. Komarova, M. Modesti, C. Wyman, C.C. Hoogenraad, H.V. Goodson, R.P. Lemaitre, D.N. Drechsel, E. van Munster, T.W. Gadella, Jr., F. Grosveld, N. Galjart, G.G. Borisy, and A. Akhmanova. 2004. Conformational changes in CLIP-170 regulate its binding to microtubules and dynactin localization. *J Cell Biol*. 166:1003-14.

Lee, L., J.S. Tirnauer, J. Li, S.C. Schuyler, J.Y. Liu, and D. Pellman. 2000. Positioning of the mitotic spindle by a cortical-microtubule capture mechanism. *Science*. 287:2260-2.

Lee, T., K.J. Langford, J.M. Askham, A. Bruning-Richardson, and E.E. Morrison. 2008. MCAK associates with EB1. *Oncogene*. 27:2494-500.

Longtine, M.S., A. McKenzie, 3rd, D.J. Demarini, N.G. Shah, A. Wach, A. Brachat, P. Philippsen, and J.R. Pringle. 1998. Additional modules for versatile and economical PCR-based gene deletion and modification in Saccharomyces cerevisiae. *Yeast*. 14:953-61.

Manna, T., S. Honnappa, M.O. Steinmetz, and L. Wilson. 2008. Suppression of microtubule dynamic instability by the +TIP protein EB1 and its modulation by the CAP-Gly domain of p150glued. *Biochemistry*. 47:779-86.

Miller, R.K., S.C. Cheng, and M.D. Rose. 2000. Bim1p/Yeb1p mediates the Kar9p-dependent cortical attachment of cytoplasmic microtubules. *Mol Biol Cell*. 11:2949-59.

Miller, S.A., M.L. Johnson, and P.T. Stukenberg. 2008. Kinetochore attachments require an interaction between unstructured tails on microtubules and Ndc80(Hec1). *Curr Biol*. 18:1785-91.

Mimori-Kiyosue, Y., I. Grigoriev, G. Lansbergen, H. Sasaki, C. Matsui, F. Severin, N. Galjart, F. Grosveld, I. Vorobjev, S. Tsukita, and A. Akhmanova. 2005. CLASP1 and CLASP2 bind to EB1 and regulate microtubule plus-end dynamics at the cell cortex. *J Cell Biol*. 168:141-53.

Mimori-Kiyosue, Y., I. Grigoriev, H. Sasaki, C. Matsui, A. Akhmanova, S. Tsukita, and I. Vorobjev. 2006. Mammalian CLASPs are required for mitotic spindle organization and kinetochore alignment. *Genes Cells*. 11:845-57.

Mishima, M., R. Maesaki, M. Kasa, T. Watanabe, M. Fukata, K. Kaibuchi, and T. Hako-shima. 2007. Structural basis for tubulin recognition by cytoplasmic linker protein 170 and its autoinhibition. *Proc Natl Acad Sci U S A*. 104:10346-51.

Mitchison, T., and M. Kirschner. 1984. Dynamic instability of microtubule growth. *Nature*. 312:237-42.

Moritz, M., M.B. Braunfeld, V. Guenebaut, J. Heuser, and D.A. Agard. 2000. Structure of the gamma-tubulin ring complex: a template for microtubule nucleation. *Nat Cell Biol*. 2:365-70.

Newton, C.N., M. Wagenbach, Y. Ovechkina, L. Wordeman, and L. Wilson. 2004. MCAK, a Kin I kinesin, increases the catastrophe frequency of steady-state HeLa cell microtubules in an ATP-dependent manner in vitro. *FEBS Lett*. 572:80-4.

Norden, C., M. Mendoza, J. Dobbelaere, C.V. Kotwaliwale, S. Biggins, and Y. Barral. 2006. The NoCut pathway links completion of cytokinesis to spindle midzone function to prevent chromosome breakage. *Cell*. 125:85-98.

Pereira, G., and E. Schiebel. 2003. Separase regulates INCENP-Aurora B anaphase spindle function through Cdc14. *Science*. 302:2120-4.

Perez, F., G.S. Diamantopoulos, R. Stalder, and T.E. Kreis. 1999. CLIP-170 highlights growing microtubule ends in vivo. *Cell*. 96:517-27.

Pierre, P., J. Scheel, J.E. Rickard, and T.E. Kreis. 1992. CLIP-170 links endocytic vesicles to microtubules. *Cell*. 70:887-900.

Rogers, S.L., G.C. Rogers, D.J. Sharp, and R.D. Vale. 2002. Drosophila EB1 is important for proper assembly, dynamics, and positioning of the mitotic spindle. *J Cell Biol*. 158:873-84.

Sandblad, L., K.E. Busch, P. Tittmann, H. Gross, D. Brunner, and A. Hoenger. 2006. The Schizosaccharomyces pombe EB1 homolog Mal3p binds and stabilizes the microtubule lattice seam. *Cell*. 127:1415-24.

Schwartz, K., K. Richards, and D. Botstein. 1997. BIM1 encodes a microtubule-binding protein in yeast. *Mol Biol Cell*. 8:2677-91.

Severin, F., B. Habermann, T. Huffaker, and T. Hyman. 2001. Stu2 promotes mitotic spindle elongation in anaphase. *J Cell Biol*. 153:435-42.

Shang, C., T.R. Hazbun, I.M. Cheeseman, J. Aranda, S. Fields, D.G. Drubin, and G. Barnes. 2003. Kinetochore protein interactions and their regulation by the Aurora kinase Ipl1p. *Mol Biol Cell*. 14:3342-55.

Slep, K.C. 2009. Structural and mechanistic insights into microtubule end-binding proteins. *Curr Opin Cell Biol*. 22:88-95.

References

Slep, K.C., S.L. Rogers, S.L. Elliott, H. Ohkura, P.A. Kolodziej, and R.D. Vale. 2005. Structural determinants for EB1-mediated recruitment of APC and spectraplakins to the microtubule plus end. *J Cell Biol*. 168:587-98.

Slep, K.C., and R.D. Vale. 2007. Structural basis of microtubule plus end tracking by XMAP215, CLIP-170, and EB1. *Mol Cell*. 27:976-91.

Steigemann, P., C. Wurzenberger, M.H. Schmitz, M. Held, J. Guizetti, S. Maar, and D.W. Gerlich. 2009. Aurora B-mediated abscission checkpoint protects against tetraploidization. *Cell*. 136:473-84.

Su, L.K., M. Burrell, D.E. Hill, J. Gyuris, R. Brent, R. Wiltshire, J. Trent, B. Vogelstein, and K.W. Kinzler. 1995. APC binds to the novel protein EB1. *Cancer Res*. 55:2972-7.

Su, L.K., and Y. Qi. 2001. Characterization of human MAPRE genes and their proteins. *Genomics*. 71:142-9.

Sun, L., J. Gao, X. Dong, M. Liu, D. Li, X. Shi, J.T. Dong, X. Lu, C. Liu, and J. Zhou. 2008. EB1 promotes Aurora-B kinase activity through blocking its inactivation by protein phosphatase 2A. *Proc Natl Acad Sci U S A*. 105:7153-8.

Tanaka, T.U., N. Rachidi, C. Janke, G. Pereira, M. Galova, E. Schiebel, M.J. Stark, and K. Nasmyth. 2002. Evidence that the Ipl1-Sli15 (Aurora kinase-INCENP) complex promotes chromosome bi-orientation by altering kinetochore-spindle pole connections. *Cell*. 108:317-29.

Tanenbaum, M.E., N. Galjart, M.A. van Vugt, and R.H. Medema. 2006. CLIP-170 facilitates the formation of kinetochore-microtubule attachments. *EMBO J*. 25:45-57.

Thomas, S., and K.B. Kaplan. 2007. A Bir1p Sli15p kinetochore passenger complex regulates septin organization during anaphase. *Mol Biol Cell*. 18:3820-34.

Tirnauer, J.S., E. O'Toole, L. Berrueta, B.E. Bierer, and D. Pellman. 1999. Yeast Bim1p promotes the G1-specific dynamics of microtubules. *J Cell Biol*. 145:993-1007.

Vaughan, K.T., and R.B. Vallee. 1995. Cytoplasmic dynein binds dynactin through a direct interaction between the intermediate chains and p150Glued. *J Cell Biol*. 131:1507-16.

Vinh, D.B., J.W. Kern, W.O. Hancock, J. Howard, and T.N. Davis. 2002. Reconstitution and characterization of budding yeast gamma-tubulin complex. *Mol Biol Cell*. 13:1144-57.

Vitre, B., F.M. Coquelle, C. Heichette, C. Garnier, D. Chretien, and I. Arnal. 2008. EB1 regulates microtubule dynamics and tubulin sheet closure in vitro. *Nat Cell Biol*. 10:415-21.

Wang, H.W., and E. Nogales. 2005. Nucleotide-dependent bending flexibility of tubulin regulates microtubule assembly. *Nature*. 435:911-5.

Watson, P., and D.J. Stephens. 2006. Microtubule plus-end loading of p150(Glued) is mediated by EB1 and CLIP-170 but is not required for intracellular membrane traffic in mammalian cells. *J Cell Sci*. 119:2758-67.

Wei, R.R., J. Al-Bassam, and S.C. Harrison. 2007. The Ndc80/HEC1 complex is a contact point for kinetochore-microtubule attachment. *Nat Struct Mol Biol*. 14:54-9.

Weisbrich, A., S. Honnappa, R. Jaussi, O. Okhrimenko, D. Frey, I. Jelesarov, A. Akhmanova, and M.O. Steinmetz. 2007. Structure-function relationship of CAP-Gly domains. *Nat Struct Mol Biol*. 14:959-67.

Westermann, S., H.W. Wang, A. Avila-Sakar, D.G. Drubin, E. Nogales, and G. Barnes. 2006. The Dam1 kinetochore ring complex moves processively on depolymerizing microtubule ends. *Nature.* 440:565-9.

Wilson-Kubalek, E.M., I.M. Cheeseman, C. Yoshioka, A. Desai, and R.A. Milligan. 2008. Orientation and structure of the Ndc80 complex on the microtubule lattice. *J Cell Biol.* 182:1055-61.

Winey, M., C.L. Mamay, E.T. O'Toole, D.N. Mastronarde, T.H. Giddings, Jr., K.L. McDonald, and J.R. McIntosh. 1995. Three-dimensional ultrastructural analysis of the Saccharomyces cerevisiae mitotic spindle. *J Cell Biol.* 129:1601-15.

Wong, J., Y. Nakajima, S. Westermann, C. Shang, J.S. Kang, C. Goodner, P. Houshmand, S. Fields, C.S. Chan, D. Drubin, G. Barnes, and T. Hazbun. 2007. A protein interaction map of the mitotic spindle. *Mol Biol Cell.* 18:3800-9.

Zanic, M., J.H. Stear, A.A. Hyman, and J. Howard. 2009. EB1 recognizes the nucleotide state of tubulin in the microtubule lattice. *PLoS One.* 4:e7585.

11. Acknowledgements

I would like to thank Stefan for his constant support and the scientific guidance during my PhD.

I am grateful to all members of the Westermann Lab for lots of help, inspiring discussions and spending time together in a friendly and creative atmosphere.

I would also like to acknowledge members of the Peters, Cowan, Clausen and Stolt-Bergner Labs for support and help during my project.

Dziękuje swoim ukochanym rodziciom i siostrze za wszystkie życzliwe słowa, wiare i ciągłe wsparcie.

12. Curriculum vitae

Personal information:

Name: Tomasz Zimniak
Nationality: Polish
Date of Birth: 8th March 1982
Place of Birth: Lubsko, Poland
Email: zimniak@imp.ac.at
Language skills: Polish, English, German

Education:

2006- present	*University of Vienna, Austria* PhD study in Molecular Biology Thesis: "Molecular insights into the function and regulation of the budding yeast EB1 homolog Bim1p "
2006	*University of Wroclaw, Institute of Biochemistry and Molecular Biology, Poland* Magister in Biotechnology – Molecular Biology Thesis: "Interactions *in vivo* and *in vitro* of chromosome partitioning proteins ParA and ParB from *Mycobacterium tuberculosis*"
2004	*University of Wroclaw, Institute of Biochemistry and Molecular Biology, Poland* B.Sc. in Biotechnology Thesis: "Application of viral vectors in gene therapy"

Research experience:

2006– present	*Research institute of Molecular Pathology, Vienna, Austria* PhD thesis in the laboratory of Dr. Stefan Westermann
2004-2006	*Polish Academy of Science, L. Hirszfeld Institute of Immunology and Experimental Therapy, Laboratory of Molecular Biology of Microorganisms, Wroclaw, Poland* Master Thesis : "Interactions *in vivo* and *in vitro* of chromosome partitioning proteins ParA and ParB from *Mycobacterium tuberculosis*" Thesis Supervisor: Dr. Dagmara Jakimowicz
II-VI 2006	*Dresden University of Technology, Medical Faculty "Carl Gustav Carus" Department of Pharmacology and Toxicology, Dresden, Germany*

Research Project : „Characterisation of antiarrhithmic agents: dofetilide, flecainide and AVE 0118 on potassium currents I_{K1} and $I_{K,ACh}$ in human atrial cardiomyocytes from patients with SR and cAF"

Project Supervisor: Dr. med. Dobromir Dobrev

Publications:

Zimniak, T., K. Stengl, K. Mechtler, and S. Westermann. 2009. Phosphoregulation of the budding yeast EB1 homologue Bim1p by Aurora/Ipl1p. *J Cell Biol*. 186:379-91.

Voigt, N., N. Rozmaritsa, A. Trausch, **T. Zimniak**, T. Christ, E. Wettwer, K. Matschke, D. Dobrev, and U. Ravens. 2009. Inhibition of I(K,ACh) current may contribute to clinical efficacy of class I and class III antiarrhythmic drugs in patients with atrial fibrillation. *Naunyn Schmiedebergs Arch Pharmacol*.

Jakimowicz, D., A. Brzostek, A. Rumijowska-Galewicz, P. Zydek, A. Dolzblasz, A. Smulczyk-Krawczyszyn, **T. Zimniak**, L. Wojtasz, A. Zawilak-Pawlik, A. Kois, J. Dziadek, and J. Zakrzewska-Czerwinska. 2007. Characterization of the mycobacterial chromosome segregation protein ParB and identification of its target in Mycobacterium smegmatis. *Microbiology*. 153:4050-60.